Physicochemical Studies on Photolytic Metal Nanoparticles in Thin Films of Polysaccharide Derivatives

多糖類誘導体薄膜中の光分解金属ナノ粒子に関する物理化学的研究

January 2005

Graduate School of Engineering
Osaka City University

Toshihito Miyama

御山　稔人

Contents

General Introduction

A beautiful color of a stained glass has attracted our eyes from a distant past. Nowadays, it is known that the origin of these colors is the surface plasmon resonance of metal nanoparticles, such as gold and silver. The physical and optical properties of metal nanoparticles as well as their chemical properties depend on certain extrinsic conditions; size, shape, aggregation, structure, composition, and their environments. Such features offer a possibility of creating novel materials for catalysis, sensors, optics, and optoelectronics.[1–3]

Fabrication of metal nanoparticles and metal thin films can be achieved through a wide variety of routes. They are mainly fallen into two types of processes; break-down process and building-up process. In the break-down process, bulk metals are smashed into nanometer-sized particles. On the other hand, in the building-up process, the constituents of small particles (atoms, clusters) are made to accumulate under controlled conditions. Wide varieties of physical and chemical methods are employed to perform those processes. In most physical methods, bulk metals are initially decomposed into the constituents by means of, e.g., vacuum heating, sputtering, laser ablation, and then those constituents are deposited on certain substrates. They are often operated under severe reaction conditions by using large-scale equipments like high-vacuum system, high-frequency power source, laser source, and so on.

In the chemical methods, metal atoms formed by certain chemical reactions are made to grow into metal particles (building-up process). Except for the chemical vapor deposition method, chemical methods are usually operated under milder conditions than physical ones; liquid-phase reactions, room temperature, in air. Synthesis of gold and silver particles by reduction of $AuCl_4^-$ and Ag^+ ions, respectively, has been popular in colloid chemistry. Among them, photoreduction of $AuCl_4^-$ ions and Ag^+ ions in solutions containing certain protective agents yields the corresponding metal nanoparticles. The photoreduction method has many advantages; it is usually operated under mild conditions, e.g., in aqueous solutions at room temperature and moreover, it can be initiated at will by introducing "reducing agents" to the reactor by UV irradiation from the outside. Therefore, our research group has concerned in the fabrication of silver and gold nanoparticles by photoreduction method. Three types of protective agents; surfactant, polyelectrolyte, well-dispersed "solid" particle, have been tested, all of which have enabled us to obtain high-quality silver and gold nanoparticles.[4]

Yonezawa et al. demonstrated the formation of colloidal silver and gold by irradiation of $AgClO_4$ and $HAuCl_4$ solutions, respectively, with 253.7-nm light in the presence of protective

agents; sodium dodecylsulfate (SDS), sodium alginate (ALNa), colloidal silica (SiO_2).[4] Structure formulas of SDS and ALNa are given in Scheme 1. For example, silver particles obtained from 1 mM $AgClO_4$–35 mM SDS–0.1 M i-C_3H_7OH solution were $2a$ = 10–30 nm in size and showed a surface plasmon band (SP-band) at λ_{SP} = 390–400 nm in the UV-visible extinction spectrum. Gold nanoparticles obtained from the 1 mM $HAuCl_4$–35 m M SDS–0.1M i-C_3H_7OH solution were $2a$ = 40–60 nm in size and showed the SP-band at λ_{SP} = 540–550 nm.

The author should note that the formation of metal nanoparticles by reduction of metallic ions is not so simple as it looks. In the course of net reactions, metal atoms (Ag^0, Au^0) grow into metal nanoparticles via metal clusters, Ag_n, Au_n, composed of n atoms (n = 1–10^2). Accordingly, these reactions consist of complex multi-step processes in themselves. What is more, metal nanoparticles can coalesce themselves, sometimes giving rise to colloidal aggregate taking a fractal structure.[5] Those situations hinder us from complete understanding of the reaction-growth mechanism. Photoreduction of Ag^+ or $AuCl_4^-$ ions and formation of the corresponding metal particles in aqueous solutions are believed to proceed by consecutive reactions as shown in Scheme 2.

The colloidal solutions in which nanoparticles are stabilized with suitable protective agents are useful for spectroscopic and other basic studies, but they are not suitable for the device applications because of the handling problems, as well as evaporation or leakage of the liquid host, etc. To overcome such limitations, variety of approaches has been considered to synthesize metal nanoparticles and thin films in solid matrixes by adopting chemical, sonolytic, radiolytic, electric, and photolytic reactions.[4,6]

(A)

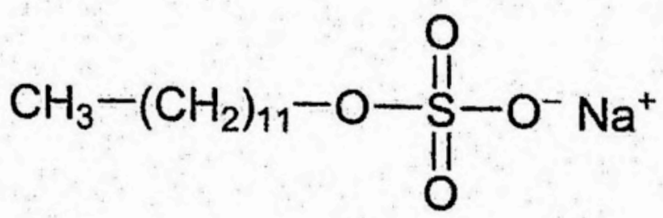

(B)

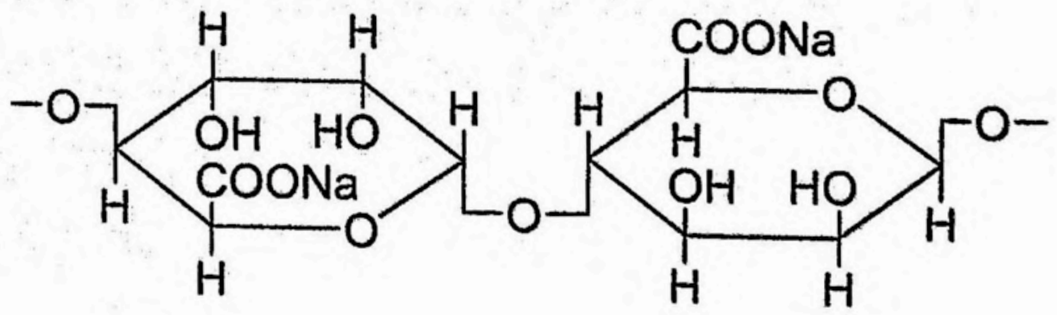

Scheme 1. Chemical structures of SDS (A) and ALNa (B).

(A)

$$Ag^{+} + H_2O \xrightarrow{h\nu} Ag^{0} + H^{+} + \dot{O}H$$

$$nAg^{0} \longrightarrow Ag_n$$

(B)

$$AuCl_4^{-} \xrightarrow{h\nu} AuCl_3^{-} + \dot{C}l \cdot$$

$$2AuCl_3^{-} \longrightarrow AuCl_4^{-} + AuCl_2^{-}$$

$$AuCl_2^{-} \xrightarrow{h\nu} Au^{0} + \dot{C}l + Cl^{-}$$

$$nAu^{0} \longrightarrow Au_n$$

Scheme 2. Scheme of photochemical reactions of Ag^{+} (A) and $AuCl_4^{-}$ (B) in solution.

Photoreduction of silver ions in polymer films has long been investigated by the research group in Kyoto University. They have fabricated silver particles and silver mirror by photolysis of thin films of silver salt of high molecular weight carboxylic acids.[7–9] Next, the author may briefly review their studies. It has long been known that irradiation of silver salts of low molecular weight carboxylic acids, for example, acetic acid, propionic acid, and oxalic acid, with UV light forms bulk silver. Konishi and coworkers found that silver particulate film is formed by photolysis of silver salt of alginic acid films (ALAg films). Alginic acid (AL) is a block heteropolymer of D-mannuronic acid and L-guluronic acid produced by brown algae, which distributes widely in nature. On irradiation with a sterilization lamp in wet air at room temperature, a large amount of silver is precipitated and the irradiated surface finally changes into a clear silver mirror with a low sheet resistance. Yonezawa et al. restarted research works on the photochemistry of the ALAg film because a renewed interest has arisen to surface-enhanced electromagnetic phenomena, nonlinear optics, as well as other size-dependent physical and chemical properties of metal nanoparticles.[10,11] High-resolution scanning electron microscope and transmission electron microscope were used for the characterization of the silver particulate films. It was revealed that the irradiated surface of the ALAg film is densely covered with 10–50 nm sized silver nanoparticles. Further, a diffusion model to simulate the segregation of silver particles at the film surface has been proposed.[12]

In this thesis, as a significant extension of the previous works of Konishi and Yonezawa on ALAg, the formation and characterization of silver and gold nanoparticles and thin films

formed by photolysis of metal salts of polysaccharide derivatives; carboxymethylcellulose (CMC), and chitosan (CTO), have been studied. CMC and CTO are typical derivatives of cellulose and chitin, respectively. Partial carboxymethylation of cellulose gives rise to CMC.[13] CTO is the deacetylated product of chitin.[14] Cellulose and chitin are widespread biosynthetic products formed by β-D-glucopyranose and *N*-acetyl-β-D-glucopyranose units linked together by (1-4) glycosidic bonds.[15] Chitin has identical structure with cellulose except that the secondary hydroxyl group on the α-carbon atom is substituted with an acetamide group and plays the same skeletal role in arthropods as cellulose does in plants. CMC and CTO are anionic and cationic polyelectrolytes, respectively, suitable to prepare aqueous solutions. Casting and drying those solutions on solid plates gave rise to corresponding polymer films. Alginic acid, cellulose and chitin are biosynthetic polymer existing with the large amount on the earth, so industrial applications of these materials attract much attention. They have been used for medicals, food products, biocompatible materials and so on. Recently, fabrication of the metal nanoparticles by using CMC or CTO as the protective agent has been reported. Kapoor and Gopinathan have employed CMC as a protective agent to fabricate silver nanoparticles in solutions by radiolytic reduction.[16] They have studied early aggregation processes of silver atoms and small clusters stabilized by CMC molecules at ambient temperature. Magdassi et al. have prepared concentrated silver nanoparticles for the use of pigments in ink-jet inks, using CMC as a polymeric stabilizer.[17] CTO/gold layered composite has been reported by Huang and Yang.[18] They have successfully constructed a multilayer gold nano-particulate assembly through electrostatic interactions on CTO functionalized electrodes by the alternate treatment of the electrode with solution of citrate-stabilized gold nanoparticles (negatively charged) and CTO solution (positively charged). Esumi et al. have fabricated gold nanoparticles in the presence of CTO via reduction of $HAuCl_4$ with sodium borohydride.[19] The catalytic activity of CTO/gold nanocomposites upon elimination of hydroxyl (OH) radicals formed in an $H_2O_2/FeSO_4$ system has been examined.

In this thesis, the author has discussed spectroscopic properties of silver and gold particles in polymer films. So that, historical background of size-dependent optical properties of precious metal particles is briefly discussed. It is known that, by 1856, Michael Faraday postulated that the beautiful color of ruby glass, as well as aqueous suspensions of gold (mixed with either SO_3 or phosphorus), is due to finely dispersed gold nanoparticles.[20] It is interesting that Faraday did not have a quantitative theoretical picture, but reached a correct answer based on an intuitive understanding of high reflectivity and scattering of metal surface. The first

attempt at a quantitative theoretical description of the colors of metal nanoparticles was made in 1904 by J. C. Maxwell-Garnett.[21] He used the expressions of the polarizability for spherical particles derived by Rayleigh and Lorenz to estimate effective dielectric constants of composite materials. In 1908, Mie published a rigorous theoretical study on the optical properties of spherical particles based on Maxwell's electromagnetic equations.[22] A Mie's theory can afford extinction, scattering and absorption coefficients for nanoscopic gold particles which are compared well with the observed extinction spectra of gold sols. After Mie, scattering of electromagnetic waves by spheres[23], cylinders[24] as well as ellipsoids[25] have been treated by many groups. It was the discovery of the surface-enhanced Raman scattering (SERS)[26–28] that sparked a renewed interest in physics and optics of metal nanoparticles. SERS is a phenomenon that the molecules adsorbed at the surface of precious metals such as gold, silver, and copper display unusually strong Raman scattering. An observation indicating the connection between electromagnetic enhancement of SERS and surface plasmon resonance[29] has provided the impetus for experimental and theoretical studies of the particle shape and aggregation of metal nanoparticles.[30,31] Although many groups became interested primarily in the SERS effect during the mid-1970s and early 1980s, their works have provided important insights into the fundamental linear and nonlinear optical properties of metal nanoparticles.[32–34]

Besides spectroscopic properties, gold and silver nanoparticles have relevance for electron microscopy (contrast agents),[35] analytical chemistry (chemical and biological sensors),[36–39] electronics (single-electron transistors, electrical connects),[40,41] and catalysis (CO oxidation on Au/TiO_2 composites).[42,43] Concerning the applications of matrix supported gold and silver nanoparticles, surface metallization of thin films has been applied for circuit pattern formation and imaging materials. Tabei et al. proposed a "photochemical circuit process" for the formation of printed circuits on solid substrates.[44] Thermography based on the chemical reduction of silver salts of long-chain organic acids, e.g. the dry silver process (3M Company), has been established.[45] Mazur et al. proposed a write-once, high-density optical information storage system based on sintering silver interlayers in polyimide films.[46] Tominaga et al. fabricated three-dimension aggregate of silver nanoparticles of 20–30-nm size on disk by hydrogen reduction of AgO layer. They have attempted to apply the silver particulate film to high-density optical data storage using the surface-enhanced plasmon resonance.[47] The author has found the reduction of $AuCl_4^-$ ions in the CTO matrix during a etching process by argon ion bombardment, indicating a possible application to lithography. A new strategy for metal patterning of polymer surfaces with mild UV light has been presented by Korchev et al. Silver

ions in the polymer films made from blends of poly(vinyl alcohol) and sulfonated poly-(ether-ether)keton have been photolyzed with 350-nm light, yielding silver nanoparticle-rich surface layers on both side of the film.[48] Biosensors based on surface plasmon resonance (SPR) of metal nanoparticles and metal thin films have been intensively examined and commercially available in part, making real-time biomolecular interaction analysis accessible to those in biochemistry-related fields. Natan and Lyon have examined the tag-amplified SPR methods: colloidal Au-enhanced biosensing.[49] Gold and silver nanoparticles have a potentially useful for nonlinear optical devices because of their exceptionally high density of delocalized electrons.[50] Sato et al. measured third-order nonlinear susceptibility $\chi^{(3)}$ of colloidal silver dispersion prepared by photoreduction.[51] Prolonged irradiation of aqueous solution containing 0.2 wt% ALNa and 1 mM $AgClO_4$ with 253.7-nm light caused the aggregation of silver nanoparticles. Accompanied with aggregation, about 10^2 times increase of $\chi^{(3)}$ was observed. They have also observed a proportional relation between $\chi^{(3)}$ and the SERS intensity of the silver nanoparticle dispersion, indicating that the increase of $\chi^{(3)}$ is caused by the enhanced local electric field due to SPR. As cited above, gold and silver nanoparticles are assumed to have a great capability for practical applications in a variety of fields of material technology.

Scope of this thesis

The author has tried to provide a convenient method to fabricate metal nanoparticles and metal thin films using naturally occurring polymer derivatives as a matrix to promote the applications of metal nanoparticles and natural resources for industrial materials. Detailed characterization of metal nanoparticles and particulate films has been mentioned. Further, the author has analyzed the SERS, a typical surface-enhanced electromagnetic phenomena, as well as quenching of dye fluorescence due to excitation energy transfer on the basis of classical electromagnetic theory, which may be useful not only for our system but also for a number of metal-matrix systems.

In Chapter 1, photolysis of silver salt of CMC films (CMCAg films) and chloroauric acid salt of CTO films (CTOAu films) with UV light under several reaction conditions has been examined. Fabrication and characterization of the silver and gold nanoparticles in polymer films, and the corresponding metal mirrors at the film surface have been discussed.

Chapter 2 dealt with the detailed surface characterization of the CMCAg films irradiated with UV light in wet air at room temperature. The formation of silver mirror at the film surface and the mechanism of photochemical reactions of the CMCAg have been examined with the

aids of field emission type scanning electron microscope (FE-SEM) and X-lay photoelectron spectroscopy (XPS).

In Chapter 3, the CTOAu films photolyzed in wet air at room temperature have been subjected to surface characterization with FE-SEM and XPS. A direct evidence of the aggregation of photolytic gold from cluster to colloidal particles has been obtained. Details of photochemical reactions of the CTOAu have been examined.

Chapter 4 dealt with the SERS of CMC and AL molecules adsorbed on silver particles. Variations of the SERS enhancement factor of the symmetric stretching vibration of carboxylate ions with the aggregation of silver particles have been examined.

In Chapter 5, a tractable formula for the enhancement efficiency of the local electric field, Q_{NF}, has been defined on the basis of Mie theory. Q_{NF} has been compared with many features of SERS of the CMCAg and ALAg in Chapter 4.

Chapter 6 dealt with the quenching of dye fluorescence by silver nanoparticles. Silver particulate films formed by photolysis of the CMCAg films were used as the substrates to deposit dye monolayers. The dependence of quenching of dye fluorescence by silver particles on the layer separation was examined with aids of classical electromagnetic theory.

References

1. D. L. Feldheim and C. A. Foss, Jr. eds., *Metal Nanoparticles: Synthesis, Characterization and Applications*, Marcel Dekker, New York (2002).
2. V. P. Kamat, *J. Phys. Chem. B*, **106**, 7729 (2002).
3. A. Heilmann, *Polymer Films with Embedded Metal Nanoparticles*, Springer, Berlin (2002).
4. Y. Yonezawa, T. Sato, M. Ohno, and H. Hada, *J. Chem. Soc., Faraday Trans. 1*, **83**, 1559 (1987).
5. D. A. Weitz and M. Oliveria, *Phys. Rev. Lett.*, **52**, 1433 (1984).
6. H. Anders, *Thin Films in Optics*, Focal Press, London (1967).
7. Y. Konishi, H. Hada, and M. Tamura, *J. Chem. Soc. Jpn.*, **86**, 1132 (1965).
8. Y. Konishi, H. Hada, and M. Tamura, *J. Chem. Soc. Jpn.*, **92**, 829 (1971).
9. Y. Konishi, H. Saijo, H. Hada, and M. Tamura, *Nature (London)*, **268**, 709 (1977).
10. Y. Yonezawa, A. Takami, T. Sato, K. Yamamoto, T. Sasanuma, H. Ishida, and A. Ishitani, *J. Appl. Phys.*, **68**, 1297 (1990).
11. Y. Yonezawa, Y. Konishi, H. Hada, K. Yamamoto, and H. Ishida, *Thin Solid Films*, **218**, 109 (1992).

12. Y. Yonezawa and M. Kijima, *J. Soc. Photogr. Sci. Tech. Jpn.*, **56**, 3 (1993).

13. A. A. R. Muzzarelli, *Chitin*, Pergamon Press, Oxford (1977).

14. J. V. Karabinos and M Hindert, *Adv. Carbohydrate Chem.*, **9**, 285 (1954).

15. A. B. Foster and J. M. Webber, *Adv. Carbohydrate Chem.*, **15**, 371 (1960).

16. S. Kapoor and C. Gopinathan, *Radiat. Phys. Chem.*, **53**, 165 (1998).

17. S. Magdassi, A. Bassa, Y. Vinetsky, and A. Kamyshny, *Chem. Mater.*, **15**, 2208 (2003).

18. H. Huang and X. Yang, *Coll. Surf. A, Physicochem. Eng. Aspects*, **226**, 77 (2003).

19. K. Esumi, T. Nakao, and T. Yoshimura, *Coll. Surf. B, Biointerfaces*, **32**, 117 (2003).

20. L. P. Wlllimas ed., *The Selected Correspondence of Michael Faraday*, Cambridge University Press, London, Vol. 2 (1971).

21. J. C. Maxwell-Garnett, *Philos. Trans. R. Soc. A*, **203**, 385 (1904).

22. G. Mie, *Ann. Phys.*, **25**, 377 (1908).

23. P. Debye, *Ann. Phys.*, **30**, 57 (1909).

24. H. C. van de Hulst, *Light Scattering by Small Particles*, Dover, New York (1981).

25. S. Asano and M. Sato, *Appl. Optics*, **19**, 962 (1980).

26. M. Fleischmann, P. J. Hendra, and A. J. McQuillan, *Chem. Phys. Lett.*, **26**, 163 (1974).

27. A. J. McQuillan, P. J. Hendra, and M. Fleischmann, *J. Electroanal. Chem.*, **65**, 933 (1975).

28. J. P. Jeanmarie and R. P. van Duyne, *J. Electroanal. Chem.*, **84**, 1 (1977).

29. M. Moskovits, *Rev. Mod. Phys.*, **57**, 783 (1985).

30. R. K. Chang, T. E. Furtak eds., *Surface Enhanced Raman Scattering*, Plenum Press, New York (1982).

31. M. Kerker ed., *Selected Papers on Surface-Enhanced Raman Scattering*, SPIE Optical Engineering, Bellingham (1990).

32. M. Meier and A. Wokaun, *Optics Lett.*, **8**, 851 (1983).

33. E. J. Zeman and G. C. Schatz, *J. Phys. Chem.*, **91**, 634 (1987).

34. P. W. Barber, R. K. Chang, and H. Massoudi, *Phys. Rev. B*, **27**, 7251 (1983).

35. M. A. Hayat, *Colloidal Gold: Principles, Methods, and Applications*, Academic Press, San Diego, Vol. 3 (1993).

36. W. P. Wuelfing and R. W. Murray, *J. Phys. Chem. B*, **106**, 3139 (2002).

37. N. Krasteva, I. Besnard, B. Guse, R. E. Bauer, K. Mullen, A. Yasuda, and T. Vossmeyer, *Nano Lett.*, **2**, 551 (2002).

38. Y. J. Kim, R. C. Johnson, and J. T. Hupp, *Nano Lett.*, **1**, 165 (2001).

39. C. A. Mirkin, *Inorg. Chem.* **39**, 2258 (2000).

40. D. L. Klein, P. L. McEuen, J. E. B. Katari, R. Roth, and A. P. Alivisatos, *Appl. Phys. Lett.*, **68**, 2574 (1996).

41. T. Sato, H. Ahmed, D. Brown, and B. F. G. Johnson, *J. Appl. Phys.*, **82**, 696 (1997).

42. G. R. Bamwenda, S, Tsubota, T. Nakamura, and M. Haruta, *Catal. Lett.*, **44**, 83 (1997).

43. J. J. Poetron, R. M. Stroud, and D. R. Rolison, *Nano Lett.*, **2**, 545 (2002).

44. H. Tabei, S. Nara, and K. Matsuyama, *Photogr. Sci. Eng.*, **20**, 246 (1976).

45. J. Kosar, *Light-Sensitive Systems: Chemistry and Application of Nonsilver Halide Photographic Processes*, Wiley, New York (1965).

46. S. Mazur and S. Reich, *J. Phys. Chem.*, **90**, 1365 (1986).

47. J. Tominaga, J. Kim, H. Fuji, D. Büchel, T. Kikukawa, L. Men, H. Fukuda, A. Sato, T. Nakano, A. Tachibana, Y. Yamakawa, M. Kumagai, T. Fukaya, and N. Atoda, *Jpn. J. Appl. Phys.*, **40**, 1831 (2001).

48. A. S. Korchev, M. J. Bozack, B. L. Slaten, and G. Mills, *J. Am. Chem. Soc.*, **126**, 10 (2004).

49. R. C. Johnson and J. T. Hupp, *Metal Nanoparticles: Synthesis, Characterization and Applications (Chapter 6)*, ed. by D. L. Feldheim and C. A. Foss, Jr., Marcel Dekker, New York (2002).

50. M. J. Natan and L. A. Lyon, *Metal Nanoparticles: Synthesis, Characterization and Applications (Chapter 8)*, ed. by D. L. Feldheim and C. A. Foss, Jr., Marcel Dekker, New York (2002).

51. T. Sato, T. Ichikawa, T. Ito, Y. Yonezawa, K. Kadono, T. Sakaguchi, and M. Miya, *Chem. Phys. Lett.*, **242**, 310 (1995).

Chapter 1

Formation of Metal Nanoparticles and Thin Films by Photolysis of Metal Salts of Polysaccharide Derivatives

1. 1 Introduction

On the way to the exploration of raw materials useful for industrial purposes, renewed interest in naturally occurring polymers has arisen because of their compatibility with environments. Cellulose and chitin are biosynthetic products which widely distributed in nature. Chitin has identical structure with cellulose except that the secondary hydroxyl group on the α-carbon atom is substituted with an acetamide group and plays the same skeletal role in arthropods as cellulose does in plants. Partial carboxymethylation of cellulose gives rise to carboxymethylcellulose (CMC).[1] Chitosan (CTO) is the deacetylated product of chitin.[2] CMC and CTO, typical derivatives of cellulose and chitin, are anionic and cationic polyelectrolyte soluble to water and various acidic solvents, respectively. Schematic structures of CMC and CTO are shown in Scheme 1-1.

Complexation of CMC and CTO with metal ions has attracted much attention.[3] When films of CMC and CTO are immersed in certain metal salt solutions, water-insoluble films are formed. As CMC and CTO are available for the protective agent of colloidal metal particles in solutions,[4] they are relevant to the fabrication of thin metal films by using those materials as the polymer support. Konishi et al. have found that a clear silver mirror was formed by photolysis of silver salt films of alginic acid, a typical polysaccharide produced by brown algae.[5] In this Chapter, thin films of silver salt of CMC (CMCAg films) and chloroauric acid

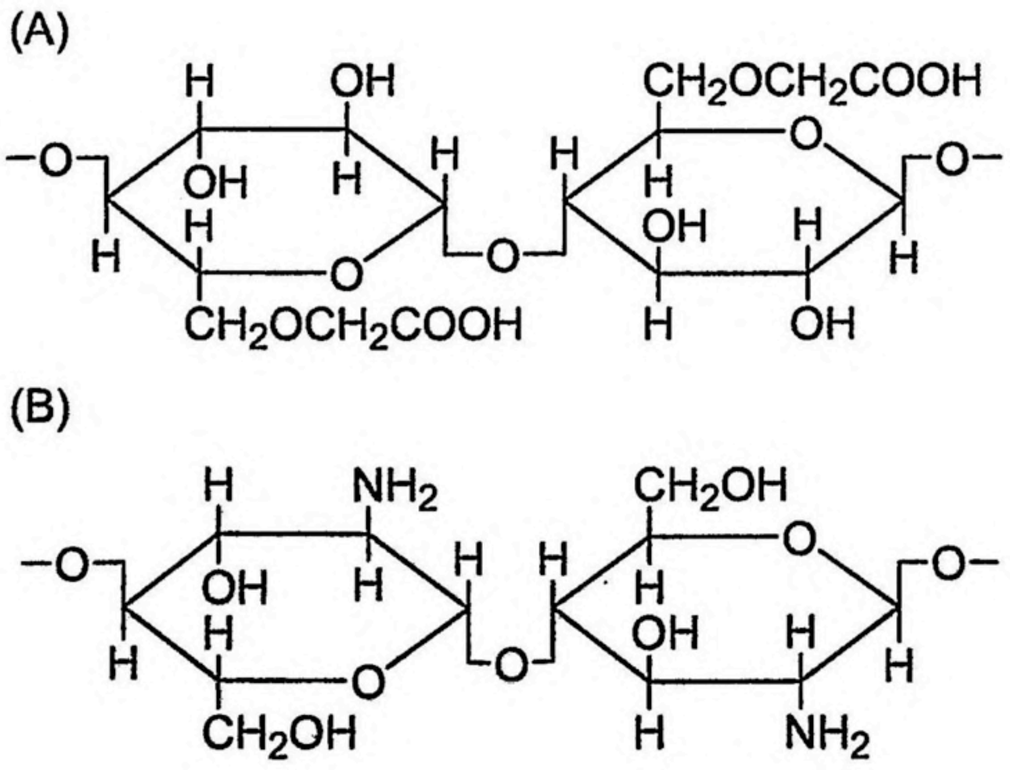

Scheme 1-1. Schematic structures of CMC (A) and CTO (B).

salt of CTO (CTOAu films) have been taken up. The CMCAg films and the CTOAu films were photolyzed with UV light under several reaction conditions and examined the changes of aggregation state of photolytic metals.

1. 2 Experimental

1. 2. 1 Preparation

A 0.5 wt% aqueous solution of sodium salt of CMC (CMCNa) (Nacalai Tesque Co., Daicel Chem. Ind. Ltd.) was prepared and spread on the quartz plate ($10 \times 30 \times 1\ mm^3$) by the amount of 0.05 $mL \cdot cm^{-2}$. The degree of carboxymetylation was about 20–30%. The CMCNa film was dried and then immersed in 0.1 M (1 M = 1 $mol \cdot dm^{-3}$) $AgNO_3$ aqueous solution for 60 min to substitute Na^+ with Ag^+ ions. The film was washed with distilled water and dried again in the dark. The CMCAg film was colorless and transparent. The thickness of the film fabricated in this manner was 1–5 μm.

CTO was purchased from Wako Pure Chemical Industries, Ltd. The degree of deacetylation was about 80%. A 0.5 wt% aqueous solution of CTO in 1 vol% acetic acid was spread on the quartz plate ($10 \times 30 \times 1\ mm^3$) by the amount of 0.05 $mL \cdot cm^{-2}$. The CTO film was dried and then immersed in 0.01 M $HAuCl_4$ aqueous solution for 60 min to form $AuCl_4^-$ salt. After washing with distilled water and drying in the dark, the light-yellow and transparent CTOAu film was formed. Cooling of the CTO film, $AuCl_4^-$ solution and distilled water by ice was helpful to prepare high-quality CTOAu films. The thickness of the CTOAu film was 1–5 μm.

The CMCAg film on the quartz plate was exposed to 253.7 nm light from a 15-W sterilization lamp (Toshiba Co.) in the reaction chamber with controlled temperature for 288–298 K and relative humidity more than 70%. The incident intensity of 253.7-nm light was monitored with the aid of a photometer, type IL-600 (International Light Co.). The number of incident photons as estimated by the ferrioxalate actinometer[6,7] was about 10^{17} $cm^{-2} \cdot min^{-1}$. As the quality of thin gold films was sensitive to reaction conditions, the author had to pay special attention to temperature and humidity during photolysis of the CTOAu film. Relative humidity and temperature in the reaction chamber were controlled to be 70–85% and more than 293 K, respectively. The author should note that a clear gold mirror was not formed at temperature below 293 K and humidity more than 85%.

1. 2. 2 Instrumentation

To estimate the amount of unreacted metal ions and the amount of deposited metal, atomic absorption spectrometry was employed by using a Hitachi Z-6100 spectrophotometer. The amount of Ag^+ ions per 1 cm^2 before photolysis was 0.64 μmol·cm^{-2} in the CMCAg film. That of $AuCl_4^-$ ions in the CTOAu film was 1.18 μmol·cm^{-2}. Transmittance spectra of the films were recorded on a UV-2200 spectrophotometer (Shimadzu Co.). The morphology of the films was examined by a high-resolution scanning electron microscope of the field emission type, Hitachi Model S-900. The accelerating voltage was 6 kV. The X-ray diffraction (XRD) data were collected on a Shimadzu XD-610 with a CuKα radiation.

1. 3 Results

1. 3. 1 Photolysis of CMCAg films

On irradiating with UV light in wet air at room temperature, the CMCAg film became yellow-brown colored due to the formation of colloidal silver. When irradiation was continued, the irradiated surface of the film gradually assumed metallic luster and finally changed into a clear silver mirror. Variation of transmittance spectra with irradiation is given in Figure 1-1(A). The colloidal absorption band of silver which was located at λ = 400–410 nm developed with irradiation time. Finally, almost continuous absorption of the silver metal film was observed. The XRD profile of the irradiated film is added to Figure 1-1(A). After 360 min of photolysis, the diffraction line of the (111) face of the face-centered cubic (f.c.c.) silver lattice is evident (JCPDS card 4-0783(Ag)). A broad diffraction line after 30 min of irradiation indicates the formation of colloidal silver particles. The dependence of the amount of photolytic silver (ΔN_{Ag}) on irradiation time is given in Figure 1-2(A). It is shown that ΔN_{Ag} was increased with irradiation time and became almost constant after 180 min. The conversion efficiency of Ag^+ ions at this stage was about 64%. A scanning electron micrograph of the CMCAg film after UV irradiation is shown in Figure 1-3(A). Before irradiation, the surface of the CMCAg film looked fairly smooth. After 600 min of irradiation, the surface was densely covered with colloidal silver particles of several 10 nm size.

1. 3. 2 Photolysis of CTOAu films

When the CTOAu film was irradiated with UV light in wet air at room temperature, the film first maintained the original color and then became blue-violet colored due to the formation of colloidal gold. After a prolonged irradiation, the irradiated surface changed into a clear gold

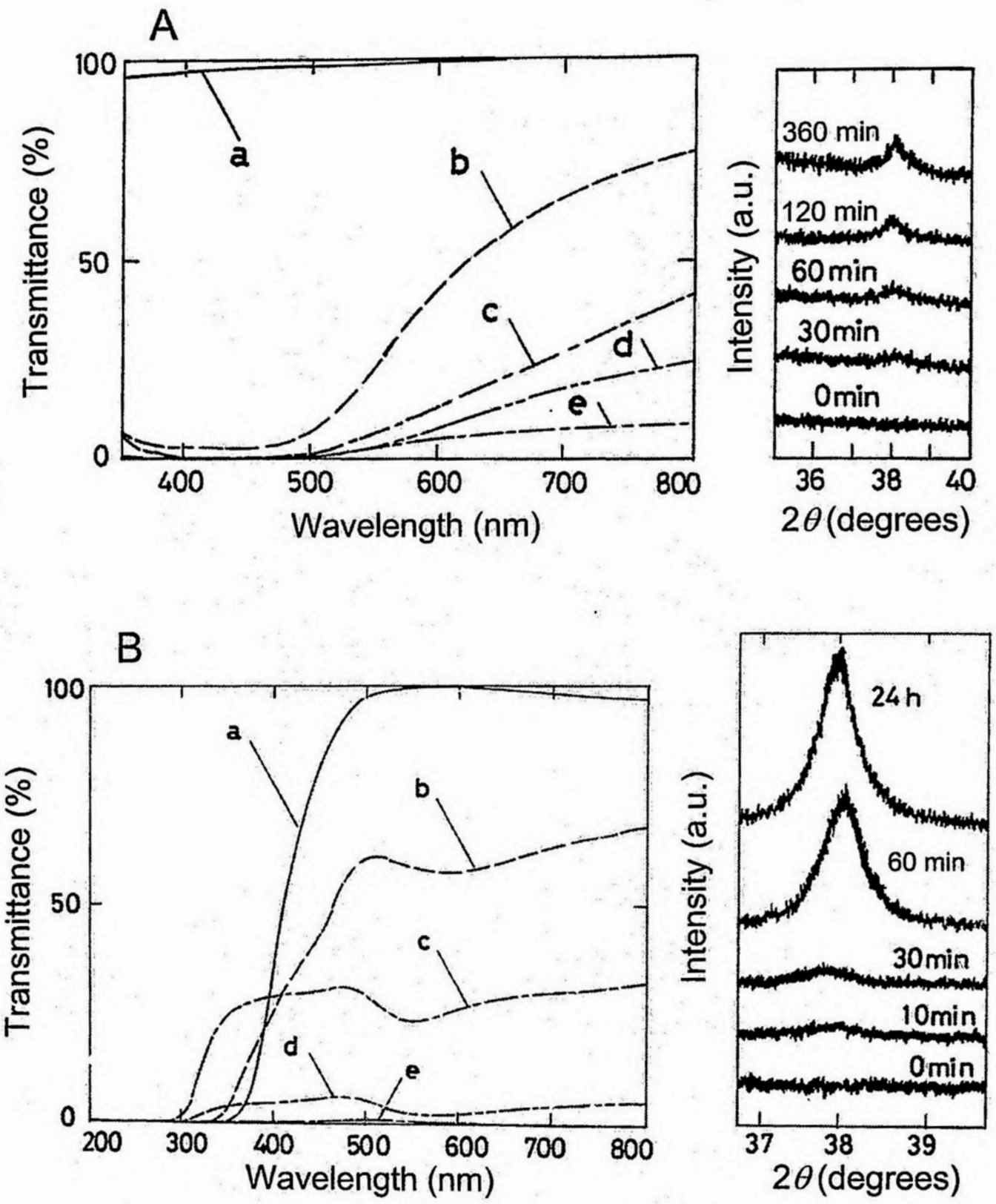

Figure 1-1. Variations of transmittance spectra and XRD profiles for the CMCAg film (A) and the CTOAu film (B) with UV irradiation. Irradiation time: (A) (a) 0 min, (b) 10 min, (c) 30 min, (d) 60 min, (e) 24 h. (B) (a) 0 min, (b) 20 min, (c) 40 min, (d) 60 min, (e) 120 min.

mirror. Variation of transmittance spectra with irradiation is given in Figure 1-1(B). The transmittance spectrum of the CTOAu film before irradiation was characterized by absorption shorter than $\lambda = 400$ nm due to ligand-to-metal charge transfer (LMCT) band.[8] On irradiation, the LMCT band was decreased and the colloidal absorption band of gold at $\lambda = 540$–560 nm developed. The colloidal absorption band got broader and finally, almost continuous absorption of the gold metal film was observed. The XRD profile of the irradiated film is added to Figure 1-1(B). After 60 min of photolysis, diffraction line of the (111) face of the f.c.c. gold lattice is evident (JCPDS card 4-0784(Au)). Photolytic gold after 24-h irradiation is in a highly

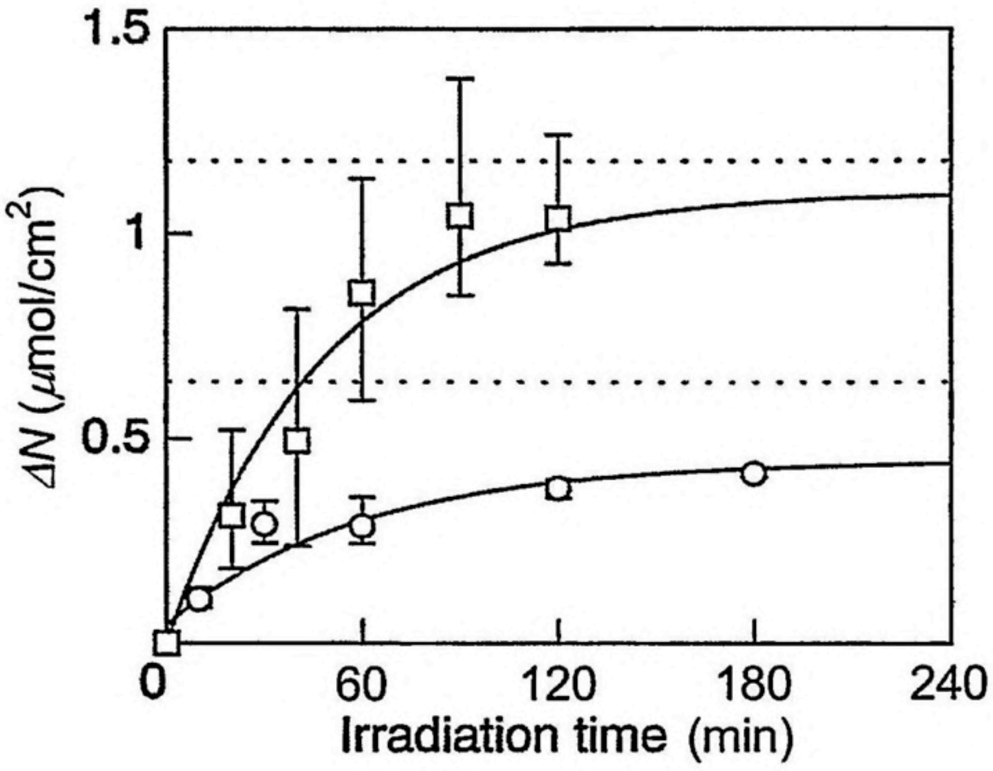

Figure 1-2. Growth of the amount ΔN of deposited silver (circle) and gold (square) with UV irradiation. ΔN (μmol·cm^{-2}) is given per square centimeter of the film.

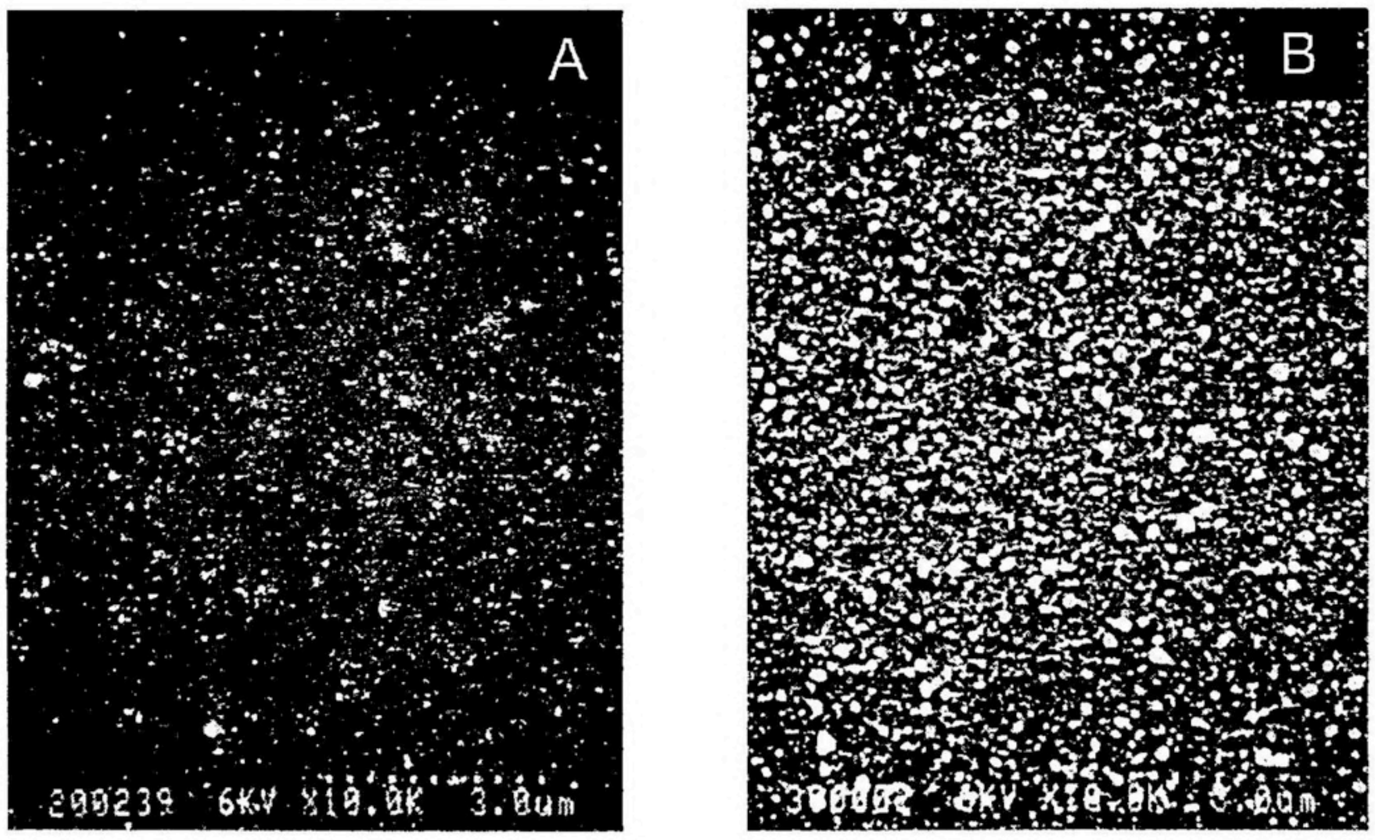

Figure 1-3. Scanning electron micrographs of the CMCAg film (A) and CTOAu film (B) after photolysis. Irradiation time: (A) 600 min, (B) 120 min. The marker corresponds to 3 μm.

crystalline state. The dependence of the amount of photolytic gold (ΔN_{Au}) on irradiation time is included in Figure 1-2(B). Apart from relatively large errors, it appeared that ΔN_{Au} was increased with irradiation time and became almost constant after 90 min. The conversion efficiency of $AuCl_4^-$ ions at this stage was about 88%. A scanning electron micrograph of the CTOAu film is shown in Figure 1-3(B). After photolysis for 120 min, the surface was densely covered with colloidal gold particles (10–100 nm size).

1. 4 Discussion

Preparation of precious metal particles by reducing metal salts has been studied extensively.[9] For example, chemical reduction of Ag^+ and $AuCl_4^-$ in the presence of chitosan[4] and imogolite[10] has been reported. The author has focused on photoreduction method because of the flexibility of reaction conditions.[11] Overall photochemical reactions in the CMCAg film and the CTOAu film are expressed as Scheme 1-2. In these films, silver atoms (Ag^0) or gold atoms (Au^0) initially formed at the Ag^+ ion or $AuCl_4^-$ ion site migrate and yield metal clusters, Ag_n or Au_n, composed of $1–10^2$ atoms. At room temperature in wet air, metal atoms and clusters could diffuse in the films and aggregate themselves, forming colloidal metal particles. Finally, these small particles aggregate at the irradiated surface, giving rise to either silver or gold mirror.

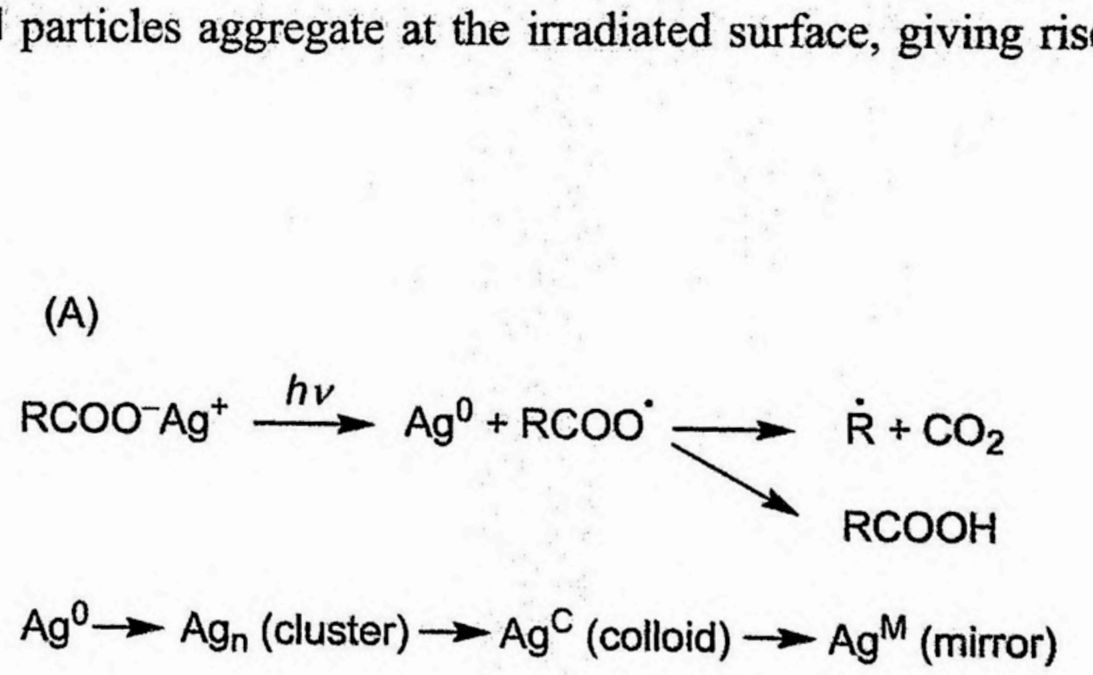

Scheme 1-2. Gross of photochemical reactions in the CMCAg film and CTOAu film.

It is likely that evacuation and low temperature can suppress migration of metal atoms and clusters in the polymer matrix. The author has examined photolysis of the CMCAg film in vacuum at liquid nitrogen temperature (77 K). The film was set in the cryostat and irradiated through the quartz window with 253.7-nm light from a 200 W low-pressure mercury lamp (Ushio Denki Co.). Variation of absorption spectra of the CMCAg film with irradiation in vacuum at 77 K, followed by dark storage in vacuum at room temperature is shown in Figure 1-4(A). The 240 min of irradiation at 77 K resulted in the broad absorption in the λ = 200–600 nm range, together with a shoulder around $\lambda \sim 330$ nm (a–d). Such spectrum is considerably different from that obtained when the film was photolyzed in wet air at room temperature, having a strong absorption band of colloidal silver around λ = 400–410 nm [Figure 1-1(A)]. The film was heated until room temperature and kept in vacuum in the dark (e–g). In consequence, peaks at λ = 300 nm, 335 nm and the colloidal absorption band of silver at λ = 400–410 nm were developed at very low speed. After introduction of air, a slight decrease of the 335 nm peak and an increase of the colloidal absorption band were noticed [Figure 1-4(B)]. Therefore, it is reasonable that peaks at λ = 300 nm and 335 nm are assigned to certain silver clusters stabilized in the polymer matrix.[12,13]

The author has also photolyzed the CTOAu film in vacuum at liquid nitrogen temperature. Figure 1-5(A) shows the variation of absorption spectra of the CTOAu film with UV irradiation in vacuum at 77 K. Irradiation for 180–600 min in vacuum at 77 K did not yield any definite peaks (b, c). When the 600-min irradiated film was heated to room temperature and kept for 180 min, a slight change of the spectra was observed in Figure 1-5(B)(a, b). However, after introduction of air to sample b, the colloidal absorption band of gold at λ = 550–560 nm and shorter wavelength band (λ < 400 nm) probably due to photolytic gold were developed rapidly (c, d). The colloidal absorption band in these spectra was similar to that of photolyzed in wet air at room temperature [Figure 1-1(B)]. Accordingly, it is plausible that the main products at low-temperature photolysis are gold atoms and clusters stabilized in the CTO matrix.[14] These results also indicate that the air and moisture introducing the polymer film play an important role for growth and aggregation of metal atoms and clusters. The importance of air and moisture to grow colloidal metal particles would be supported by the results of photolysis of the CMCAg and CTOAu films in vacuum at room temperature. These results are shown in Appendix.

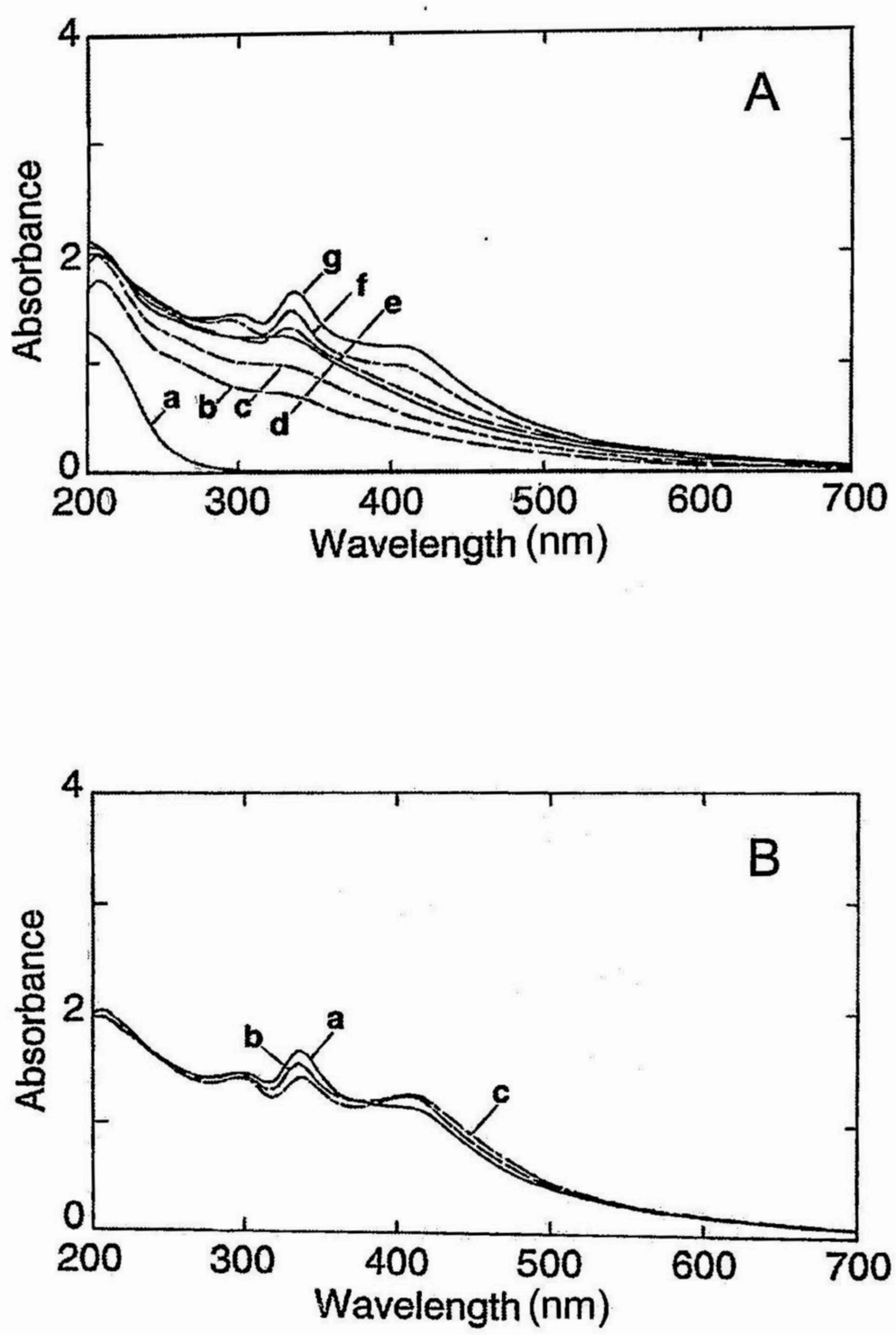

Figure 1-4. Variations of absorption spectra of the CMCAg film with UV irradiation. (A) Irradiation in vacuum at liquid nitrogen temperature (a–d), followed by dark storage in vacuum at room temperature (e–g). Irradiation time: (a) 0 min, (b) 60 min, (c) 120 min, (d) 240 min. Dark storage time after 240 min of irradiation: (e) 30 min, (f) 60 min, (g) 20 h. (B) After introduction of air to sample A and dark storage at room temperature. Dark storage time: (a) 0 min, (b) 5 min, (c) 600 min.

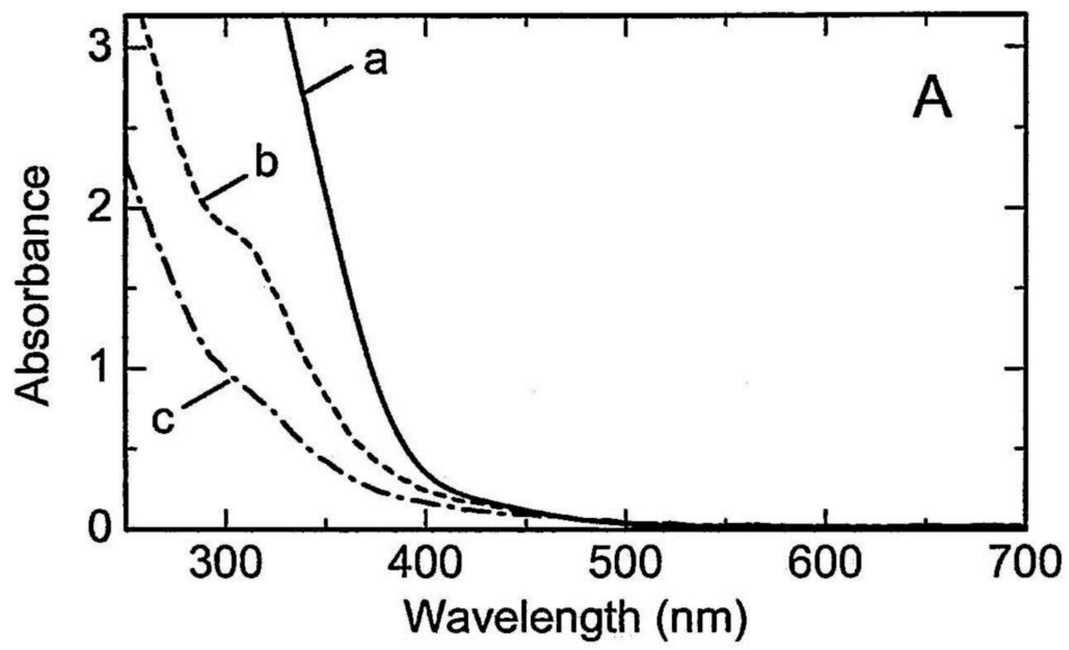

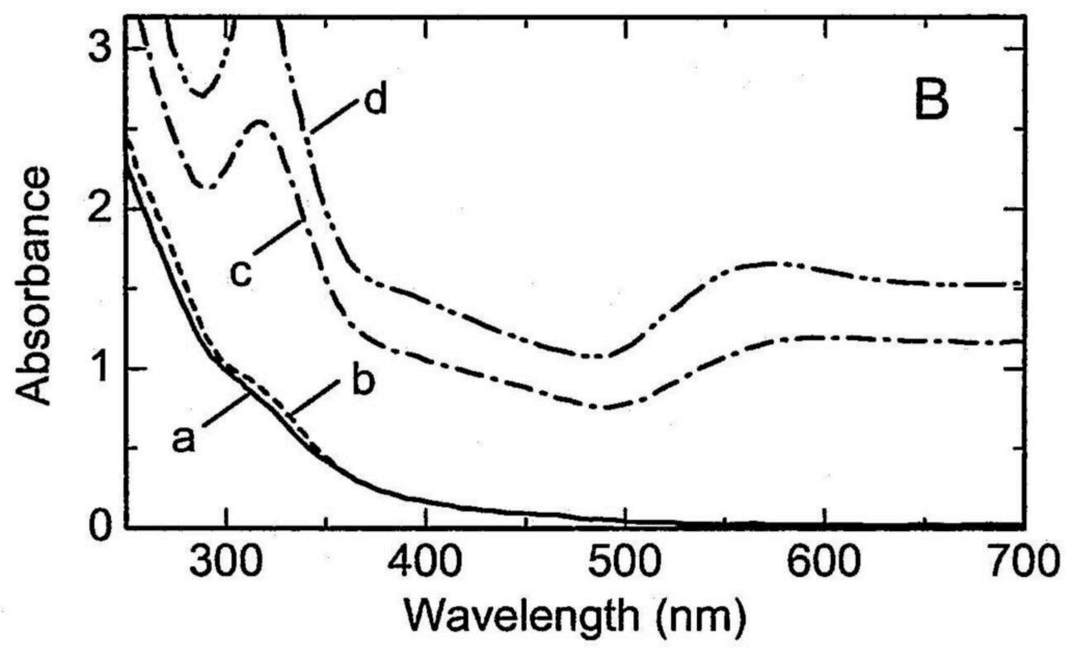

Figure 1-5 Variations of absorption spectra of the CTOAu film with UV irradiation. (A) Irradiation in vacuum at liquid nitrogen temperature. Irradiation time: (a) 0 min, (b) 180 min, (c) 600 min. (B) After heating sample A until room temperature and dark storage in vacuum at room temperature, followed by introduction of air to sample b and dark storage in air at room temperature. Dark storage time in vacuum: (a) 0 min, (b) 180 min. Dark storage time in air: (c) 15 min, (d) 120 min.

The author has so far examined photolysis of metal salts of polysaccharide derivatives, CMC and CTO. The silver salt of polymethacrylic acid (PMA) is interesting because of considerably different structure of the monomer unit. Schematic structure of PMA is shown in Scheme 1-3(A). Thin film of silver salt of PMA (PMAAg film) was fabricated from polymethacrylic acid (Scientific Polymer Products Inc.) and photolyzed. Variations of absorption spectra of the PMAAg film with UV irradiation are given in Figure 1-6. In this film, a peak at λ = 345 nm, probably due to certain silver clusters, appeared after 10 min of irradiation in wet air at room temperature [A(c)]. Prolonged irradiation caused the development of the colloidal absorption band at λ = 440–450 nm, along with the decrease of the 345 nm peak [A(d, e)]. Irradiation more than 40 h yielded a silver mirror [A(f)]. On the other hand, photolysis in vacuum at 77 K resulted in broad structureless absorption (λ = 200–600 nm), together with a peak around λ = 345 nm [B(b, c)]. Heating until room temperature [B(d–f)] and the introduction of air caused the decrease of the 345 nm peak and a little increase of the colloidal absorption band [C(a–c)]. Considering the long time irradiation necessary to obtain the silver mirror, it is likely that migration of silver atoms and clusters in the PMA matrix is not so easy as in the polysaccharide derivative films.

(A)

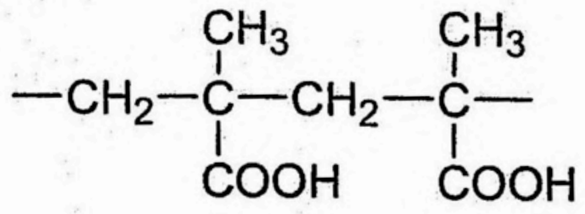

(B)

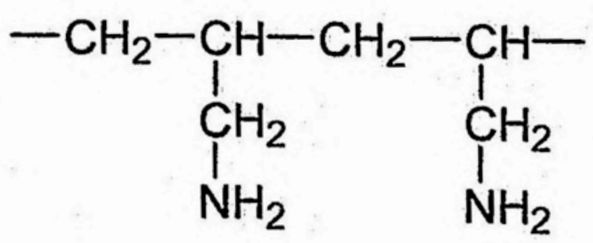

(C)

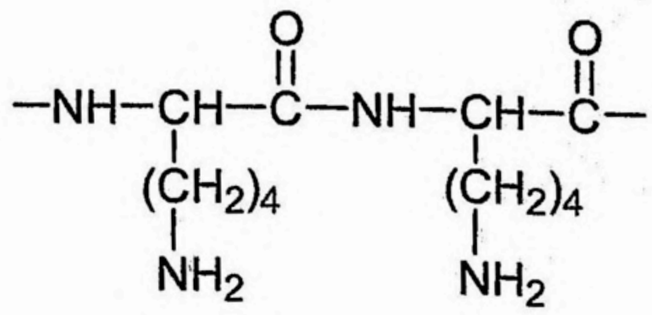

Scheme 1-3. Schematic structures of synthetic polymer used in this study. (A) PMA, (B)PAL, and (C) PLS.

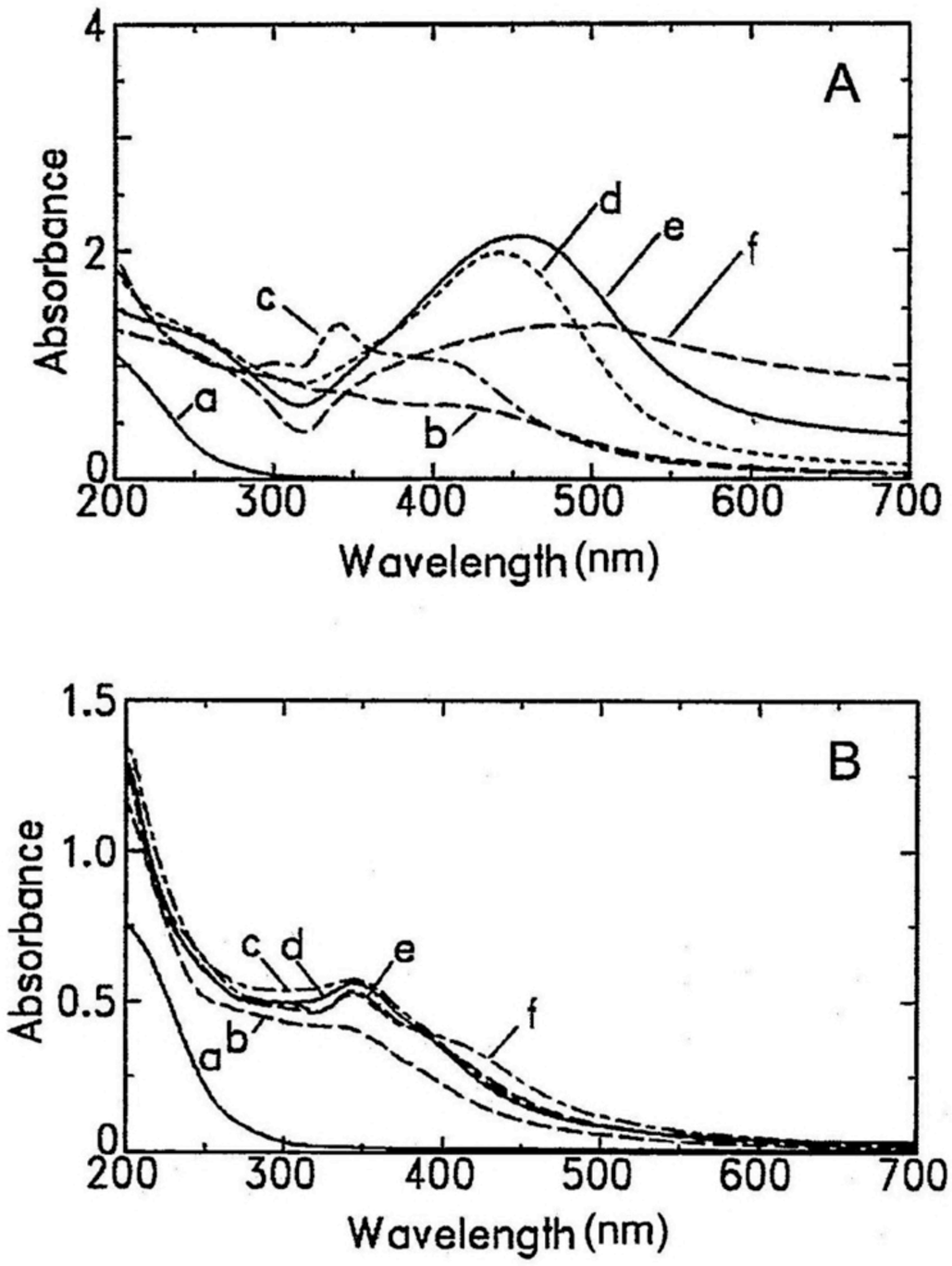

Figure 1-6. Variations of absorption spectra of the PMAAg film with UV irradiation. (A) Irradiation in wet air at room temperature. Irradiation time: (a) 0 min, (b) 2 min, (c) 10 min, (d) 180 min, (e) 600 min, (f) 40 h. (B) Irradiation in vacuum at liquid nitrogen temperature (a–c), followed by dark storage in vacuum at room temperature (d–f). Irradiation time: (a) 0 min, (b) 60 min, (c) 240 min. Dark storage time after 240-min of irradiation: (d) 30 min, (e) 60 min, (f) 20 h. (C) After introduction of air to sample B and dark storage at room temperature. Dark storage time: (a) 0 min, (b) 60 min, (c) 600 min.

The author has made a preliminary examination of photolysis of $AuCl_4^-$ ions in polyallylamine (Aldrich) films (PALAu films) and polylysine (Sigma) films (PLSAu films). Schematic structures of PAL and PLS are shown in Scheme 1-3(B) (C). Irradiation of the films with UV light in wet air at room temperature caused the formation of colloidal gold particles similar to the CTOAu film case. However, prolonged irradiation for 120–480 min did not form a clear gold mirror at both films surface. Absorption spectra of the PALAu film and the PLSAu film before and after UV irradiation are shown in Figure 1-7. Relatively low absorbance of both films would indicate the low conversion efficiency of $AuCl_4^-$ ions. The polymer matrix plays the roles not only of the protective agent of photolytic metal, but also of the reagent for photolysis. The predominance of the CMCAg and CTOAu films superior to the PMAAg, PALAu, and PLSAu films may be at least in part due to the presence of six-membered ring and higher reactivity of photoreduction of metal ions.

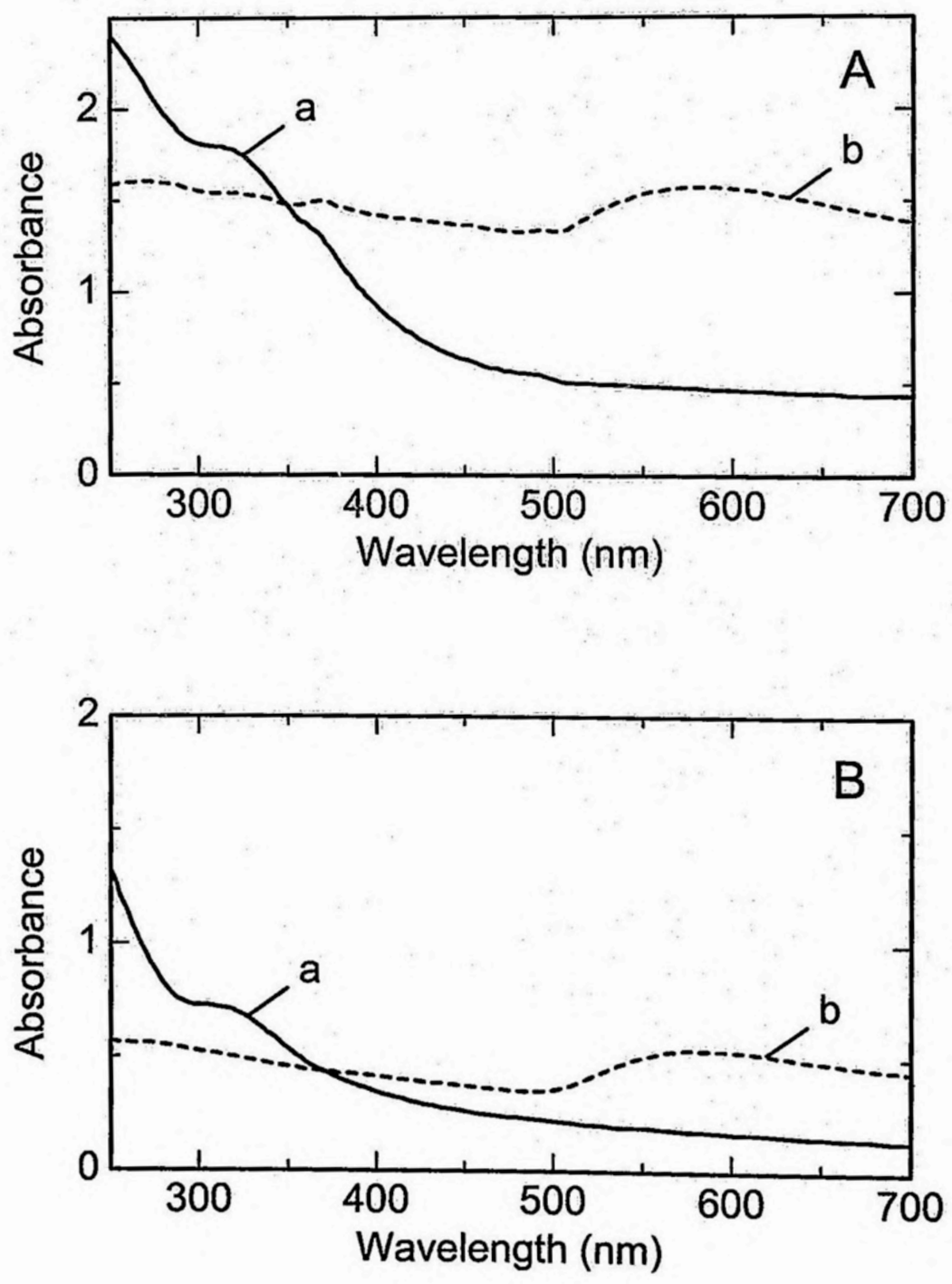

Figure 1-7. Variations of absorption spectra of the PALAu film (A) and PLSAu film (B) with UV irradiation in wet air at room temperature. Irradiation time: (A) (a) 0 min, (b) 480 min, and (B) (a) 0 min, (b) 120 min.

1.5 Summary

Thin films of CMCAg and CTOAu were photolyzed with 253.7-nm light under several reaction conditions. At room temperature in wet air, the irradiated surface of the films finally changed into clear silver or gold mirror. When the CMCAg film was photolyzed in vacuum at 77 K and then heated, 300 nm and 335 nm peaks overlapped with the structureless absorption appeared. These peaks are assigned to certain silver clusters. Although no distinct peaks were noticed in the CTOAu film photolyzed in vacuum at 77 K, heating the film until room temperature, followed by the introduction of air, brought about the development of colloidal absorption band of gold. These observations are indicative of migration and aggregation of metal atoms and clusters in the films. Considering the control of the aggregation state of photolytic metal by reaction conditions – from cluster to metal film –, metal salts of CMC and CTO are promising starting materials for matrix-supported metal particles.

1.6 Appendix: Photolysis in vacuum at room temperature

Absorption spectra of the CMCAg film and CTOAu film irradiated in vacuum at room temperature are shown in Figures 1-A1 and 1-A2, respectively.

Absorption band around 345 nm and broad peak around 360–400 nm developed with irradiation time, indicating the formation of silver particles less than several nm size [Figure 1-A1(A)]. After introduction of air, these bands were decreased and an increase of the colloidal absorption band around $\lambda = 400$–410 nm was noticed (B).

Absorption spectra of the CTOAu film after UV irradiation in vacuum at room temperature [Figure 1-A2(A)] is similar to that obtained when the film is photolyzed in vacuum at liquid nitrogen temperature [Figure 1-5(A)]. Also in the CTOAu film photolyzed in vacuum at room temperature, colloidal absorption band of gold around $\lambda = 560$–580 nm considerably developed after introduction of air [Figure 1-A2(B)]. These observations indicate that the role of moisture is very important for migration of metal atoms and clusters, forming larger colloidal particles and their aggregates in the CMCAg and CTOAu films.

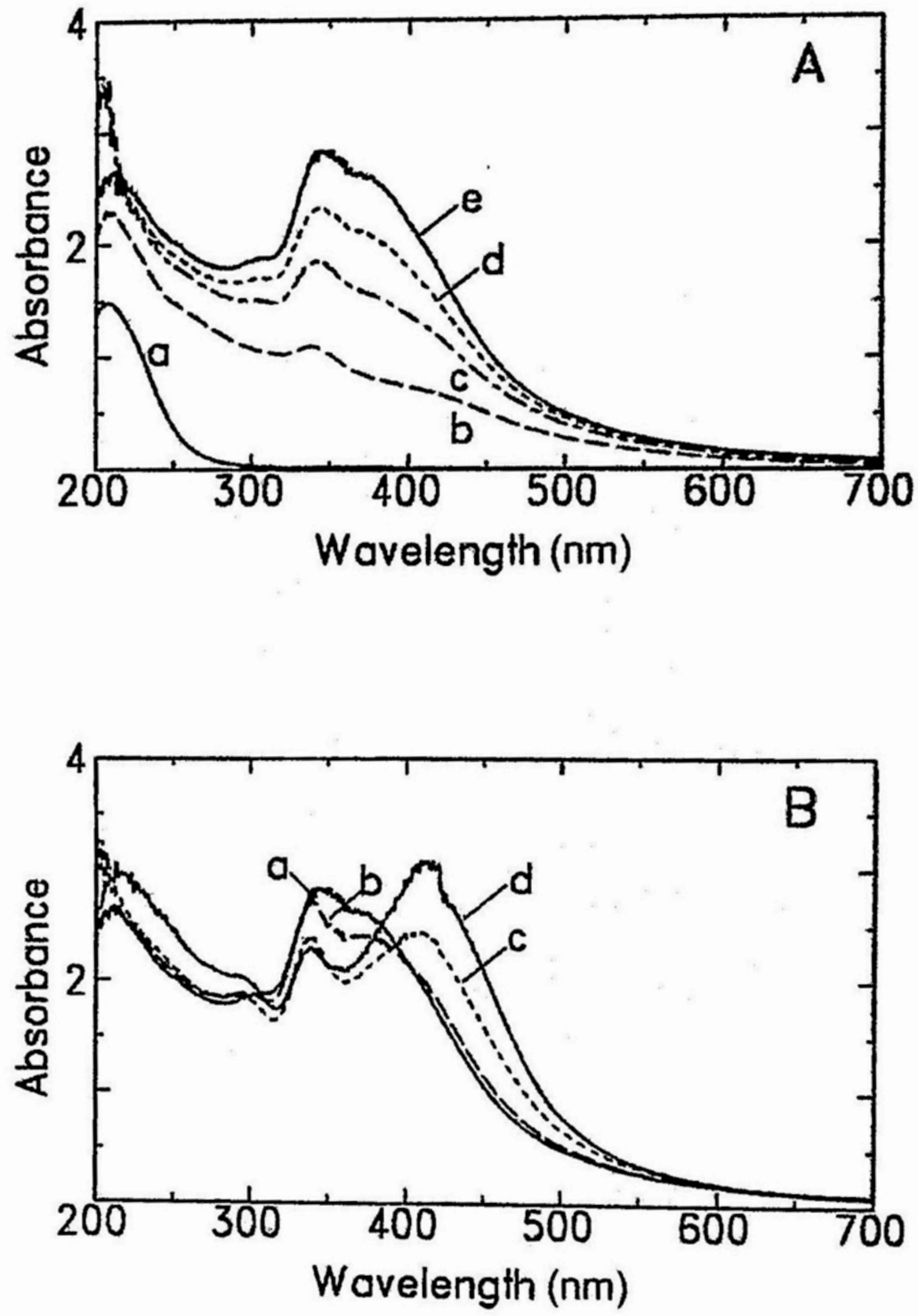

Figure 1-A1. Variations of absorption spectra of the CMCAg film with UV irradiation in vacuum at room temperature (A). Irradiation time: (a) 0 min, (b) 10 min, (c) 30 min, (d) 60 min, (e) 120 min. After introduction of air to sample A and dark storage at room temperature (B). Dark storage time: (a) 0 min, (b) 60 min, (c) 20 h, (d) 50 h.

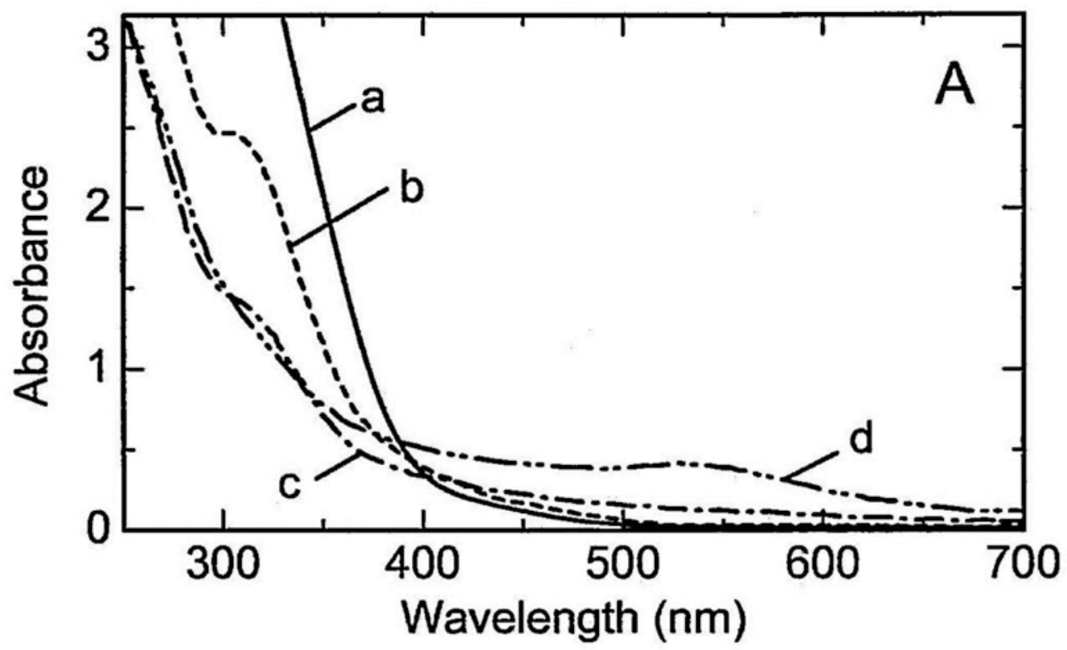

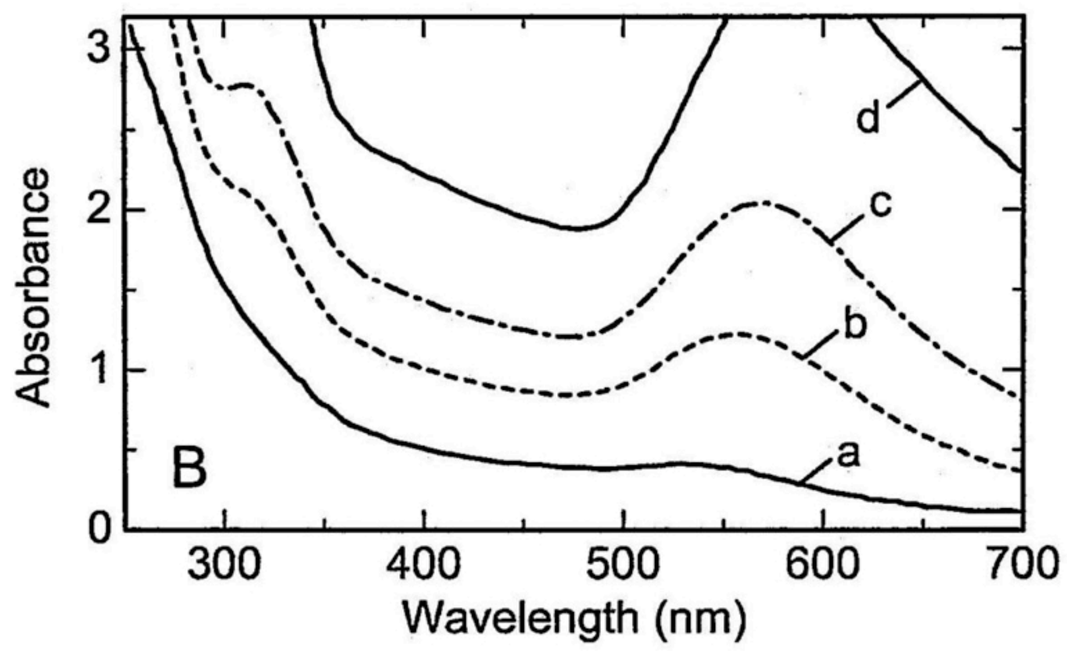

Figure 1-A2. Variations of absorption spectra of the CTOAu film with UV irradiation in vacuum at room temperature (A). Irradiation time: (a) 0 min, (b) 180 min, (c) 720 min, (d) 36 h. After introduction of air to sample A and dark storage at room temperature (B). Dark storage time: (a) 0 min, (b) 15 min, (c) 60 min, (d) 720 min.

References

1. J. V. Karabinos and M. Hindert, *Adv. Carbohydrate Chem.*, **9**, 285 (1954).
2. A. B. Foster and J. M. Webber, *Adv. Carbohydrate Chem.*, **15**, 371 (1960).
3. M. Yabuki, *Kichin Kitosan no Oyo (Applications of Chitin and Chitosan)*, Ed. by Chitin Chitosan Kenkyukai, Gihoudo Shuppan, Tokyo (1990).
4. N. Ishizuki, K. Torigoe, K. Esumi, and K. Meguro, *Colloids and Surfaces*, **55**, 15 (1991).
5. Y. Yonezawa, A. Takami, T. Sato, K. Yamamoto, T. Sasanuma, H. Ishida, and A. Ishitani, *J. Appl. Phys.*, **68**, 1297 (1990).
6. C. A. Parker, *Proc. R. Soc. Lond. A*, **220**, 104 (1953).
7. C. G. Hatchard and C. A. Parker, *Proc. R. Soc. Lond. A*, **235**, 518 (1956).
8. A. K. Gangopadhayay and A. J. Chakravorty, *J. Chem. Phys.*, **35**, 2206 (1961).
9. J. Turkevich, P. C. Stevenson, and J. Hillier, *Discuss. Faraday Soc.*, **11**, 55 (1951).
10. L. M. Liz-Marzan and A. P. Philipse, *J. Phys. Chem.*, **99**, 15120 (1995).
11. Y. Yonezawa, T. Sato, M. Ohno, and H. Hada, *J. Chem. Soc., Faraday Trans. 1*, **83**, 1559 (1987).
12. S. Fedrigo, W. Harbich, and J. Buttet, *Phys. Rev. B*, **47**, 10706 (1993).
13. S. Fedrigo. W. Harbich, and J. Buttet, *J. Chem. Phys.*, **99,** 5712 (1993).
14. D. G. Duff, A. Baiker, and P. P. Edwards, *Langmuir*, **9**, 2301 (1993).

Chapter 2

Aggregation of Photolytic Silver Nanoparticles at the Surface of Carboxymethylcellulose Films

2. 1 Introduction

Metal nanoparticles have been extensively studied because of their size-dependent physical and chemical properties.[1,2] Especially, metal nanoparticles embedded in solid matrices have attracted much attention with a view of technological applications to optical and optoelectronic devices as well as novel catalysts.[3–5] Carboxymethylcellulose (CMC), a typical derivative of cellulose, is an anionic polyelectrolyte soluble to water. Irradiation of the silver salt of CMC films, denoted as CMCAg films, with UV light caused photoreduction of Ag^+ ions, yielding silver nanoparticles. In Chapter 1, the control of the aggregation states of silver nanoparticles; atom, cluster, colloid, and bulk metal in the polymer matrix has been examined by changing reaction conditions. It has been proved that the prolonged irradiation of the CMCAg film in wet air at room temperature produced a clear silver mirror at the irradiated surface.

In this Chapter, the detailed surface characterization of the CMCAg films photolyzed with UV light in wet air at room temperature has been attempted. In Scheme 2-1, the structure formula of CMC and gross reaction scheme of photolysis of the CMCAg film are shown. As the author has focused on the precipitation of silver nanoparticles at the irradiated surface of the film, the surface characterization has been carried out with aids of high-resolution scanning electron microscopy and X-ray photoelectron spectroscopy (XPS).

(A)

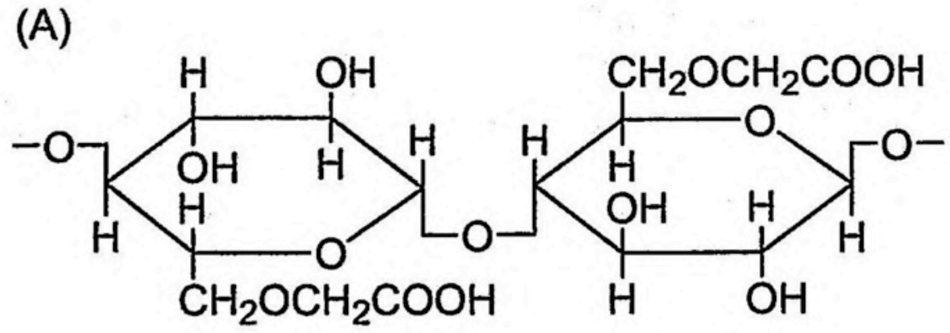

(B)

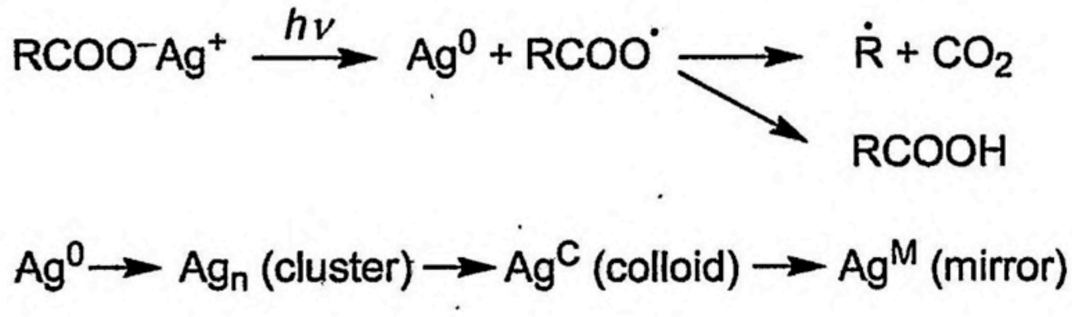

Scheme 2-1. Chemical structure of CMC (A) and gross of photochemical reactions in the CMCAg film (B).

2. 2 Experimental

2. 2. 1 Preparation

A 0.5 wt% aqueous solution of sodium salt of CMC (CMCNa) (Nacarai Tesque Co.) was spread on the quartz plate ($10 \times 30 \times 1$ mm^3) by the amount of 0.05 mL·cm^{-2}. The CMCNa film was dried and then immersed in 0.1 M (1 M = 1 mol·dm^{-3}) $AgNO_3$ solution for 60 min to substitute Na^+ to Ag^+. After washing with distilled water and drying in the dark, a clear and transparent CMCAg film was formed. Judging from the analysis of silver by atomic absorption spectrometry, the amount of Ag^+ ions per 1 cm^2 before photolysis was 0.64 μmol.[8] The thickness of the film fabricated in this manner was 1–5 μm. As the CMCAg film showed a broad absorption band that extended from the wavelength shorter than 200 nm to about 300 nm, the author employed 253.7-nm light as actinic light. The CMCAg film on the quartz plate was exposed to the 253.7-nm light from a 15-W sterilization lamp (Toshiba Co.) in the reaction chamber with a controlled temperature of 298–303 K and a relative humidity of 70–90%. The incident intensity of 253.7-nm light was monitored with the aid of a photometer, type IL-600 (International Light Co.). The number of incident photons as estimated by the ferrioxalate actinometer[11,12] was about 10^{17} cm^{-2}·min^{-1}.

2. 2. 2 Instrumentation

Absorption spectra of the films were recorded on a UV-visible spectrophotometer UV-260 (Shimadzu Co.). XPS measurements were made using a Shimadzu/Kratos AXIS-165 electron spectrometer with a monochromatic Al Kα X-ray radiation at 1486.6 eV. The power level of the Al Kα X-ray was 75 W for the wide scan and 105 W for the narrow scan. The pass energy was 80 eV. Neutralization by the low-energy flood gun with suitable conditions was performed to reduce the sample charging during the XPS measurements. The binding energies were calibrated by setting the lowest binding energy component of the C(1s) electron band to be 284.5 eV. This peak was attributed to the C-C fundamental structure of CMC and surface adventitious carbon.[13] The standard program supplemented to the AXIS-165 electron spectrometer enabled us to carry out the relative composition analysis of each element. The percent concentration of each element in the film was estimated from the relative peak area and sensitivity factor.[14] In the quantitative analysis, because the C(1s) and O(1s) bands are affected by the contamination due to carbon and certain organic substances, the error of the relative compositions of each element was 5–10%. The morphology of the films was examined by a high-resolution scanning electron microscope of the field emission type (FE-SEM), Hitachi

Model S-4500. A thin layer of Pt was deposited on the sample surface by sputtering. The accelerating voltage was 5 kV, and the electric current was 10 mA. To examine the cross section of the irradiated CMCAg film, the thick film of CMCAg (10–20 μm) was fabricated and irradiated with UV light for 600 min in wet air at room temperature. The irradiated film was peeled from the quartz plate and an appropriate section was cut and potted in the epoxy resin. The cross section was microtomed and provided to the transmission electron microscopy (TEM) observation. The measurement was made using a JEOL JEM-1200EX II transmission electron microscope with an accelerating voltage of 120 kV.

2. 3 Results and Discussion

2. 3. 1 Formation of silver nanoparticles by photolysis

When the CMCAg film was irradiated with UV light in wet air at room temperature, the film first became yellow-brown ~ dark-brown colored, indicating the formation of colloidal silver (irradiation time; t = 5–120 min). After a prolonged irradiation, the irradiated surface wore a metallic luster for about 180 min, and finally, it changed into a clear silver mirror (t = 600 min). The variation of absorption spectrum with irradiation time is given in Figure 2-1. Before irradiation, a broad absorption band less than 300 nm due to the electron transfer from $RCOO^-$ to Ag^+ ions was observed in the spectrum (a). On irradiation with 253.7-nm light, absorption bands at the wavelength shorter than 300 nm and $\lambda \sim$ 410 nm appeared, and developed with irradiation time (b, c). These bands are assigned to the photolytic silver.[6] In particular, the latter band is characteristic of colloidal silver. A small shoulder at 338 nm was

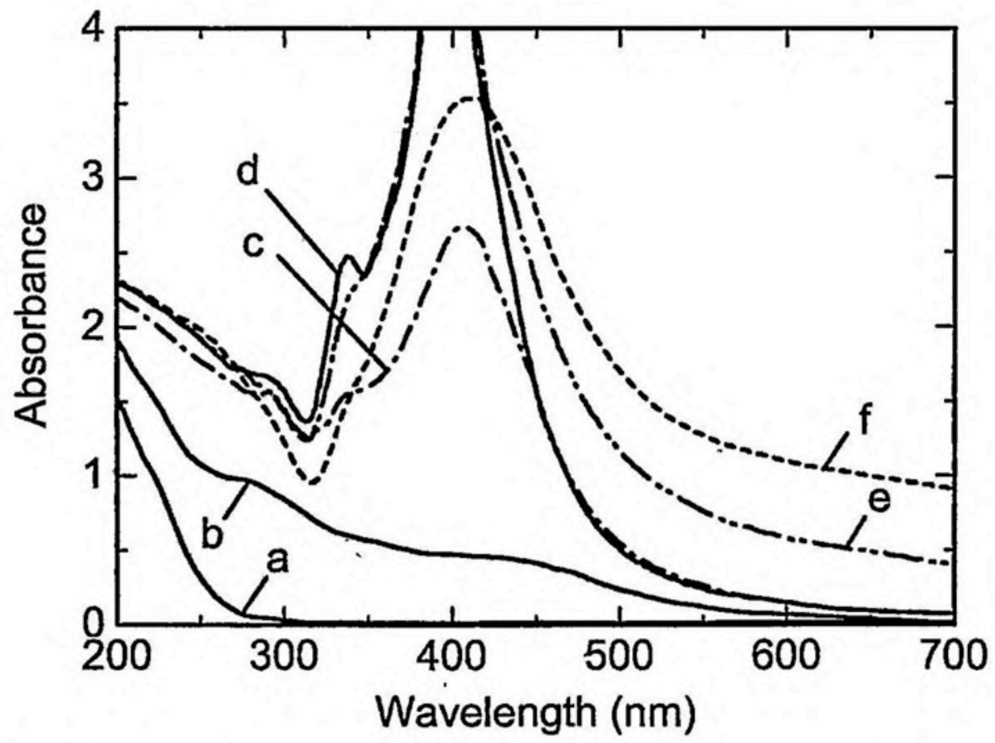

Figure 2-1. Absorption spectra of the CMCAg film before and after UV irradiation. Irradiation time: (a) 0 min, (b) 1 min, (c) 5 min, (d) 30 min, (e) 180 min, (f) 600 min.

noticed in the film irradiated for 5 min (c), which grew to a distinct peak after 30 min of irradiation (d). This peak is assigned to the silver clusters less than ~1 nm in size.[10] When irradiation was continued, the small peak at 338 nm was reduced (d), then colloidal absorption band ($\lambda \sim 410$ nm) gradually got broader, and the absorbance of the long-wavelength tail was increased (f). These observations indicate the growth and aggregation of colloidal silver particles.

2. 3. 2 Aggregation of silver nanoparticles at the film surface

Scanning electron micrographs of the CMCAg films before and after irradiation are shown in Figure 2-2. Before irradiation, the film surface looked smooth and silver nanoparticles were hardly observed in the whole surface (a). Photolysis for 30 min generated silver nanoparticles of 10–20 nm in size sparsely distributed at the surface (b). After 60 min of irradiation, the surface was covered with silver nanoparticles of relatively uniform size (c). When irradiation was continued, number density of silver nanoparticles was increased and the particles grew in size (d). Most particles were in spherical shape and the distribution of silver nanoparticles at the film surface was almost homogeneous. After 600 min of irradiation, the surface was densely covered with colloidal silver particles (e). The size distribution of the silver

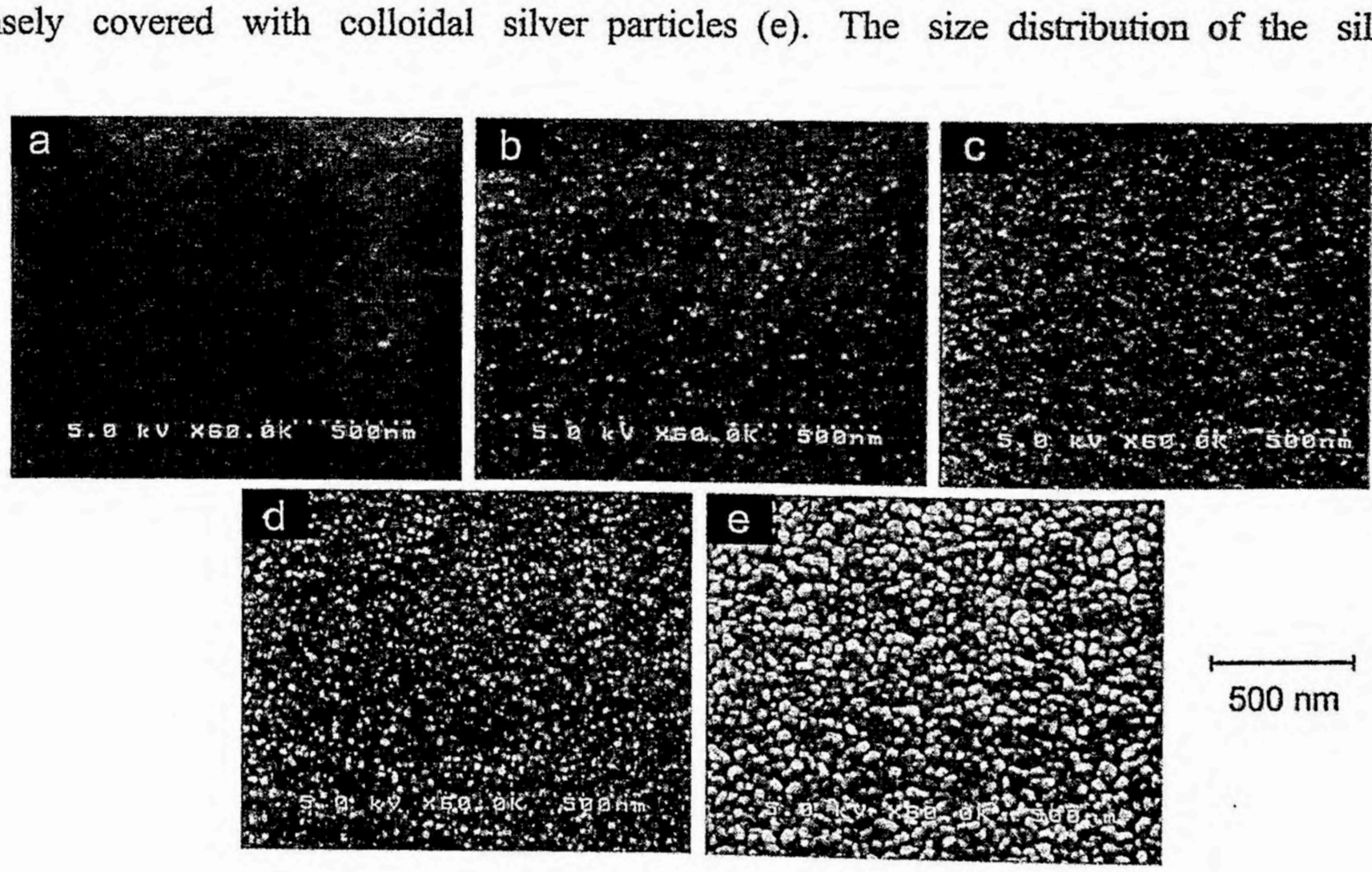

Figure 2-2. Scanning electron micrographs of the CMCAg film before and after UV irradiation. Irradiation time: (a) 0 min, (b) 30 min, (c) 60 min, (d) 180 min, (e) 600 min.

nanoparticles formed after varying the irradiation time is shown in Figure 2-3. More than 200 individual particles were counted to estimate the particle size distributions. The particle size distribution was somewhat broad for the irradiation of 30 min (b). The mean particle diameter was 13.4 nm. The silver particles grew in size with irradiation for 60–600 min (c–e). The mean particle diameters were 10.8 nm (60 min), 15.4 nm (180 min), and 33.3 nm (600 min), respectively. The temporal decrease of the mean particle diameter in Figure 2-3 (b, c) may imply the non-monotonous particle growth in the initial stage.

Figure 2-4 shows the change of the XPS wide-scan spectrum for the CMCAg film before and after UV photolysis. The peak intensity of each spectrum is normalized to the highest peak. In these spectra, the peaks of the C(1s), O(1s), Ag(3p), and Ag(3d) lines (marked by the dotted lines) were observed. While the relative intensities of the silver peaks [Ag(3p), Ag(3d)] were increased after 600 min of irradiation, the peak intensities of other elements were decreased. These observations would demonstrate the increase in the Ag concentration at the surface layer of several nm range; that is, precipitation of photolytic silver particles at the irradiated side of the film. XPS narrow scan spectra of each element were measured and used for detailed chemical composition analysis.

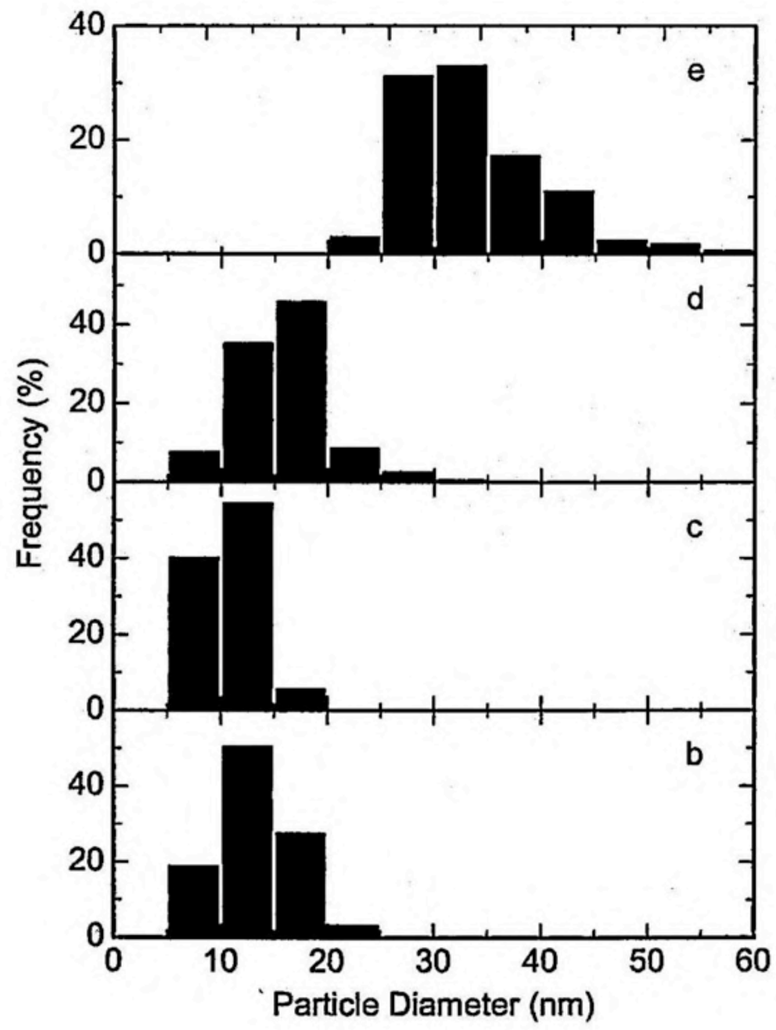

Figure 2-3. Particle size distributions of silver particles at the surface of the CMCAg film after UV irradiation. Irradiation time: (b) 30 min, (c) 60 min, (d) 180 min, (e) 600 min. As silver nanoparticles are hardly observed before irradiation, the figure (a) corresponding to (a) 0 min is omitted.

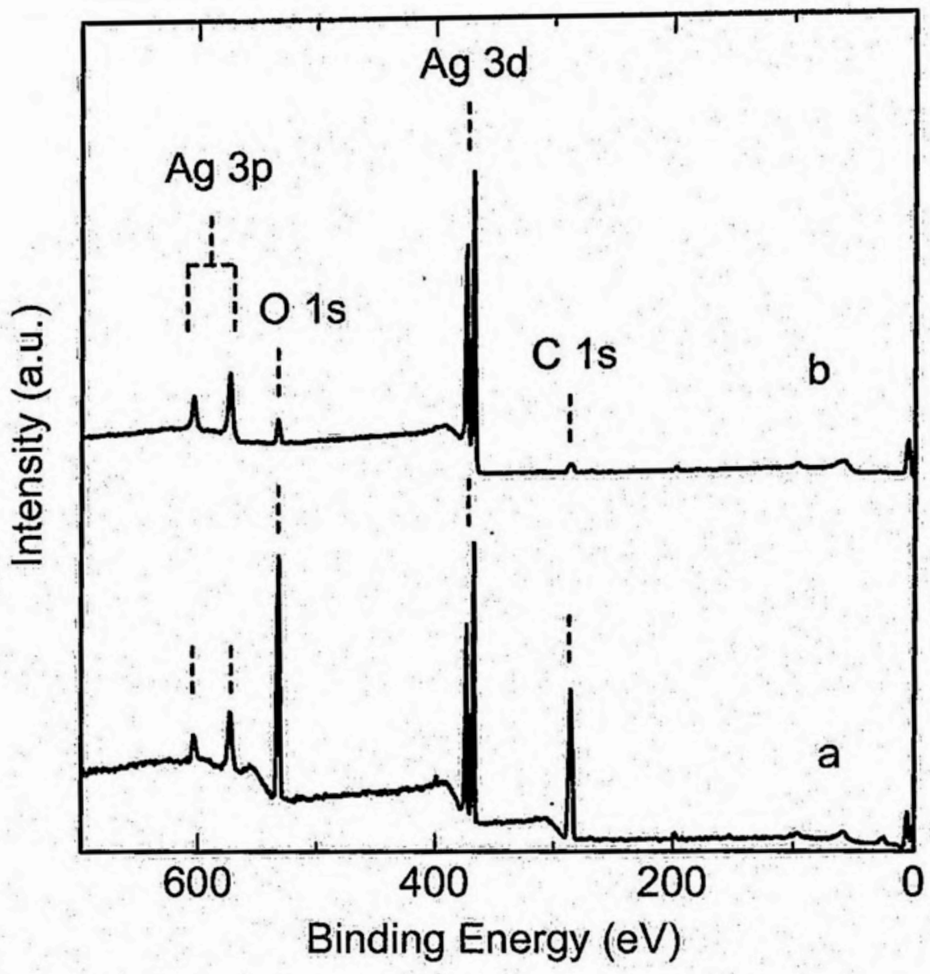

Figure 2-4. Wide-range XPS spectra of the CMCAg film before and after UV irradiation. Irradiation time: (a) 0 min, (b) 600 min. Dashed lines are a guide to the eyes.

The variation of the Ag($3d_{5/2}$) and Ag($3d_{3/2}$) lines of the XPS spectrum of the CMCAg film with UV irradiation is shown in Figure 2-5. The author has certified that the spectral line shape of the XPS does not change so much in course of the measurements (about 60 sec per 1 element of the specimen). Before irradiation (a), two lines for Ag($3d_{5/2}$) (368.0 eV) and Ag($3d_{3/2}$) (374.0 eV) assigned to Ag^+ ions were observed.[13] The author has focused on the peak position and the full width of half-maximum (FWHM) of the Ag($3d_{5/2}$) line. The peak was gradually shifted to higher binding energy (368.1–368.4 eV) with UV irradiation. Furthermore, the band width was somewhat decreased from 1.6 eV to 1.3 eV with irradiation time. The variations of the core binding energy and FWHM of the Ag($3d_{5/2}$) line with irradiation time are plotted in Figure 2-6. The peak position after more than 180 min of irradiation is accord with the literature value of bulk silver (368.3 ± 0.1 eV).[13] The author has observed that the core binding energy of Ag($3d_{5/2}$) band for Ag^+ ions is 0.3 eV lower and the FWHM of Ag^+ ions is 0.3 eV larger than those of bulk silver, respectively. The gradual changes of the peak position and FWHM observed in 0–180 min of irradiation seem to be responsible for the conversion of Ag^+ ions to silver metals. These results would suggest that Ag^+ ions at the film surface almost disappear after more than 120–180 min of irradiation. Therefore, the increase in Ag concentration after prolonged irradiation is nothing but the increase of photolytic silver at the surface layer.

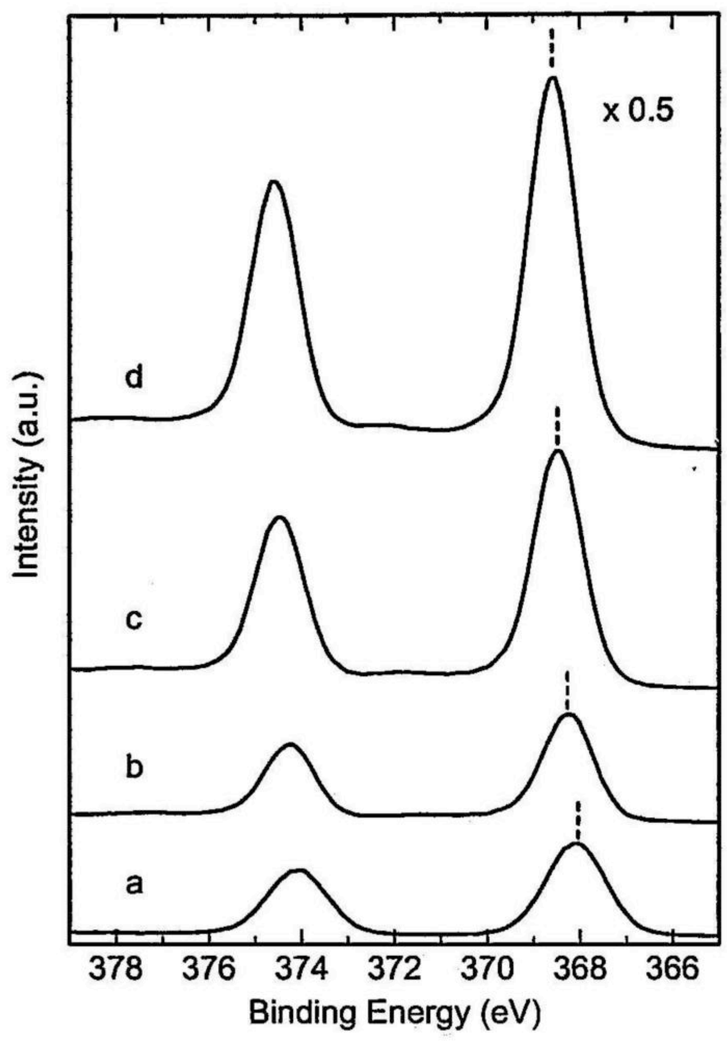

Figure 2-5. XPS spectra in the Ag(3d) region for the CMCAg film before and after UV irradiation. Irradiation time: (a) 0 min, (b) 60 min, (c) 120 min, (d) 600 min. Dashed lines are a guide to the eyes.

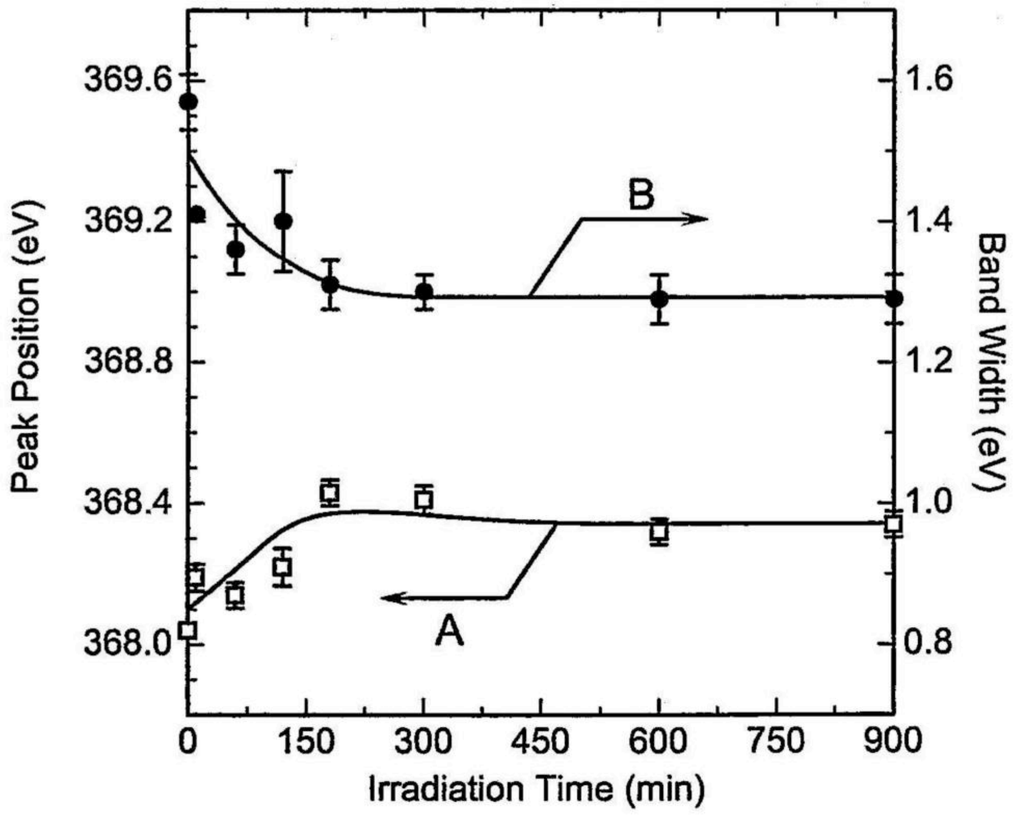

Figure 2-6. Changes of the peak position (A) and FWHM (B) of Ag($3d_{5/2}$) line in the XPS spectrum of the CMCAg film with UV irradiation.

The dependence of the core binding energy of the metal clusters on size has been studied by many groups. Mason reported that the core binding energy of supported silver clusters on the carbon substrate is about 0.4 eV larger than that of bulk silver.[15] However, the author did not

detect such higher energy shift of the Ag(3d) core binding energy from bulk silver in the irradiated CMCAg film. Furthermore, a direct evidence of the existence of silver atoms and small clusters was difficult to obtain by the FE-SEM employed in this study because of the resolution limit of about 5 nm. These results may indicate that the lifetime of small silver clusters at the film surface would be very short. On the other hand, in the UV-visible absorption spectrum of the CMCAg film irradiated for 5–30 min, a 338 nm absorption peak assigned to silver clusters was noticed [Figure 2-1(c, d)]. This result indicates that small silver clusters exist at least inside of the film at the early stage of photolysis.

Detailed chemical composition analysis was attempted with the help of the peak area and sensitivity factor of the XPS spectra. Figure 2-7 shows the XPS spectra of the C(1s) and O(1s) regions. Variations of atomic concentrations of carbon, oxygen, and silver (sum of Ag^+ ions and reduced silver) with irradiation time are plotted in Figure 2-8(I). The total Ag percentage was increased with the irradiation time (C), while the atomic concentrations of other elements (carbon and oxygen) were decreased in return (A, B). Variations of mass concentration (wt%) of each element are added in Figure 2-8(II) for convenience sake. The increase in the Ag concentration clearly indicates that silver atoms and clusters can migrate inside the film and precipitate at the irradiated side of the film surface, yielding stable silver nanoparticles.

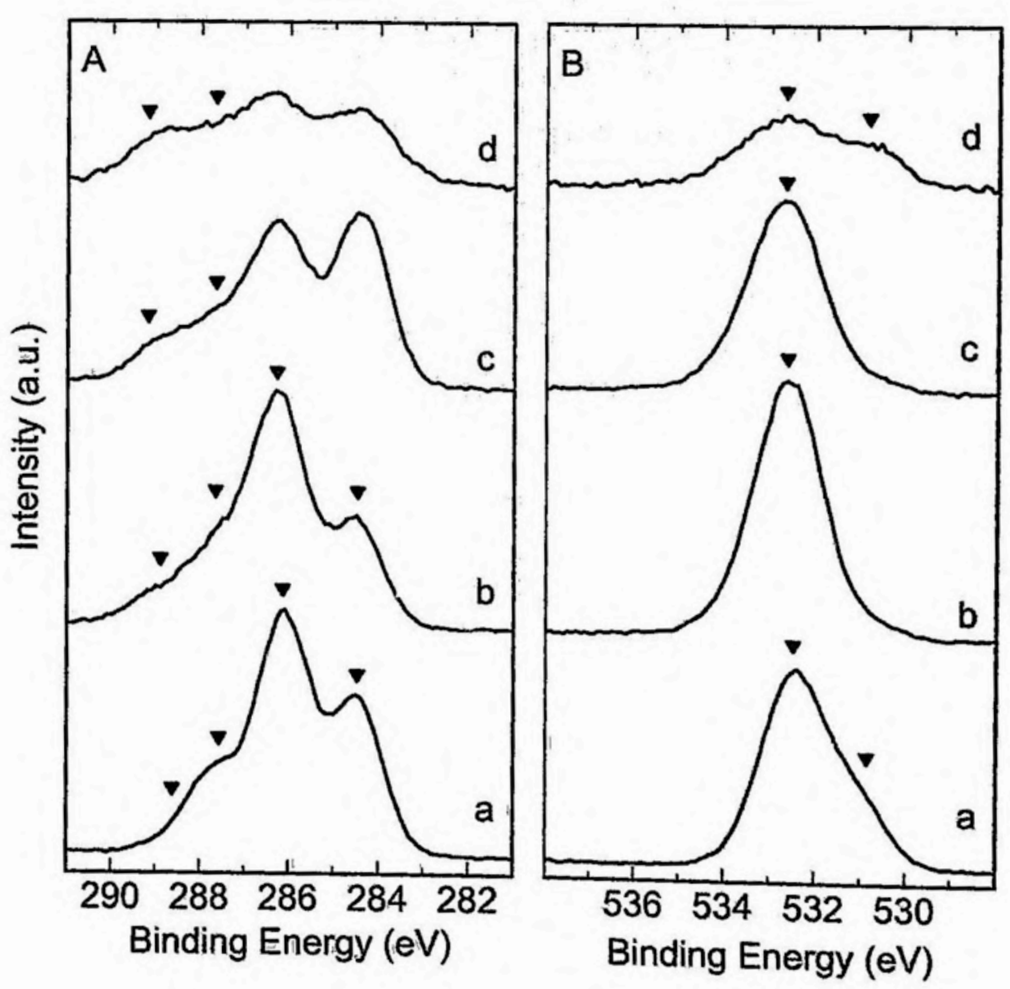

Figure 2-7. XPS spectra in the regions of C(1s) (A) and O(1s) (B) for the CMCAg film before and after UV irradiation. Irradiation time: (a) 0 min, (b) 60 min, (c) 120 min, (d) 600 min. (▼) Peak position of the noticeable component of each element.

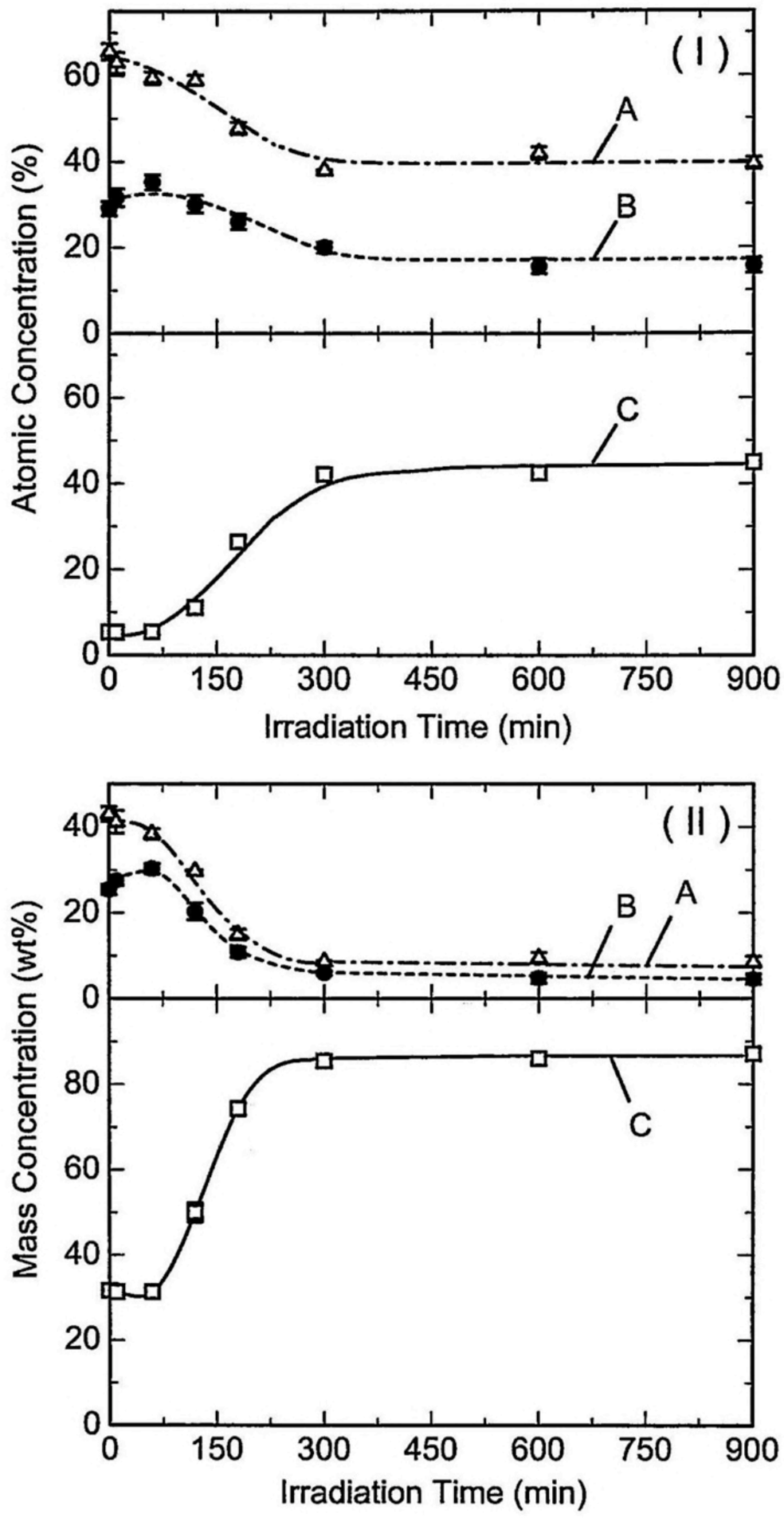

Figure 2-8. Changes of atomic concentration (I) and mass concentration (II) of the elements at the surface of the CMCAg film with UV irradiation. (A) carbon, (B) oxygen, (C) silver.

The author has confirmed that the diffraction line of the (111) face of the face-centered cubic silver lattice is evident in the X-ray diffraction profile of the CMCAg film photolyzed for longer than 360 min in Chapter 1. The author has also measured the change of direct current (DC) electrical resistance, R Ω, of the irradiated surface. Before UV irradiation, R was larger than 10^{10} Ω. After formation of the clear silver mirror, that is, after 600 min of irradiation, R was decreased to 10^2–10^3 Ω. Even after the formation of the silver mirror, 55 atomic % (13

wt%) organic components still remained at the film surface (Figure 2-8). Accordingly, it is reasonable that the silver nanoparticles and thin films would be partly covered with an ultra-thin layer of CMC and degraded CMC. Such an assumption is not inconsistent with a relatively large DC resistance of the CMCAg mirror compared with that of the bulk silver film.

The author has tried a preliminary observation of the cross section of the irradiated CMCAg film. Figure 2-9 shows TEM micrographs of the cross section. A silver layer comprising of densely packed silver nanoparticles was seen whose thickness is ca. 100 nm. The micrograph

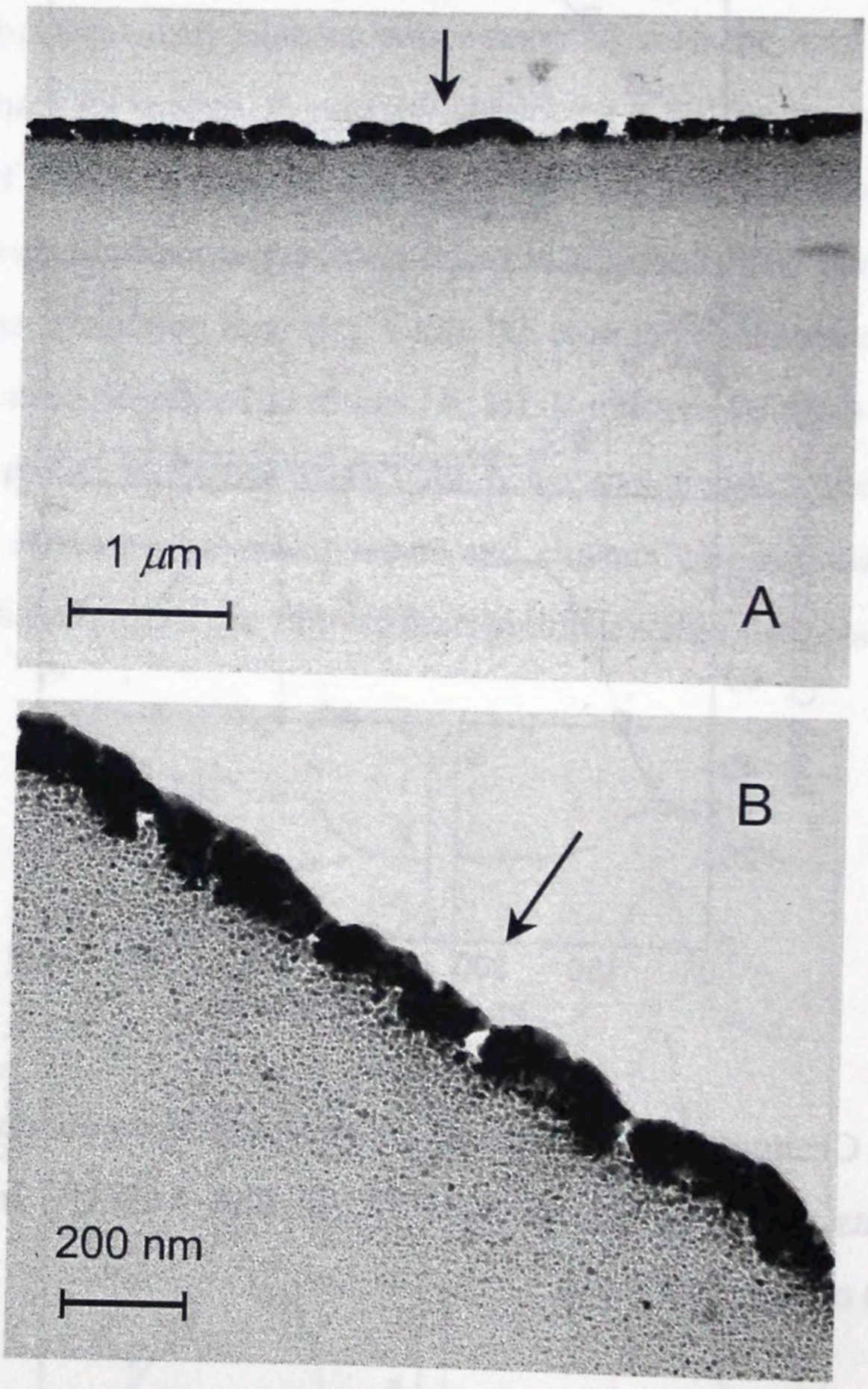

Figure 2-9. Transmission electron micrographs of a cross section of the CMCAg film irradiated for 600 min. (A) Lower magnification micrograph. The arrow is the direction of incident light for photolysis. (B) Enlarged micrograph of A.

directly reconfirms a tendency that the photolytic silver nanoparticles would precipitate at the irradiated side of the film. The author has also noticed in the enlarged micrograph (B), that the silver nanoparticles less than 5 nm are sparsely distributed inside the film. Accordingly, the author can suggest that silver atoms and small clusters can migrate inside the film under present reaction condition. Migration of silver atoms and clusters to the surface of polymer films under illumination has been reported by Bokhonov et al.[16] and by Korchev et al.[17] According to the former works on photolysis of silver alginate films,[7,18] it has been assumed that the amount of photolytic silver is decreased when the reaction chamber is either evacuated or filled with dry air. Furthermore, the formation of a clear silver mirror in the CMCAg film was suppressed by evacuation as shown in Chapter 1. Water molecules contained in the film would facilitate the segmental motions of the polymer and promote migration of silver atoms and clusters. Silver nanoparticles produced at the surface could play a role of the concentration center, which continue growing with a supply of silver atoms and clusters from inside the film. These are the reasons the silver particulate film and the silver mirror are formed at the irradiated side of the surface. Yonezawa & Kijima have examined the growth mechanism of thin silver films on the basis of the diffusion of small silver particles in silver alginate films.[19] Because excess Ag^+ ions were carefully removed from the CMCAg film and the silver alginate films, the contribution of the diffusion of the Ag^+ ions would be not so important as that of silver atoms and clusters. These results have demonstrated that CMC is an effective matrix for the fabrication of the densely packed silver particulate films in fairly mild conditions.

2. 3. 3 Mechanism of photochemical reaction of CMCAg

The author has found that photolytic silver nanoparticles form the densely packed particulate film at the irradiated surface of the CMCAg film. The author will discuss some details of the mechanism of photochemical reactions of the CMCAg [Scheme 2-1(B)] with the aids of XPS[13,20] and IR absorption spectroscopy. In Figure 2-7(A), major peaks were observed at 284.5 eV (C-C; fundamental structure of polymer), 286.1–286.2 eV (C-OH of pyranose ring, C-O-C of carboxymethyl group), 287.6 eV (O-C-O of pyranose ring), and 288.6–289.0 eV (O-C=O of carboxylate) in the XPS spectra of the CMCAg film before irradiation (a) and after 60 min of irradiation (b). After more than 120 min of irradiation (c, d), the broad bands due to carbonyl carbon (C=O) and carboxylic carbon (O-C=O of carboxylic acid) produced by the photooxidation of pyranose ring became evident in the range of 287.5–289.2 eV. The major peak of O(1s) around 532.5 eV was noticed in Figure 2-7(B). This peak originates from C-OH

and C-O-C of pyranose ring and C-O-C of carboxymethyl group. A small shoulder around 530.8 eV was also noticed which is assigned to O-C=O of carboxylate before irradiation (a). After 60–120 min of irradiation (b, c), the carboxylate peak at 530.8 eV tended to decrease probably due to the elimination of carbon dioxide from the surface carboxylate ions of the CMCAg [Scheme 2-1(B)]. After 600 min of irradiation (d), the peak around 530.8 eV appeared, which would be assigned to certain carbonyl compounds (C=O) and carboxylic acids (RCOOH) formed by photooxidation of the pyranose ring.

To get further insight into the reaction scheme, IR absorption spectra of the CMCAg films peeled from the quartz plate were recorded on a Shimadzu Fourier transform infrared spectrometer 4100 (Figure 2-10). Here, we should note that IR absorption spectra would reflect the bulk properties, while XPS analysis may afford the information of surface region of the film. In Figure 10(a), the IR spectrum of the CMCAg film before irradiation exhibited two characteristic absorption bands arising from the $RCOO^-$ structure at 1575 cm^{-1} (anti-symmetrical stretching vibration) and 1415 cm^{-1} (symmetrical stretching vibration). After UV irradiation (b), the relative intensities of those bands were decreased and a new peak at 1720 cm^{-1} and a small shoulder around 1240 cm^{-1} developed. These bands are assigned to carbonyl

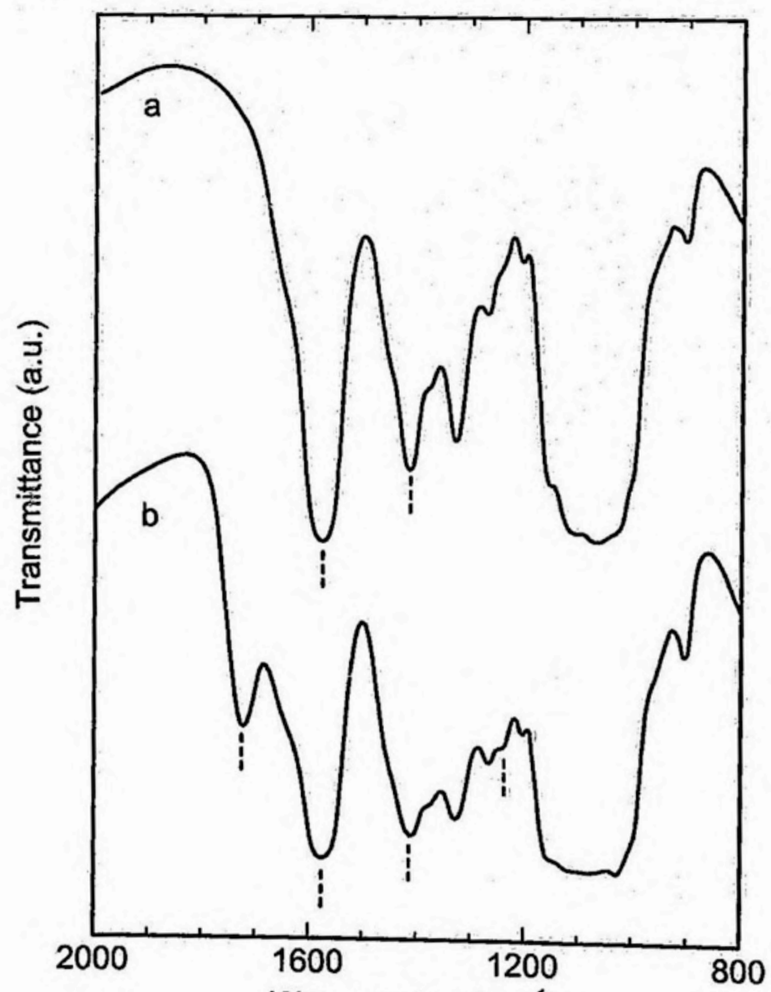

Figure 2-10. IR absorption spectra of the CMCAg film before and after UV irradiation. Irradiation time: (a) 0 min, (b) 180 min. Dashed lines are a guide to the eyes.

compounds (C=O) and carboxylic acids (RCOOH), which are produced by photolysis. These observations are on the whole consistent with the behavior of the C(1s) and O(1s) bands in the XPS spectra. The photochemical reactions in the CMCAg film are initiated by one-electron transfer from the carboxylate ion to the bound Ag^+ ion, giving rise to silver atoms [Scheme 2-1(B)]. The carboxy radical (RCOO·) either decomposes into a secondary radical (R·) and CO_2 or is converted to carboxylic acid (RCOOH) as a result of hydrogen abstraction from the C-H bond of the polymer chain. Some of the remaining radicals would be oxidized by O_2, yielding final products such as carbonyl compounds of CMC.

2. 4 Summary

Thin films of CMCAg were photolyzed with 253.7-nm light in wet air at room temperature. Detailed XPS and FE-SEM studies on the silver nanoparticles have been carried out. Surface composition analysis by XPS has been proved to be helpful to examine the mechanism of formation and growth of silver nanoparticles at the film surface, as well as photochemical reactions of the CMCAg. FE-SEM observations have demonstrated the change of the average particle size of the silver nanoparticles, from about 11 nm to 33 nm during 30–600 min of irradiation. The concentration of total silver (Ag^+, Ag) at the surface layer was increased from 5.4 atomic % (31.6 wt%) before irradiation to 45.0 atomic % (87.0 wt%) after 600 min of irradiation indicating that silver atoms and clusters can migrate inside the film and precipitate at the irradiated surface. Those results are consistent with the FE-SEM and TEM observations. The mechanism of photochemical reactions has been discussed on the basis of the C(1s) and O(1s) bands of the XPS spectra, together with the IR absorption spectra of the CMCAg film before and after photolysis.

References

1. D. L. Feldheim and C. A. Foss, Jr., *Metal Nanoparticles: Synthesis, Characterization and Applications.*, Marcel Dekker, New York (2002).
2. V. P. Kamat, *J. Phys. Chem. B*, **106**, 7729 (2002).
3. A. Heilmann, *Polymer Films with Embedded Metal Nanoparticles*, Springer, Berlin (2002).
4. Y. Gotoh, T. Kanno, Y. Fujimori, Y. Ohkoshi, M. Nagura, K. Akamatsu, and S. Deki, *Poly. J.* **35**, 960 (2003).
5. Z. H. Mbhele, M. G. Salemane, C. G. C. E. van Sittert, J. M. Nedeljković, V. Djoković, and A. S. Luyt, *Chem. Mater.*, **15**, 5019 (2003).

6. Y. Yonezawa, A. Takami, T. Sato, K. Yamamoto, T. Sasanuma, H. Ishida, and A. Ishitani, *J. Appl. Phys.*, **68**, 1297 (1990).
7. Y. Yonezawa, M. Kijima, and T. Sato, *Ber. Bunsen-Ges. Phys. Chem.*, **96**, 1828 (1992).
8. Y. Yonezawa, N. Kometani, M. Seki, T. Sakagami, H. Tanaka, S. Koyanagi, and T. Miyama, *Trans. Mater. Res. Soc. Jpn.*, **27**, 197 (2002).
9. G. A. Gaddy, J. L. McLain, E. S. Steigerwalt, R. Broughton, B. L. Slaten, and G. Mills, *J. Cluster Sci.*, **12**, 457 (2001).
10. A. V. Loginov, V. V. Gorbunova, and T. B. Boitsova, *J. Nanopart. Res.*, **4**, 193 (2002).
11. C. A. Parker, *Proc. R. Soc. Lond. A*, **220**, 104 (1953).
12. C. G. Hatchard and C. A. Parker, *Proc. R. Soc. Lond. A*, **235**, 518 (1956).
13. N. Ikeo, Y. Iijima, N. Niimura, M. Sigematsu, T. Tazawa, S. Matsumoto, K. Kojima, and Y. Nagasawa, *Handbook of X-ray Photoelectron Spectroscopy*, JEOL, Tokyo (1991).
14. C. D. Wagner, L. E. Davis, M. V. Zeller, J. A. Taylor, R. H. Raymond, and L. H. Gale, *Surf. Interface Anal.*, **3**, 211 (1981).
15. M. G. Mason, *Phys. Rev. B*, **27**, 748 (1983).
16. B. B. Bokhonov, L. P. Burleva, D. R. Whitcomb, and Yu. E. Usanov, *J. Imaging Sci. Technol.*, **45**, 259 (2001).
17. A. S. Korchev, M. J. Bozack, B. L. Slaten, and G. Mills, *J. Am. Chem. Soc.*, **126**, 10 (2004).
18. Y. Konishi, H. Hada, and M. Tamura, *J. Chem. Soc. Jpn.*, **86**, 1132 (1965).
19. Y. Yonezawa and M. Kijima, *J. Soc. Photogr. Sci. Technol. Jpn.*, **56**, 3 (1993).

Chapter 3

Aggregation of Photolytic Gold Nanoparticles at the Surface of Chitosan Films

3. 1 Introduction

Metal nanoparticles have attracted considerable attention because of their optical, electronic, and chemical properties that are size-dependent.[1,2] With a view of technological applications of metal nanoparticles to novel optoelectronic devices[2] and electronic devices[2] as well as imaging materials,[3,4] it would be important to incorporate those particles into solid matrices, for example, polymers, glasses, and ceramics. Recently, there have been many reports on metal nanoparticles in various polymer matrices.[5–7]

In this thesis, the author has studied the photochemical formation of metal nanoparticles in the films of polysaccharides and their derivatives such as alginic acid, carboxymethylcellulose, and chitosan (CTO).[8,9] In Chapter 1, the control of the aggregation state of metal nanoparticles has been examined by changing reaction conditions.[9–11] An important aspect of those reactions is that photolytic silver and gold have a tendency to precipitate on the irradiated side of the film, when these metal salt films are photolyzed in wet air.

In this Chapter, the author has focused on aggregation of photolytic gold nanoparticles in the films of chloroauric acid salt of CTO (CTOAu films) to explore the photoinduced precipitation of gold nanoparticles at the film surface. In this system, it is interesting that various states of metal, from ion to atom, cluster, colloid, and bulk metal, are formed during the

(A)

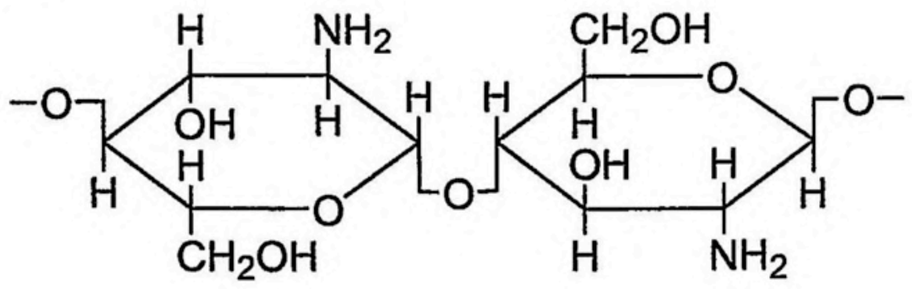

(B)

$$RNH_3^+AuCl_4^- \xrightarrow{h\nu} Au^0 + RNH_3^+Cl^- + 3\dot{C}l$$

$$Au^0 \rightarrow Au_n\ (\text{cluster}) \rightarrow Au^C\ (\text{colloid}) \rightarrow Au^M\ (\text{mirror})$$

Scheme 3-1. Chemical structure of CTO (A) and gross of photochemical reactions in the chitosan-$AuCl_4^-$ (CTOAu) film.

reaction. In Chapter 1, the author has noted that the quality of thin gold films is sensitive to temperature and humidity during the photolysis of the CTOAu films in air. The formation of gold films was suppressed by evacuation. In Scheme 3-1, the structure formula of CTO and gross reaction of photolysis of the CTOAu film are shown. In this Chapter, the detailed surface characterization has been carried out by means of high-resolution scanning electron microscopy and X-ray photoelectron spectroscopy (XPS).

3. 2 Experimental

3. 2. 1 Preparation

CTO was purchased from Wako Pure Chemical Industries, Ltd. The degree of deacetylation was about 80%. A 0.5 wt% solution of CTO in 1 vol% acetic acid was spread on the quartz plate ($10 \times 30 \times 1$ mm^3) by the amount of 0.05 mL·cm^{-2}. The CTO film was dried and then immersed in 0.01 M (1 M = 1 mol·dm^{-3}) $HAuCl_4$ solution for 60 min to prepare the chloroauric acid salt of CTO. The amount of $AuCl_4^-$ per 1 cm^2 as determined by atomic absorption spectrometry was about 1.2 μmol when the time of immersion was longer than 30 min. After washing with distilled water and drying in the dark, a light-yellow and transparent CTOAu film was formed, whose thickness was 1–5 μm. The CTOAu film on the quartz plate was exposed to 253.7-nm light from a 15-W sterilization lamp (Toshiba Co.) in the reaction chamber with a controlled temperature of 298–303 K and a relative humidity of 70–85%.

3. 2. 2 Instrumentation

Absorption spectra of the films were recorded on a UV-visible spectrophotometer V-560 (JASCO Co.). The bandwidth of the detector was 2 nm. Surface characterization of the CTOAu films was performed as the same way as Chapter 2. The morphology of the films was examined by a high-resolution scanning electron microscope of the field emission type (FE-SEM), Hitachi model S-4500. A thin layer of Pt was deposited on the film surface by sputtering. XPS measurements were made using a Shimadzu/Kratos AXIS-165 electron spectrometer with a monochromatic Al Kα X-ray radiation at 1486.6 eV. Neutralization by the low-energy flood gun with suitable conditions was performed to diminish the sample charging during the XPS measurements. The binding energies were calibrated by setting the lowest binding energy component of the C(1s) electron band to be 284.5 eV. This peak was assumed to originate from the C-C component of CTO and surface adventitious carbon. The binding energy of the C(1s) peak for adventitious carbon and the Au($4f_{7/2}$) peak for the bulk gold film

were 284.5 eV and 84.0 eV, respectively. The standard program supplemented to the AXIS-165 electron spectrometer enabled us to carry out the data processing: deconvolution of the XPS spectra by curve fitting with Gaussian-type profiles and evaluation of the peak area, as well as relative composition analysis of each element. The percent concentration of each element in the film was estimated from the relative peak area and sensitivity factor.[12] In the quantitative analysis, because the C(1s) and O(1s) bands are affected by the contamination due to carbon and certain organic substances, the error of the relative compositions of each element was 5–10%.

3. 3 Results

3. 3. 1 Formation of gold nanoparticles by photolysis

When the CTOAu film was irradiated with UV light in wet air at room temperature, the film maintained the original color for the first 10 min and then became blue-violet colored, indicating the formation of colloidal gold (irradiation time; t = 15–20 min). After a prolonged irradiation, the irradiated surface wore a metallic luster for about 40–60 min, and, finally, it changed into a clear gold mirror (t = 120 min). The variation of absorption spectra with irradiation time is given in Figure 3-1. Before irradiation, strong absorption less than λ = 400 nm due to the ligand-to-metal charge transfer (LMCT) band ($\lambda \sim$ 315 nm)[13] was observed in the spectrum (a). On irradiation, the LMCT band was decreased (b). After 30 min of irradiation, the colloidal absorption band of gold appeared around λ = 560–570 nm, and at the same time, the shorter-wavelength band (λ < 400 nm) began to develop (c). The author has assumed that

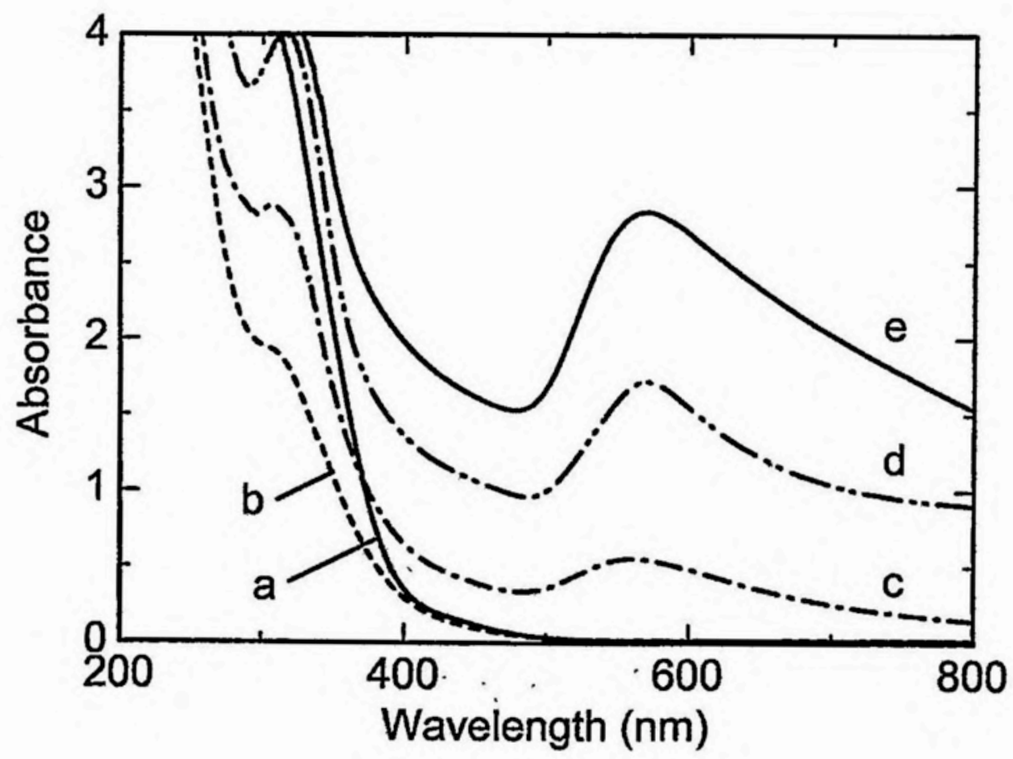

Figure 3-1. Absorption spectra of the CTOAu film before (a) and after UV irradiation. Irradiation time: (a) 0 min, (b) 10 min, (c) 30 min, (d) 60 min, (e) 120 min.

an initial decrease of the absorption band $\lambda < 400$ nm reflects the decrease of the $AuCl_4^-$ ions. The formation of photolytic gold causes the increase of absorbance at these wavelength regi The colloidal absorption band got broader, and the absorbance of the long-wavelength tail was increased (d).[14,15] Further, the interband transition (5d–6s, 6p) in the shorter wavelength region became evident, indicating the formation of the bulk gold film (e).[16,17]

Scanning electron micrographs of the CTOAu film before and after irradiation are shown in Figure 3-2. Before irradiation, the surface looked smooth (a). Photolysis for 10 min generated gold particles about 10 nm in size sparsely distributed at the film surface (b). When irradiation was continued, gold nanoparticles grew in size and number density was increased (c, d). The distribution of gold nanoparticles at the film surface was almost homogeneous. Most particles are regarded as the spherical shape. Some particles formed in the 20–40-min irradiated films are faceted with various shapes as triangular, hexagonal, and others. After 120 min of irradiation, the film surface was densely covered with colloidal gold particles (e). The size distribution of the gold particles formed after varying the irradiation time is shown in Figure 3-3. More than 300 individual particles were counted to determine the distributions regarding that they were in spherical shape. The mean particle diameter was 13 nm for 10 min of irradiation, 30 nm for 20 min of irradiation, 49 nm for 40 min of irradiation, and 50 nm for 120 min of irradiation.

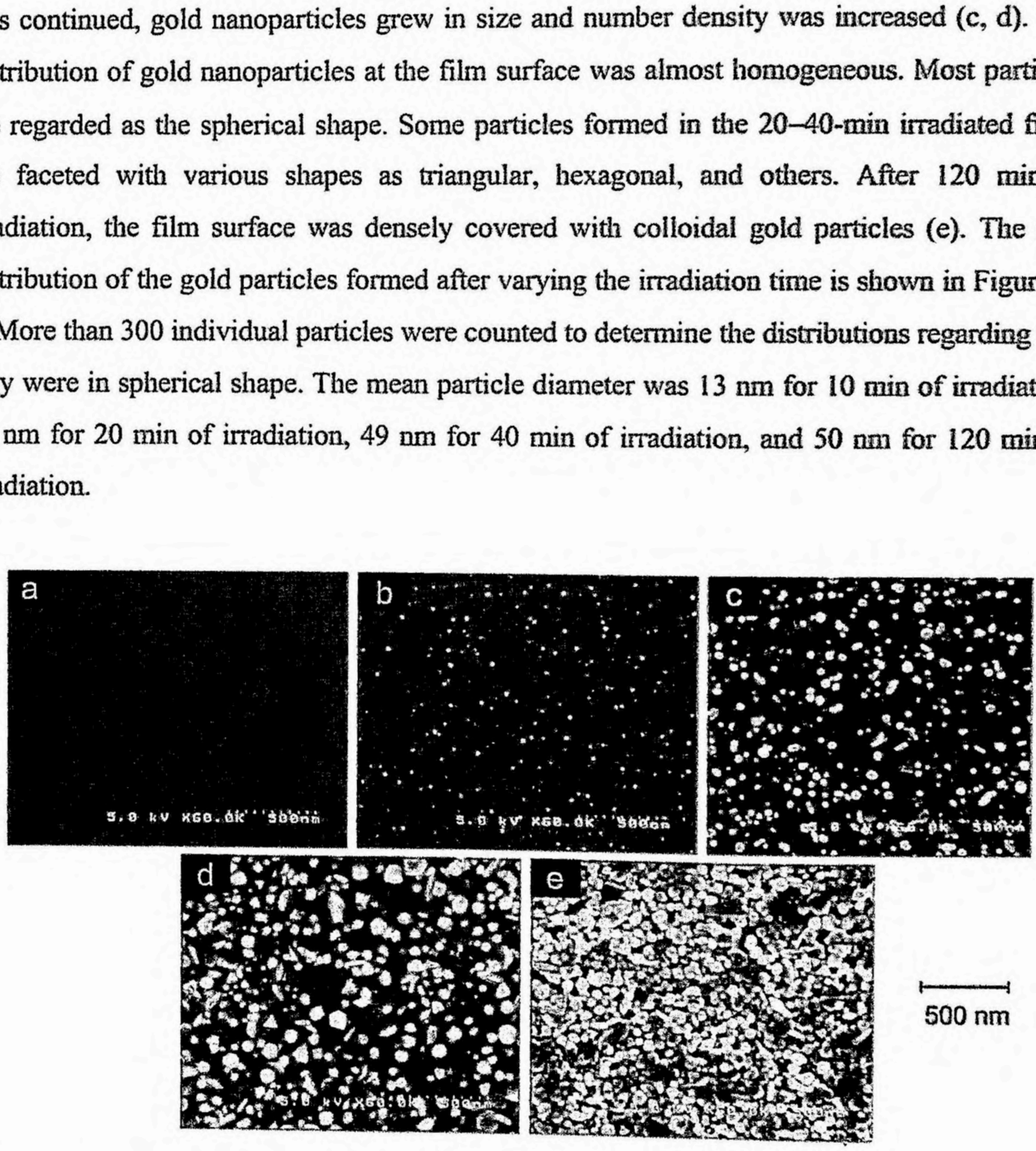

Figure 3-2. Scanning electron micrographs of the CTOAu film before and after UV irradiation. Irradiation time: (a) 0 min, (b) 10 min, (c) 20 min, (d) 40 min, (e) 120 min.

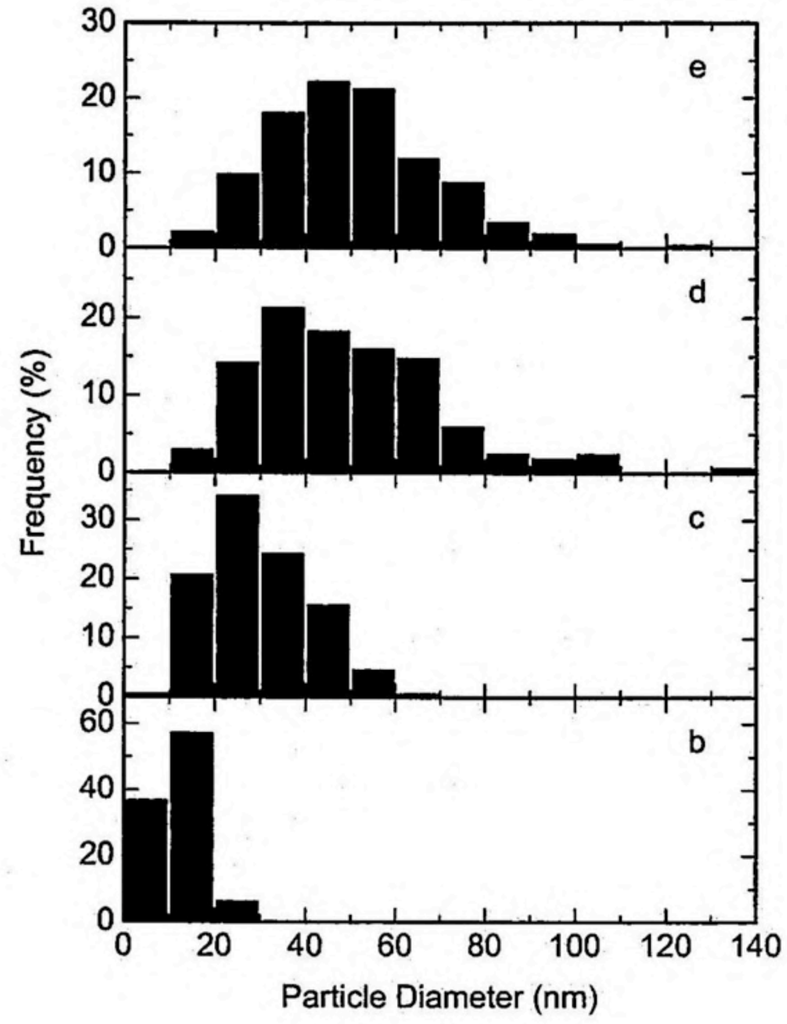

Figure 3-3. Particle size distributions of Au particles at the surface of the CTOAu film after UV irradiation. Irradiation time: (b) 10 min, (c) 20 min, (d) 40 min, (e) 120 min.

3. 3. 2 XPS study

Figure 3-4 shows variation of the XPS wide-scan spectrum for the CTOAu film before and after UV photolysis. The peak intensity of each spectrum is normalized to the highest peak. In the spectrum, the peaks of the C(1s), N(1s), O(1s), Cl(2p), Au(4d), and Au(4f) lines (marked by the dotted lines) were observed. While the relative intensities of the gold peaks [Au(4d), Au(4f)] were increased with the irradiation time, the peak intensities of other elements were decreased. These observations demonstrate the increase in the Au concentration at the film surface; that is, precipitation of photolytic gold particles at the irradiated side of the film. XPS narrow scan spectra of each element were measured and applied to detailed chemical composition analysis.

Variations of the Au($4f_{7/2}$) and Au($4f_{5/2}$) lines of the XPS spectra of the CTOAu film before and after UV photolysis are shown in Figure 3-5. The author confirmed that the spectrum change during the XPS measurement (60 sec per 1 element) is small. Before irradiation (a), two lines for Au($4f_{7/2}$) (87.4 eV) and Au($4f_{5/2}$) (91.0 eV) due to Au^{3+} were evident.[18] Deconvolution results are represented by dotted lines in the spectra. For spectrum a, in addition to the major peaks, a small peak around 84.9 eV and another minor peak at 88.7 eV were noticed. Those peaks are assigned to gold clusters (Au_n)[19,20] formed by dark reaction because they are shifted

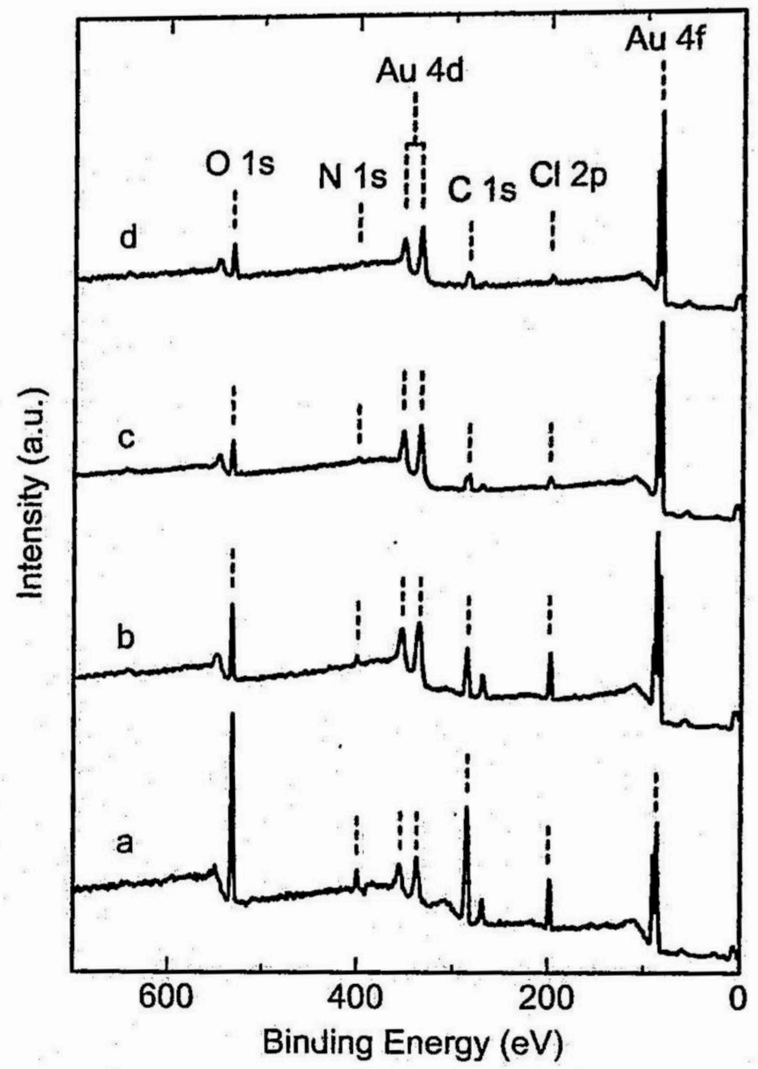

Figure 3-4. Wide-range XPS spectra of the CTOAu film before and after UV irradiation. Irradiation time: (a) 0 min, (b) 10 min, (c) 40 min, (d) 120 min. Dashed lines are a guide to the eyes.

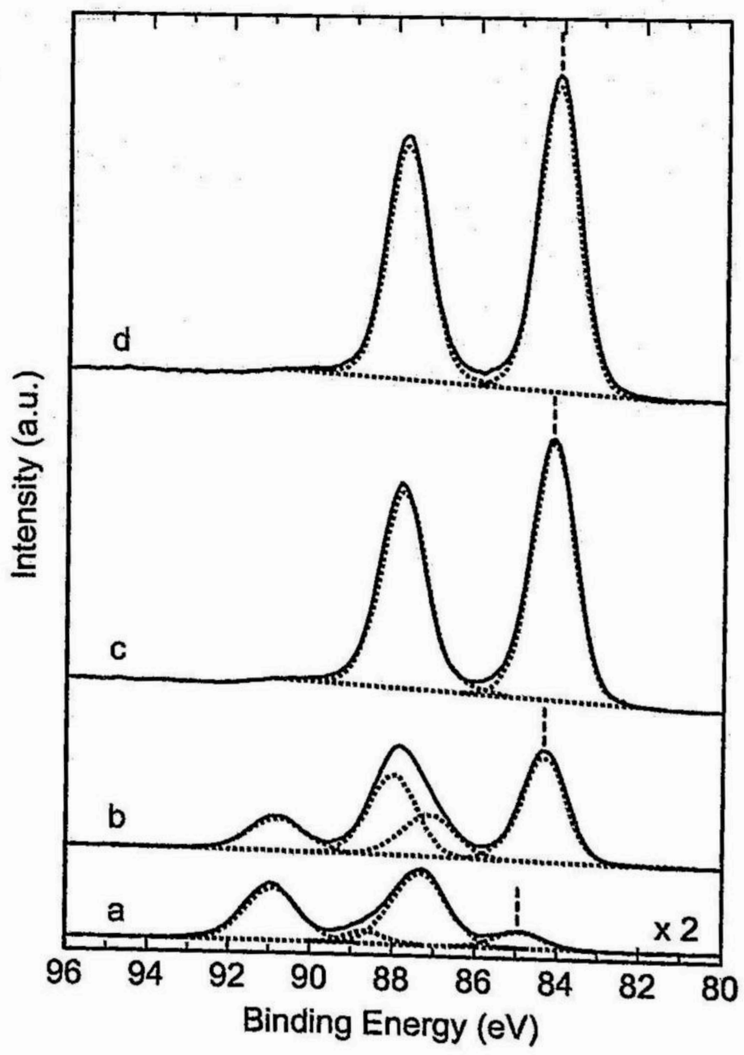

Figure 3-5. XPS spectra in Au(4f) region for the CTOAu film before and after UV irradiation. Irradiation time: (a) 0 min, (b) 10 min, (c) 40 min, (d) 120 min. Dotted lines are deconvolution results. Dashed lines are a guide to the eyes.

from the corresponding peaks of bulk gold [Au($4f_{7/2}$), 84.0; Au($4f_{5/2}$), 87.7 eV].[18] After 10 min of irradiation (b), the peaks due to Au^{3+} were decreased and the peaks due to Au_n became evident in return. After more than 40 min of irradiation (c, d), the Au^{3+} peaks almost disappeared and the peak position of the Au_n lines approached to those of bulk gold. The author has focused on the peak position of the Au($4f_{7/2}$) line and plotted the variation of the core binding energy with irradiation time (Figure 3-6). Dependence of the core binding energy of the metal clusters on size has been reported by many groups. Mason reported that the core binding energy of supported Au clusters on solid matrices is shifted 1.0–1.3 eV higher than that of bulk gold.[20] Furthermore, the full width of half-maximum (FWHM) of the Au($4f_{7/2}$) peak for the Au cluster is 0.5–0.7 eV broader than that for bulk gold. It is obvious in Figure 3-6(A) that the peak position is in 0.5–0.8 eV higher energy side than bulk gold for the CTOAu film irradiated for 0–10 min. The FWHM of the Au($4f_{7/2}$) peak is also plotted in Figure 3-6(B), which is 0.1–0.25 eV broader than bulk gold. These observations seem to be clear examples of the "cluster size effect" on the peak shift and line broadening of the XPS spectra as mentioned in the references.[19,20] Gradual changes of Au($4f_{7/2}$) peak position and FWHM, which are approaching the bulk values, are consistent with the successive growth of gold clusters to bulk gold.

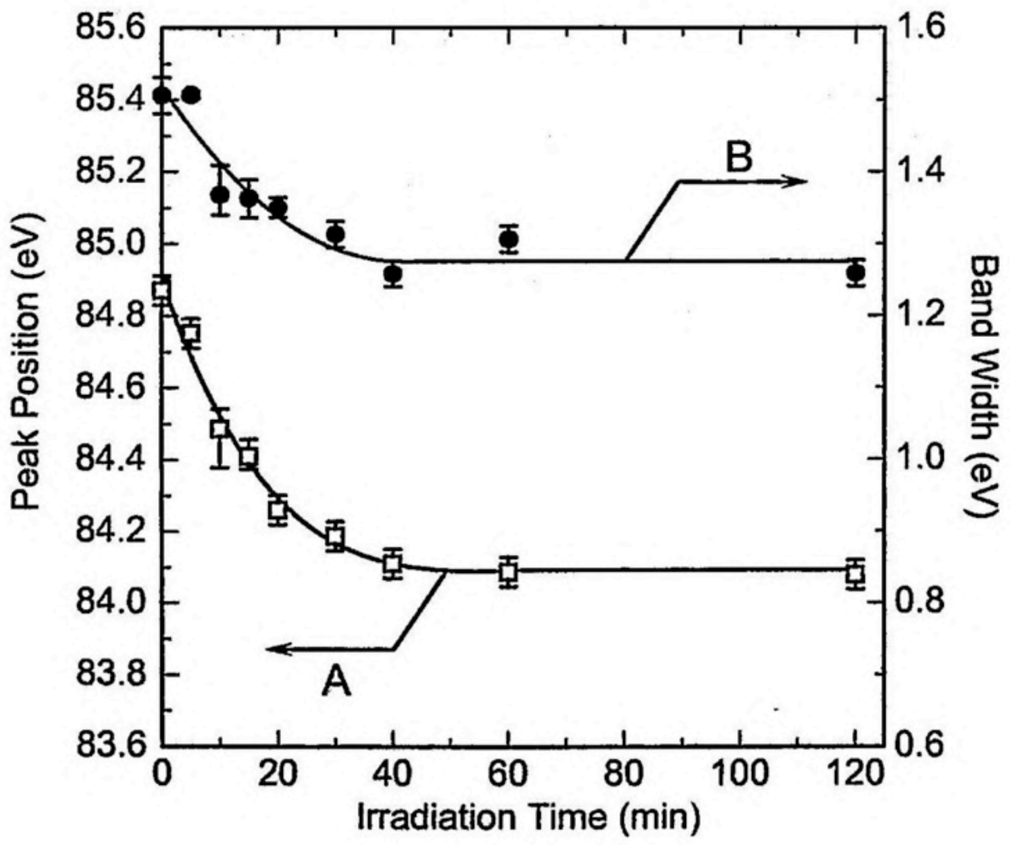

Figure 3-6. Changes of the peak position (A) and FWHM (B) of Au($4f_{7/2}$) line in the XPS spectrum of the CTOAu film with UV irradiation.

XPS spectra of the C(1s), N(1s), O(1s), and Cl(2p) regions are shown in Figure 3-7. The XPS spectra of the C(1s), N(1s), and O(1s) of CTO itself are added to Figure 3-7. Chemical composition analysis was carried out on the basis of the peak area and sensitivity factor of the XPS spectra. Variations of atomic concentrations of Au^{3+}, Au and the sum of the other elements with irradiation time are plotted in Figure 3-8. The total Au percentage (sum of Au_n and bulk gold) was increased with the irradiation time, while Au^{3+} was decreased rapidly. The sum total of other elements was decreased with the irradiation time.

3. 4 Discussion

3. 4. 1 Aggregation of gold nanoparticles at the film surface

The author has demonstrated the growth of gold nanoparticles at the surface of CTOAu films on the basis of surface morphology study (FE-SEM) and composition analysis (XPS). This is the first example of the "cluster size effect" of Au nanoparticles generated by photolysis in polymer films. Because the "cluster size effect" in our system is not so different from those observed in vacuum-deposited Au films, there is no doubt about the existence of Au clusters in the early stage of reaction. Recently, Shukla and Seal have reported a similar "cluster size effect" of gold nanoparticles in the glass matrix formed by the sol-gel method.[21] The cluster

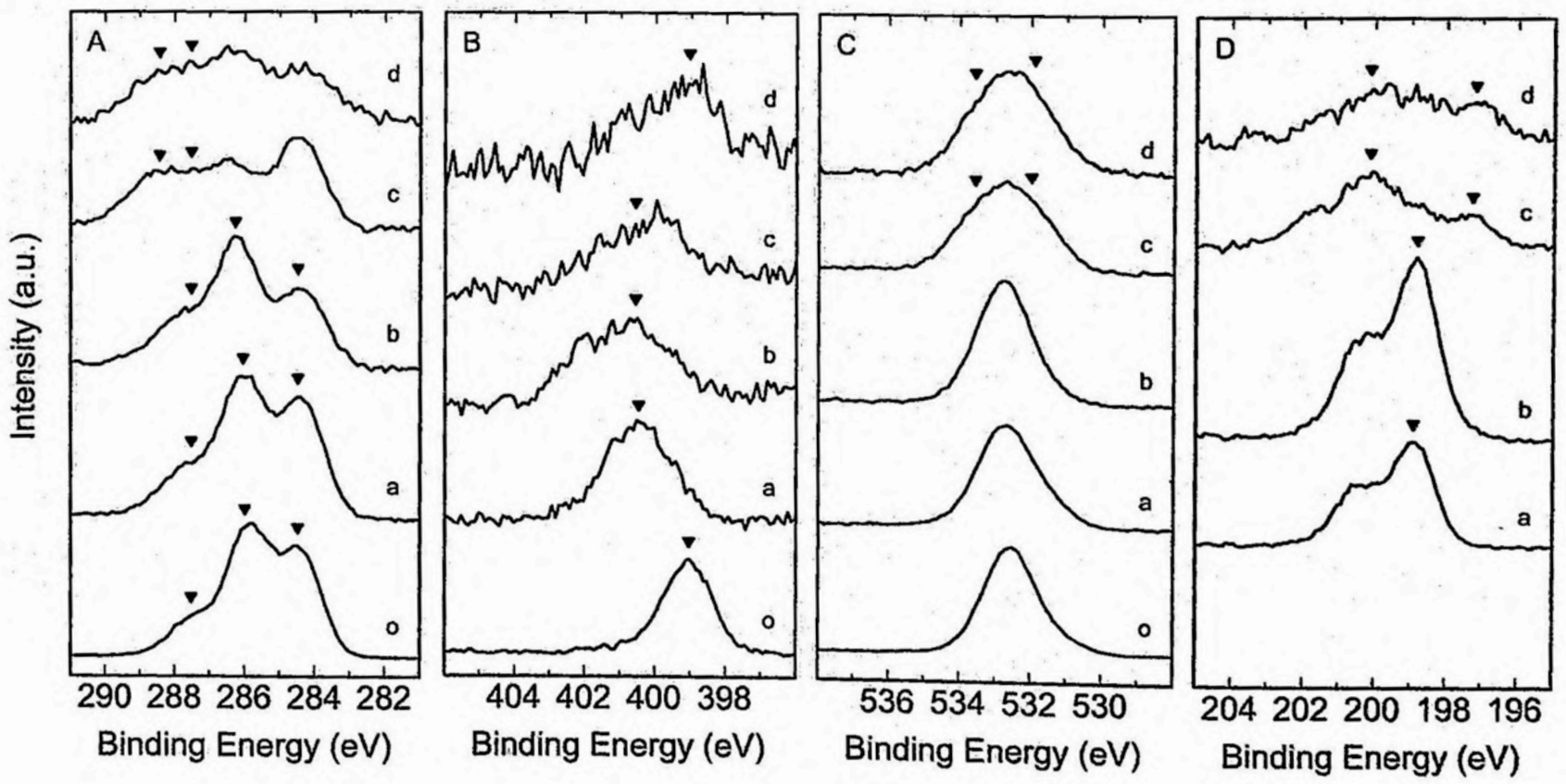

Figure 3-7. XPS spectra in regions of C(1s) (A), N(1s) (B), O(1s) (C), and Cl(2p) (D) for the CTO film (o) and CTOAu film before and after UV irradiation (a–d). Irradiation time: (a) 0 min, (b) 10 min, (c) 40 min, (d) 120 min. (▼) Peak position of the noticeable component of each element.

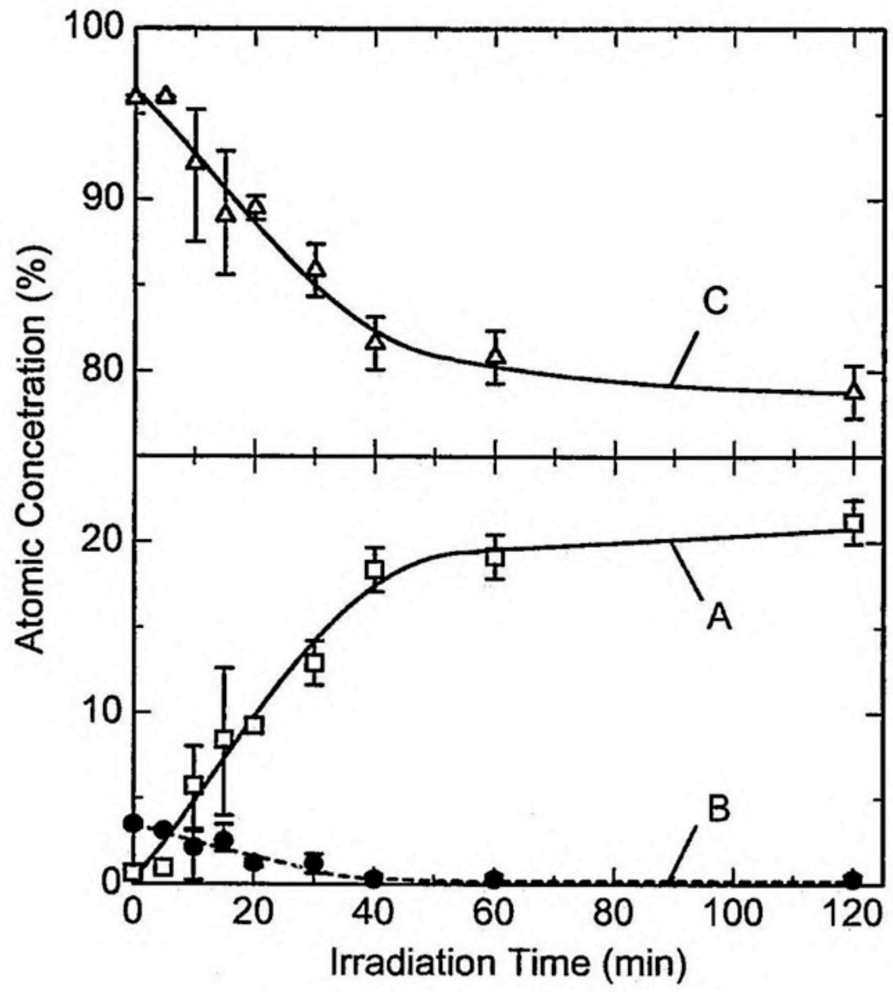

Figure 3-8. Changes of atomic concentration of the elements at the surface of the CTOAu film with UV irradiation. (A) Au, (B) Au^{3+}, (C) sum of other elements (C, N, O, and Cl).

whose size is less than 5 nm could not be detected in the FE-SEM as a result of the resolution limit of our SEM system. We could observe the "cluster size effect" in the XPS spectra for the CTOAu films. The CTOAu films irradiated with UV light for 5–30 min were kept in the dark at room temperature in air for about 12–24 h and then provided for XPS measurements. Therefore, it appeared that gold clusters produced by a short-time UV irradiation are stable enough in the CTOAu film at least 1 day or so in ambient conditions.

In the lower part of Figure 3-9, the changes of the mass concentrations of Au and Au^{3+}, as well as the amount of reduced gold, ΔN, evaluated by atomic absorption spectrometry[9] (Chapter 1) on irradiation time are shown. Although evaluation of ΔN is usually accompanied with relatively large error, it is noticed that the amount of photolytic gold is growing even after the saturation time of disappearance of Au^{3+}. Here, the author should note that the ΔN value would reflect the bulk of the CTOAu film, while XPS analysis may afford the information of the surface region on the order of several nanometers. It means that the $AuCl_4^-$ ions at the surface are reduced to form Au atoms at a stage earlier than those in the bulk film. The author has mentioned the formation of a clear silver mirror by photolysis of thin films of silver salt of carboxymethylcellulose in Chapter 2. It has been proposed that silver atoms and clusters

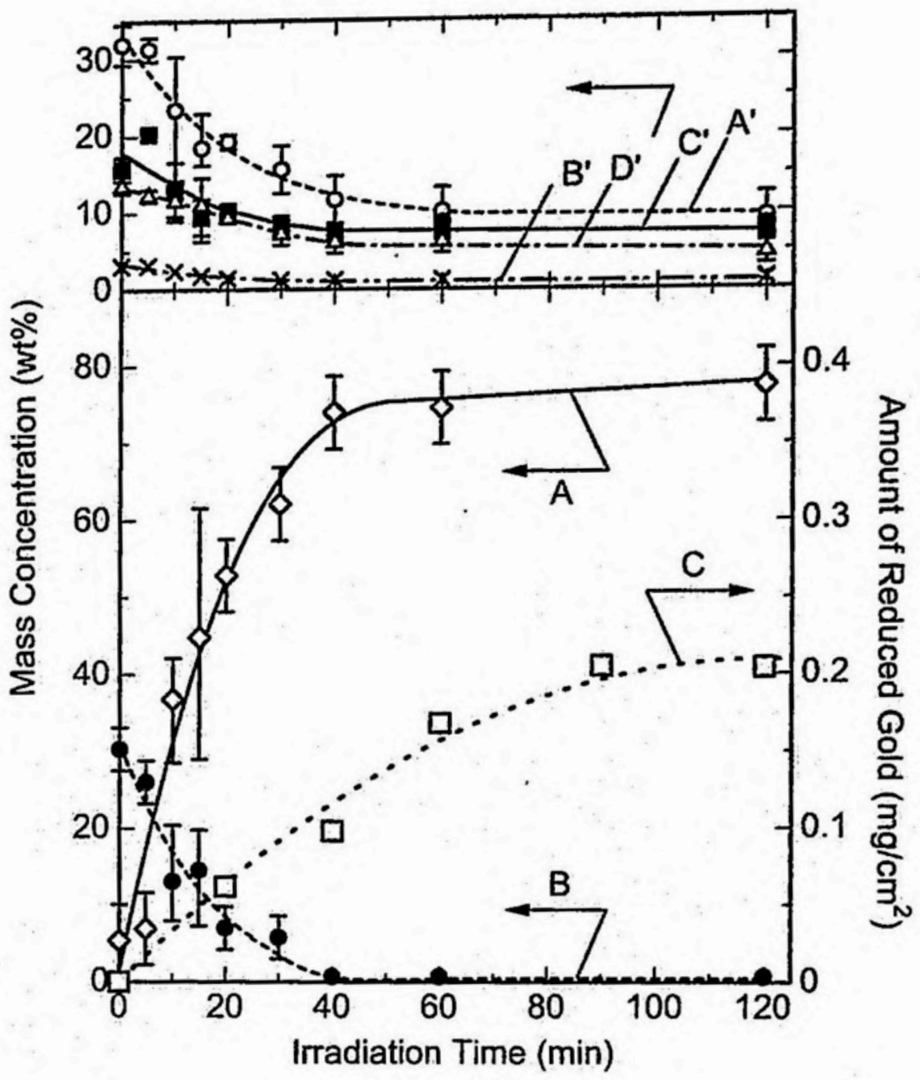

Figure 3-9. Changes of mass concentration of the elements at the surface of the CTOAu film with UV irradiation. (A) Au, (B) Au^{3+}, (A') C, (B') N, (C') O, and (D') Cl. (C) The amount of deposited gold, ΔN, with UV irradiation from Chapter 1 (□).

generated by photolysis migrate toward the irradiated side of the film and are deposited at that side, giving rise to silver metal films. These assumptions have been confirmed by a simple one-dimensional diffusion model calculation with absorbing barrier boundary conditions, which allows diffusion and deposition of silver atoms and clusters in the film and on the irradiated surface.[10,11] This model may be applicable to account for the mechanism of the formation of a gold mirror in the CTOAu films. Au nanoparticles at the surface could play a role of the concentration center, which continue growing with a supply of Au atoms and clusters from inside the film. Au atoms and clusters can migrate inside the film at room temperature when the relative humidity is high. Water molecules contained in the film would facilitate the segmental motions of the polymer and promote migration of gold atoms and clusters. These are the reasons the gold particulate film and the gold mirror are formed at the irradiated surface.

In Chapter 1, the author showed the X-ray diffraction profile of the CTOAu film. After 60 min of photolysis, the diffraction line of the (111) face of the face-centered cubic gold lattice was evident. In addition, the change of direct current (DC) electrical resistance, R Ω, of the irradiated surface was measured. Before UV irradiation, R was larger than 10^{10} Ω. After

formation of the clear gold mirror, R was decreased to 10^4–10^5 Ω. Even after the formation of the clear gold mirror, that is, after 120 min of irradiation, 20 wt% organic components still remained at the film surface (Figure 3-9). Several hypotheses would be possible to account for those observations. Gold particles and thin films may be partly covered with an ultra-thin layer of degraded CTO and certain photoproducts resulting in insufficient electric contact between them. These assumptions are not inconsistent with a relatively large DC resistance of the film compared with that of the gold bulk film.

3. 4. 2 Mechanism of photochemical reaction of CTOAu

In this Chapter, the author has found that CTO is effective to control the aggregation of the gold nanoparticles; photolytic gold nanoparticles form the densely packed particulate film at the irradiated side. The author will discuss some details of the mechanism of photochemical reactions of CTO [Scheme 3-1(B)] with the aid of the XPS study.[18,22] In Figure 3-7(A), major peaks were observed at 284.5 eV (C-C; fundamental structure of polymer),[23] 286.1–286.3 eV (C-OH), and 287.5 eV (O-C-O) in the spectra of the CTO film (o) and CTOAu film before irradiation and after 10 min of irradiation (a, b). After more than 40 min of irradiation (c, d), the broad bands due to carbonyl carbon (C=O) and carboxylic carbon (O-C=O) were noticed around 287.5–288.4 eV. In Figure 3-7(B), the peak of the amino N of CTO at 399.0 eV was shifted to a higher binding energy (400.5–400.8 eV) by the formation of CTOAu (o, a), probably as a result of complexation with $AuCl_4^-$ ions. The peak position of the amino N band seems to return partly to the original peak position of CTO after prolonged irradiation, as shown in spectrum d. These observations would support Scheme 3-1(B). In Figure 3-7(C), the peak of O(1s) around 532.3 eV was broadened as a result of the growth of two components assigned to C=O (532.0 eV) and O-C=O (533.6 eV; carbonyl oxygen and carboxylic oxygen) after more than 40 min of irradiation (c, d). In Figure 3-7(D), the peak of Cl(2p) of $AuCl_4^-$ at 198.9 eV before UV irradiation was converted to the peaks of hydrochloric acid (HCl) and the chlorinated carbon component (C-Cl) at 197.4 eV and 200.2 eV, respectively, after more than 40 min of irradiation (c, d). A somewhat more detailed scheme consistent with those observations is proposed (Scheme 3-2).

To support those assumptions, IR absorption spectra of CTO and CTOAu films after being peeled from the quartz plate were measured by using a FTS-30 Fourier transform infrared spectrometer (Bio-Rad Laboratories, Inc.) and are shown in Figure 3-10. In the spectra o and a, the NH_2 bending vibration at 1561 cm^{-1} of the CTO was decreased by immersion of the CTO

$$RNH_2 + HAuCl_4 \longrightarrow RNH_3^+AuCl_4^- \quad \text{(complexation)}$$

$$RNH_3^+AuCl_4^- \xrightarrow{h\nu} Au^0 + RNH_3^+Cl^- + 3\dot{C}l \quad \text{(reaction)}$$

(following reaction)

$$RNH_3^+Cl^- \longrightarrow RNH_2 + HCl$$

$$RNH_2 + Cl_2 \ (O_2) \longrightarrow \begin{cases} \text{carbonyl compound (C=O)} \\ \text{chlorinated compound (C-Cl)} \\ \text{hydrochloric acid (HCl)} \end{cases}$$

Scheme 3-2. Scheme of photochemical reactions and final products in the CTOAu film.

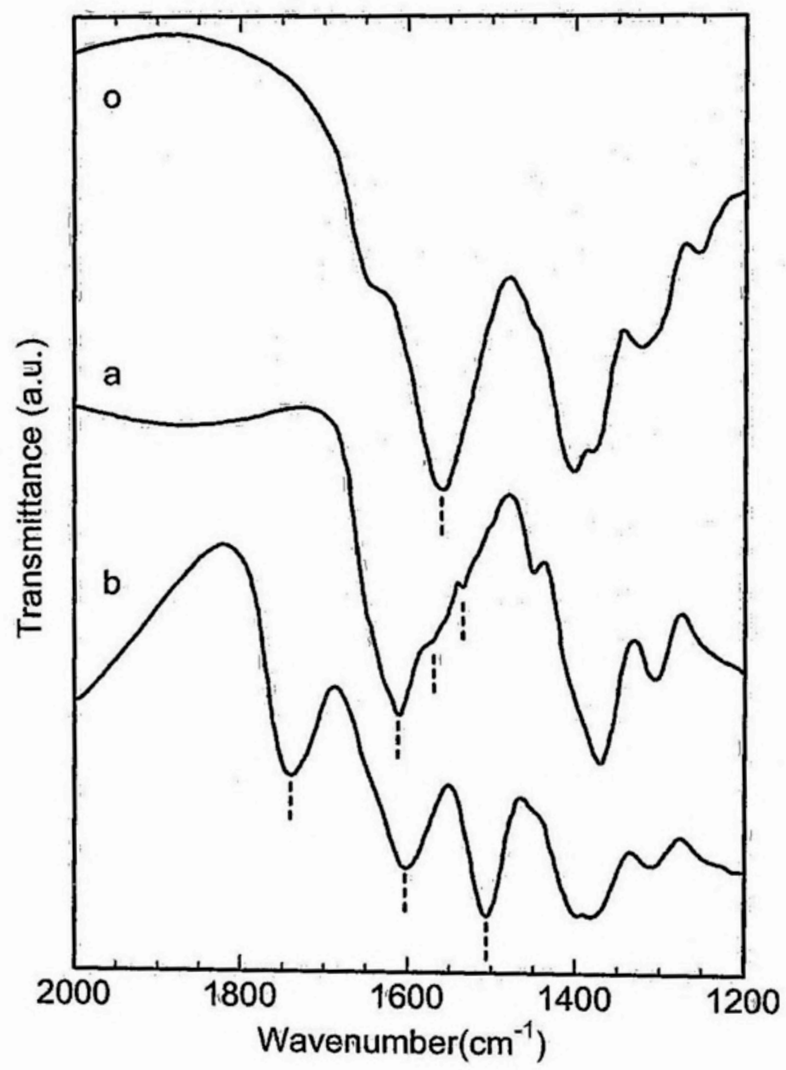

Figure 3-10. IR absorption spectra of the CTO film (o) and the CTOAu film before and after UV irradiation (a, b). Irradiation time: (a) 0 min, (b) 720 min. Dashed lines are a guide to the eyes.

film into $HAuCl_4$ solution. In return, a peak of the antisymmetric bending vibration at 1617 cm^{-1} and a shoulder of symmetric vibration at 1542 cm^{-1} of the NH_3^+ group developed. Such a change corresponds to the formation of CTOAu, $RNH_3^+AuCl_4^-$. A new peak of carbonyl stretching vibration (ν= 1744 cm^{-1}) was noticed after UV photolysis (b).[24] These observations are in accordance with the changes of C(1s), N(1s), and O(1s) bands in the XPS spectra.

Primary products of the photochemical reaction are the gold atom, quaternary ammonium chloride of CTO, and chlorine. CTO and quaternary ammonium chloride would be further oxidized by chlorine and oxygen, yielding certain carbonyl compounds and chlorinated compounds of CTO as final products.

3.5 Summary

Thin films of CTOAu were photolyzed with 253.7-nm light in wet air at room temperature. Detailed study on the aggregation of gold nanoparticles has been carried out with the aids of XPS and FE-SEM observations. Surface composition analysis by XPS proved to be helpful to examine the formation and the growth of gold nanoparticles and the mechanism of photochemical reactions of the CTOAu films. Gold clusters formed at the early stage have been characterized by the 0.5–0.8 eV peak shift and 0.1–0.25 eV line broadening of the XPS spectrum of Au($4f_{7/2}$). FE-SEM observations have demonstrated the change of the average particle size, from 13 nm (t = 10 min) to 50 nm (t = 120 min). After prolonged irradiation, peak position and FWHM of the Au(4f) line approached those of bulk gold [Au($4f_{7/2}$) 84.0 eV, FWHM 1.2 eV]. The scanning electron micrograph shows that colloidal gold particles densely cover the film surface at the irradiated side. On the basis of the spectral line shape and intensity of C(1s), N(1s), O(1s), and Cl(2p) in the XPS spectra of the CTOAu film, a detailed reaction scheme has been proposed. A part of CTO seems to be oxidized by chlorine and oxygen, finally producing carbonyl compounds or chlorinated compounds of CTO.

References

1. V. P. Kamat, *J. Phys. Chem. B*, **106**, 7729 (2002).
2. D. L. Feldheim and C. A. Foss, Jr., *Metal Nanoparticles: Synthesis, Characterization and Applications.*, Marcel Dekker, New York (2002).
3. J. M. Ware, *J. Photogr. Sci.*, **42**, 157 (1994).
4. S. Magdassi, A. Bassa, Y. Vinetsky, and A. Kamyshny, *Chem. Mater.*, **15**, 2208 (2003).
5. A. Heilmann, *Polymer Films with Embedded Metal Nanoparticles*, Springer, Berlin (2002).
6. H. Nabika, K. Akamatsu, M. Mizuhata, A. Kajinami, and S. Deki, *J. Mater. Chem.*, **12**, 2408 (2002).
7. N. N. Kariuki, L. Han, N. K. Ly, M. J. Patterson, M. M. Maye, G. Liu, and C. J. Zhong, *Langmuir*, **18**, 8255 **(2002)**.

8. Y. Yonezawa, A. Takami, T. Sato, K. Yamamoto, T. Sasanuma, H. Ishida, and A. Ishi *J. Appl. Phys.*, **68**, 1297 (1990).
9. Y. Yonezawa, N. Kometani, M. Seki, T. Sakagami, H. Tanaka, S. Koyanagi, and T. Miyama, *Trans. Mater. Res. Soc. Jpn.*, **27**, 197 (2002).
10. Y. Yonezawa, M. Kijima, and T. Sato, *Ber. Bunsen-Ges. Phys. Chem.*, **96**, 1828 (1992).
11. Y. Yonezawa and M. Kijima, *J. Soc. Photogr. Sci. Technol. Jpn.*, **56**, 3 (1993).
12. C. D. Wagner, L. E. Davis, M. V. Zeller, J. A. Taylor, R. H. Raymond, and L. H. Gale, *Surf. Interface Anal.*, **3**, 211 (1981).
13. A. K. Gangopadhayay and A. Chakravorty, *J. Chem. Phys.*, **35**, 2206 (1961).
14. D. G. Duff, A. Baiker, and P. P. Edwards, *Langmuir*, **9**, 2301 (1993).
15. A. Henglein, *Langmuir*, **15**, 6738 (1999).
16. U. Kreibig, *J. Phys. (Paris)*, **38**, C2-97 (1977).
17. R. E. Benfield, J. A. Creighton, D. G. Eadon, and G. Schmid, *Z. Phys. D.*, **12**, 533 (1989).
18. C. D. Wagner, W. M. Riggs, L. E. Davis, J. F. Moulder, and G. E. Muilenberg, *Handbook of X-ray Photoelectron Spectroscopy*, Perkin-Elmer, Eden Prairie (1978).
19. K. S. Kim and N. Winograd, *Chem. Phys. Lett.*, **30**, 91 (1975).
20. M. G. Mason. *Phys. Rev. B*, **27**, 748 (1983).
21. S. Shukla and S. Seal, *Nanostruct. Mater.*, **11**, 1181 (1999).
22. G. Beamson and D. Briggs, *High-Resolution XPS of Organic Polymers*, John Wiley & Sons, New York (1992).
23. N. Ikeo, Y. Iijima, N. Niimura, M. Sigematsu, T. Tazawa, S. Matsumoto, K. Kojima, and Y. Nagasawa, *Handbook of X-ray Photoelectron Spectroscopy*, JEOL, Tokyo (1991).
24. H. Tsubomura, T. Yagishita, and H. Toi, *Bull. Chem. Soc. Jpn.*, **46**, 3051 (1973).

Chapter 4

Surface-Enhanced Raman Scattering from Silver Salts of High Molecular Weight Carboxylic Acids Photolyzed with UV Light

4.1 Introduction

Surface-enhanced Raman scattering (SERS) characterized by a giant enhancement (10^4–10^6) of the Raman cross section of molecules in contact with precious metal surface has been intensively studied since its discovery.[1–3] Suitable substrates for adsorbed molecules include roughened electrodes, vacuum-deposited metal films, matrix-isolated metal clusters, smooth metal surfaces in the attenuated total reflection arrangement, and holographic metal gratings. Creighton and coworkers were the first to introduce colloidal silver and gold particles in solutions for the SERS study.[4] Yogev & Efrima have reported the synthesis of silver metal liquidlike films (MELLF) that are confined within two immiscible liquids and examined Raman scattering from the film surface.[5] On the other hand, the SERS studies by using photolytic silver as the substrate seem to be rather rare. Rowe et al. have obtained roughened silver surface available for the substrate by exposing a clear silver surface to iodine vapor and then photolyzing with the wavelength, λ = 488 nm laser light.[6] Ahern & Garrell have used in situ photoreduced silver nitrate ($AgNO_3$) as a substrate for surface-enhanced spectroscopy.[7] Haegel & Wokaun have prepared silver colloid adsorbing dye molecules at the surface by photoreduction of Ag^+ ions in the presence of cyanine dyes in solutions.[8] As carboxylate ions in the silver salts of high molecular weight carboxylic acids such as carboxymethylcellulose (CMC) and alginic acid (AL) may be regarded as the reactant for photochemical reactions, the protective agent, as well as the matrix of photolytic silver, the study on SERS of these compounds photolyzed with UV light could afford useful information relevant to the mechanism of photochemical reactions, aggregation of colloidal silver particles and structure of silver metal films.

AL is a polysaccharide produced by brown algae. When the silver salt of AL (ALAg) is photolyzed with UV light (λ = 253.7 nm), silver atom is formed by one electron transfer from the carboxylate ion ($RCOO^-$) to the bounded silver ion (Ag^+). Subsequent agglomeration of silver atoms produces silver clusters, colloids, and bulk metal.[9] These phenomena is fundamentally the same as the photolysis of the silver salt of CMC (CMCAg).[10] An important aspect of the photochemical method is a possibility to control aggregation states of photolytic silver by changing the reaction conditions.[11] In this chapter, the author has examined Raman

scattering form the CMCAg films and the ALAg films which are photolyzed with UV light and observed SERS effect useful for characterization of the CMCAg and ALAg films. The author has found that the aggregation of photolytic silver particles has profound effects on the Raman intensity of the symmetric COO^- stretching vibration band.

4. 2 Experimental

4. 2. 1 Preparation

Preparation of the CMCAg and ALAg films was carried out as described in Chapter 1. The author cut off a sector with an interior angle of 120° from a circular quartz plate (22.5 mm in diameter, 0.65 mm in thickness) and used it as the substrate for the film. The films of sodium salt of CMC (CMCNa: Nakarai Tesque Co.) and sodium alginate (ALNa: Nakarai Tesque Co.) on the quartz plate were immersed in 0.1 M (1 M = 1 mol·dm^{-3}) $AgNO_3$ solution to substitute Na^+ with Ag^+ ions. The film thickness was 1–5 μm and more than 85% of Na^+ ions in the CMCNa film and the ALNa film were replaced by Ag^+ ions. Then, the CMCAg film and the ALAg film were exposed to a 15-W sterilization lamp in wet air (relative humidity more than 70%) at room temperature.

4. 2. 2 Instrumentation

UV-visible absorption spectra were recorded on a Shimadzu UV-260 spectrophotometer. The experimental setup used for Raman scattering measurements is shown in Figure 4-1.[12] The film was set on the sample holder and the sector portion was replaced by a bare silicon wafer of the same shape. This configuration made it possible to use the 520–525 cm^{-1} Raman peak due to the Si lattice vibration as an external intensity standard.[13] The p-polarized excitation light (λ = 514.5 nm) with the output power of 100–300 mW from a Spectra Physics Model 2016 Ar^+ laser was incident on the film surface with an angle of incidence 60° after passing through appropriate interference filters. The sample was rotated at 3000 rpm to avoid photodegradation by laser beam. Raman scattering was observed in the direction perpendicular to the excitation beam and detected by a Photometric Model PM 512 CCD detector through a Spex Triplemate monochromator 1877. Data processing was performed by a Seki MDS program on a personal computer. The observation time was 200–600 sec. The spectral resolution and the accuracy of wavenumber readings were about 8 cm^{-1} and better than ± 0.5 cm^{-1}, respectively. The morphology of the ALAg film surface was examined by a high-resolution scanning electron microscope of the field emission type (FE-SEM), Hitachi Model S-810.

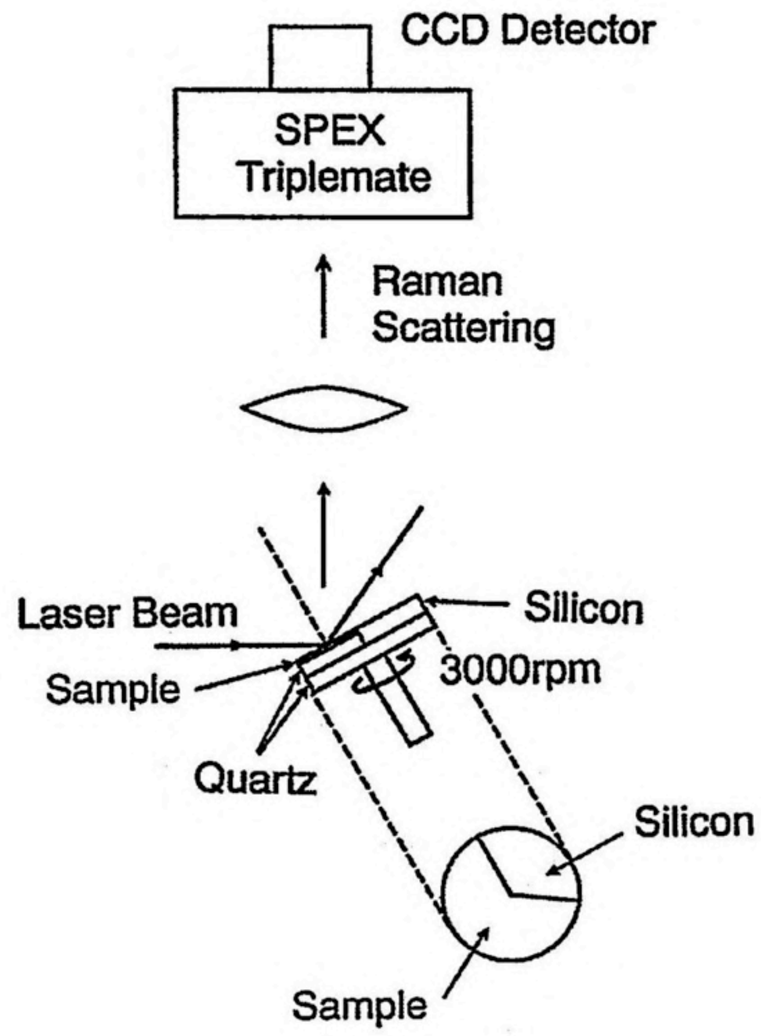

Figure 4-1. Experimental setup for obtaining Raman spectra of the CMCAg films and the ALAg flms.

4. 3 Results and Discussion

4. 3. 1 CMCAg films

Variation of the absorption spectra of the CMCAg film with UV irradiation is given in Figure 4-2. A colloidal absorption band around 410 nm developed with irradiation time. On 180-min irradiation, the film surface wore a metallic luster and at the same time, the increase in the absorbance at $\lambda > 600$ nm was observed. After 600 min of irradiation, a clear silver mirror was formed, and finally, absorption spectrum turned into a continuous absorption of silver metal film.

The author attempted to measure the Raman spectrum of the CMCAg film before irradiation. However, evident Raman spectrum was not observed due to the disturbance by unspecified fluorescence. The author then fabricated the reference film sample whose thickness was 1–5 μm on the Si wafer by dropping an aqueous solution of CMCNa and drying. Although fluorescence harmful for Raman scattering measurements was serious in the neat CMCNa film, it was made to diminish by irradiation with laser beam (300 mW) for several minutes. Raman spectrum in Figure 4-3 was obtained after such a pretreatment and without rotating the sample during the measurement. In this spectrum, the sharp peak at 520 cm^{-1} is due to a fundamental Raman band of Si.[13,14] The broad band around 940–980 cm^{-1} is assigned to an overtone of Si.

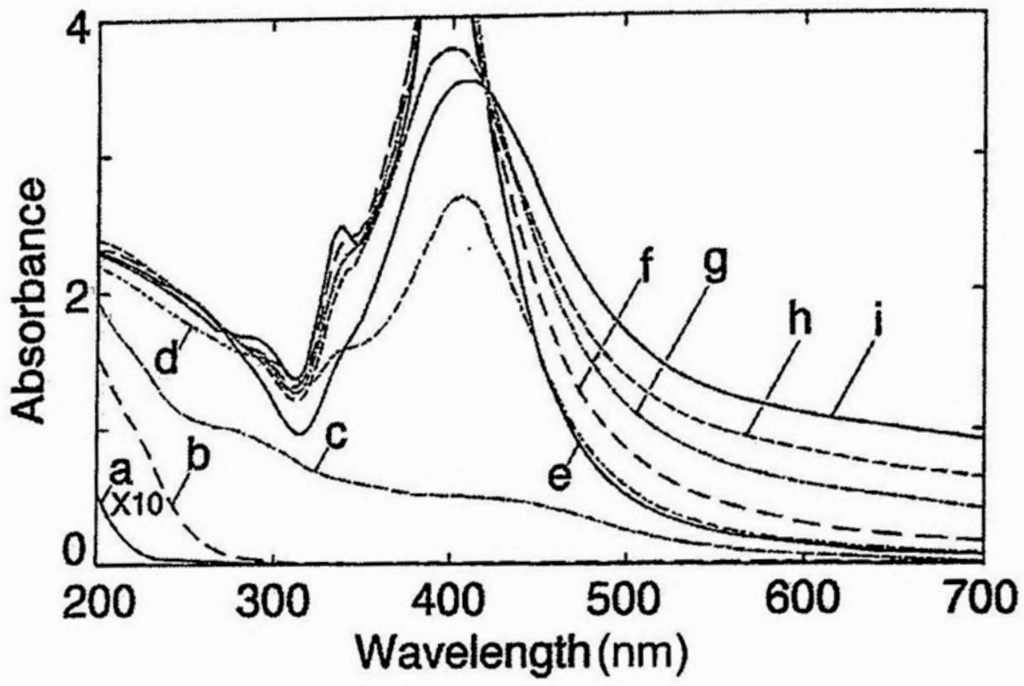

Figure 4-2. Absorption spectrum of the CMCNa film (a) and variation of the absorption spectra of the CMCAg film. Irradiation time: (b) 0 min, (c) 1 min, (d) 5 min, (e) 30 min, (f) 90 min, (g) 180 min, (h) 300 min, (i) 600 min.

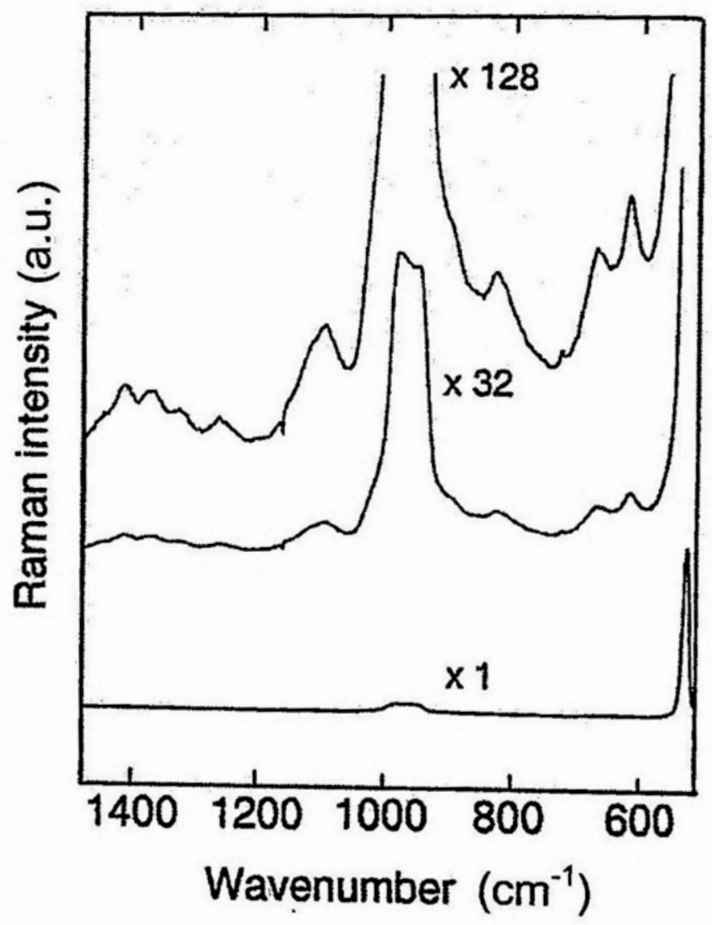

Figure 4-3. Raman spectrum of the CMCNa film on the Si wafer. ×1, ×32, and ×128 in the figure indicate the magnitude of the enlargement.

After an enlargement of the spectrum, five bands were perceived. The peak around 1410 cm^{-1} is assigned to symmetrical stretching vibration of carboxylate group (COO^-).[15] The 825 and 1094 cm^{-1} peaks are attributed to skeletal vibration of pyranose ring.[16,17] Further, the peaks at 615 and 668 cm^{-1} are assigned to deformation vibrations of COO^- group.[15]

In the case of the photolyzed CMCAg film, it turned out that harmful fluorescence was considerably decreased and measurements of Raman spectra became possible after UV photolysis for 30 min and more. The variation of the Raman spectra of the CMCAg film with UV irradiation is given in Figure 4-4. Two bands around 1396–1401 cm^{-1} and 936–945 cm^{-1} are remarkably noticed. The peak at 1396–1401 cm^{-1} is assigned to symmetrical COO^- stretching vibration and the peak at 936–945 cm^{-1} to skeletal C-C stretching vibration adjacent to COO^- group, respectively.[15] Raman bands around 767–774 cm^{-1} and 642–651 cm^{-1} assigned to CH_2 rocking vibration and COO^- deformation vibration, respectively, are also noticed. The relative Raman intensity is defined as the intensity ratio of the Raman band of CMCAg to the fundamental band of Si (520 cm^{-1}). Due to the difficulty in measuring the Raman spectrum of the CMCAg film before irradiation, the author has employed the CMCNa film as a substitute, i.e., CMCAg film for irradiation time, $t = 0$ min. Considering the intensity ratio of the Si overtone to the fundamental band (0.054) and the surface area of the Si wafer, the relative Raman intensity of symmetric COO^- stretching vibration at $t = 0$ (1410-cm^{-1} band) is 0.0042. The relative Raman intensities of four bands, symmetric COO^- stretching vibration (1396–1401 cm^{-1}), C-C (COO^-) stretching vibration (936–945 cm^{-1}), CH_2 rocking vibration (767–774 cm^{-1}), and COO^- deformation vibration (642–651 cm^{-1}), are plotted versus irradiation time in Figure 4-5. Considering the decrease of CMCAg by UV photolysis, the intensity of Raman scattering should be decreased monotonously with photolysis. In reality,

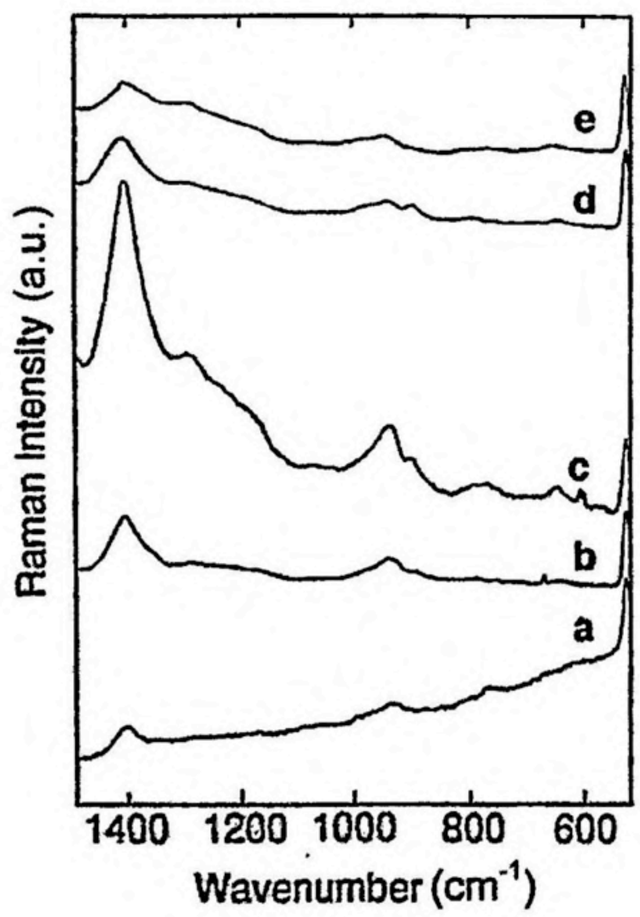

Figure 4-4. Variation of the Raman spectra of the CMCAg film. Irradiation time: (a) 30 min, (b) 90 min, (c) 180 min, (d) 300 min, (e) 600 min.

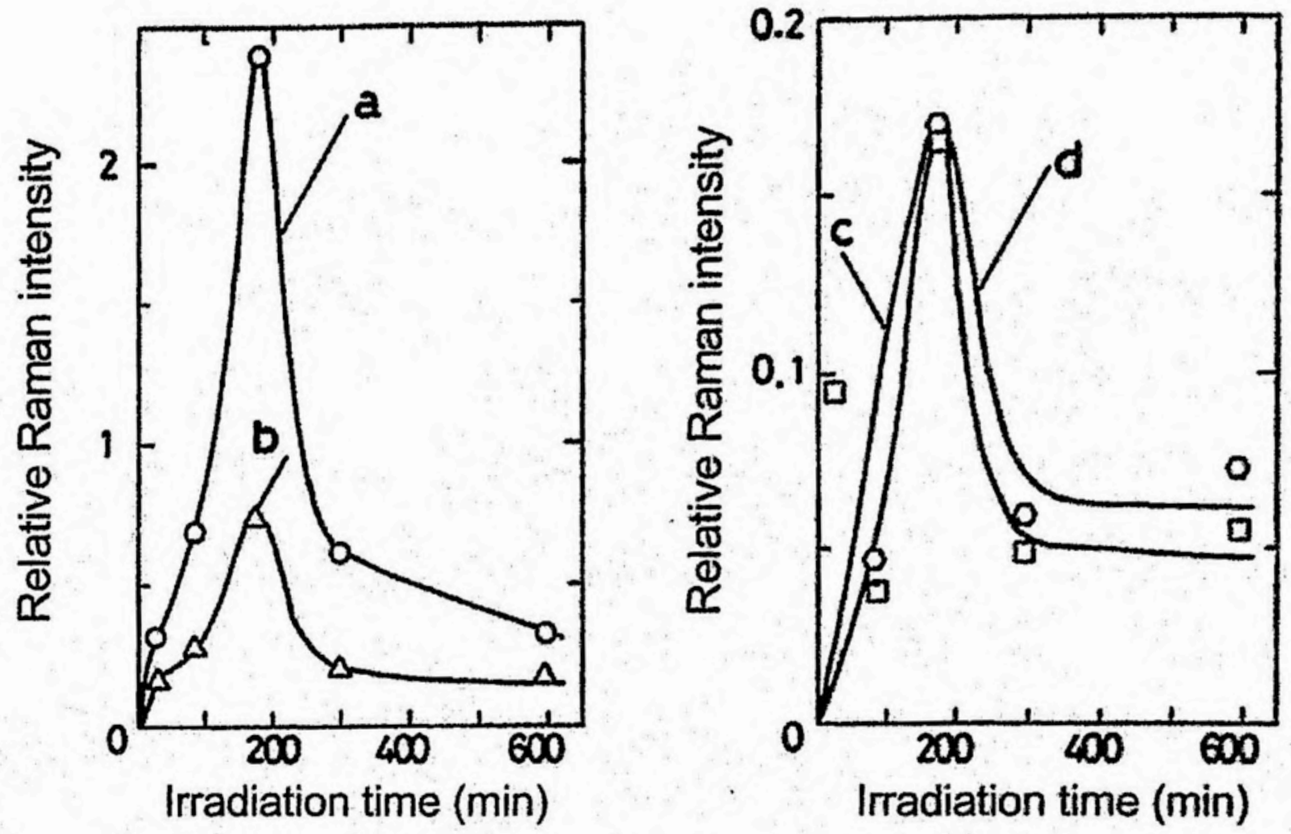

Figure 4-5. Variations of the relative Raman intensities of characteristic bands of the CMCAg film with UV irradiation time. (a) Symmetric COO^- stretching vibration (1396–1401 cm^{-1}), (b) C-C (COO^-) stretching vibration (936–945 cm^{-1}), (c) CH_2 rocking vibration (767–774 cm^{-1}), (d) COO^- deformation vibration (642–651 cm^{-1}). Raman intensity is given relative to the fundamental band of Si.

Figure 4-5 clearly shows that Raman intensities are increased by UV irradiation for 0–180 min. Therefore, it is reasonable to assume that the intensity enhancement of Raman scattering is caused by SERS.

The author has focused on the symmetric COO^- stretching vibration because SERS is most evident in this band. The author has measured the IR absorption spectra of the CMCAg film before and after photolysis in Chapter 2. Characteristic bands observed at 1575 cm^{-1} and 1415 cm^{-1} before irradiation are assigned to the asymmetric COO^- stretching and the symmetric COO^- stretching vibrations, respectively. After irradiation, the intensities of these bands were decreased and alternately, a new band at 1720 cm^{-1} appeared. This band at 1720 cm^{-1} is assigned to the antisymmetric carbonyl group (C=O) stretching vibration of CMC (RCOOH) and degraded CMC produced by the reaction. Some of RCOOH molecules produced as a result of UV photolysis may be adsorbed at the surface of the aggregated silver particles in the form of $RCOO^-$ ions, making contribution to SERS. Enhanced Raman scattering and the geometry of COO^- group would suggest that COO^- group is adsorbed at the surface of the aggregated silver particles with a tendency to orient the line joining two oxygen atoms parallel to the surface.[18,19] Such a configuration may favor the electromagnetic mechanism of SERS. In

addition, the adsorption of $RCOO^-$ ions on the aggregated silver particles could enhance Raman scattering by short-range mechanism (chemical mechanism) as well.[20,21] The remainder RCOOH molecules which existed in the film bulk as the free acid may not contribute to SERS. Compared with the enhancement of Raman scattering of the symmetric COO^- stretching vibration band, Raman bands assigned to the pyranose ring do not exhibit such an evident intensity enhancement, which is probably due to the difficulty of adsorbing at the colloidal surface.

The SERS enhancement factor of the roughened silver surface has been theoretically estimated to be 10^4–10^6.[21,22] Kerker et al.[23] and Mabuchi et al.[18] have observed SERS of the citrate ions by Ag and Au colloids prepared by chemical reduction of $AgNO_3$ and $HAuCl_4$. They have estimated the SERS enhancement factor as large as 10^5 for the incident light λ = 514.5 nm. The author has tried to estimate the SERS enhancement factor according to these groups. First, a simple ratio of the relative Raman intensity of the CMCAg film to the CMCNa film was calculated. In the CMCNa film, all of COO^- ions can contribute to Raman scattering. On the other hand, in the CMCAg film after UV photolysis, it is reasonable to assume that only carboxylate ions in contact with Ag particles contribute to SERS. Accordingly, the author has to introduce a certain assumption to estimate the number of COO^-. The number of COO^- in the CMCNa film is obtained by the amount of CMCNa casting on a substrate. The diameter of colloidal silver is assumed to be 10 nm or 40 nm with the help of SEM observations in Chapter 2. By introducing an assumption that colloidal silver particles are covered with a monolayer of carboxylate ions, each of which occupies an area of 0.4 nm^2. Then, the author has corrected the intensity ratio for the number of carboxylate ions adsorbed on the colloidal silver.[23] From the number of COO^- which contribute to SERS, the ratio γ of the number of COO^- in the CMCAg film to that in the CMCNa film has been estimated. With the additional assumption that the Raman spectrum of the CMCAg before irradiation is nearly equal to that of the CMCNa, the relative enhancement factor f has been calculated and summarized in Table 4-1. The degree of maximum enhancement for $2a$ = 40 nm amounts to 6×10^4–3×10^5. This value is close to that of Kerker et al.[23] and Mabuchi et al.[18] However, the author should be careful not to take such a value literally as it is because of several crude approximations, e.g., apart from the assumptions for the estimation of γ, disregard of the distribution of the particles size and the shape of the aggregated silver particles, as well as the correction of absorption of incident light and scattered light by photolytic silver in the film (filter effect).

Table 4-1. Apparent SERS enhancement factor f of symmetric COO^- stretching vibration band of the CMCAg film. The diameter of Ag particles $2a$ is either 10 nm or 40 nm

t	I	γ		f	
min		$2a$ = 10 nm	40 nm	$2a$ = 10 nm	40 nm
0	0.0042	1.0	1.0	1.0	1.0
30	0.32	0.0052	0.0013	1.5×10^4	6.0×10^4
90	0.69	0.0065	0.0016	2.5×10^4	1.0×10^5
180	2.4	0.0090	0.0023	6.5×10^4	2.6×10^5
300	0.61	0.010	0.0025	1.4×10^4	5.6×10^4
600	0.33	0.011	0.0028	7.0×10^3	2.8×10^4

The increase of I and f in t = 0–180 min implies that there is a close connection between the intensity of Raman scattering and the aggregation state of photolytic silver. Variation of the direct current electrical resistance R of the film surface and the relative Raman intensity $\tilde{I}$ are plotted in Figure 4-6. Here, $\tilde{I}$ are expressed relative to the maximum one of 2.4 (180 min). R is decreased from about $10^{10}\ \Omega$ for the unirradiated film to 10^7–$10^8\ \Omega$ for the 180-min

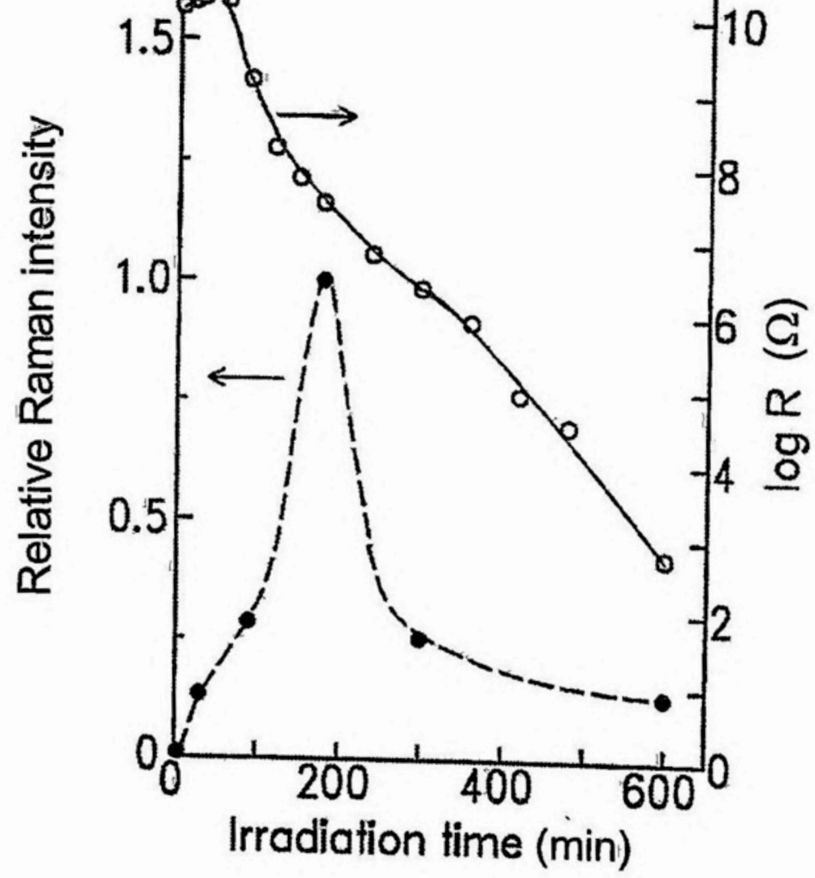

Figure 4-6. Changes of the relative enhancement factor $\tilde{I}$ and electrical sheet resistance R of the CMCAg film with irradiation time. $\tilde{I}$ is given in arbitrary units.

irradiated film, indicating the beginning of aggregation of silver particles. When metal particles begin to aggregate, a contribution of multipole plasmon resonance to SERS becomes significant.[18] The increase in $\tilde{I}$ by 180-min irradiation might be interpreted in this context. In this sense, SERS is applicable to a probe to monitor the change of the aggregation states of silver particles, such as the percolation transition of the thin silver films. The decrease in $\tilde{I}$ after 300 min of irradiation is indicative of the filter effect, i.e., absorption of incident light and Raman scattering light by photolytic silver. Ishida et al. have pointed out that the intensity of Raman scattering of pyrolytic graphite is fairly increased by deposition of 6–10-nm silver overlayer, while the intensity is rather reduced when thickness of the silver layer is more than that.[24] There is a resemblance in the intensity enhancement of the Raman bands between $RCOO^-$ ions in the CMCAg film and anisic ions in the MELLF.[5] Yogev & Efrima have stated that when the MELLF is present, the Raman signal from the organic phase much diminishes or completely disappears due to low transmittance of the film (10–60 nm thickness). Accordingly, a considerable part of the decrease in $\tilde{I}$ may arise from the filter effect.

It is interesting that even after the formation of the clear silver mirror, the Raman intensity still remains about 10% of the maximum value. It is plausible that the silver mirror is partly covered with the thin polymer films containing COO^- group. This assumption is not inconsistent with the surface composition analysis by the X-ray photoelectron spectroscopy in Chapter 2. The observation that the metallic luster of the silver mirror lasts more than 1 year in air because of the protective action of the polymer matrix also assists the assumption.

4. 3. 2 ALAg films

UV-visible absorption spectra of the ALAg film were recorded on a spectrophotometer and the results are given in Figure 4-7. After 5-min UV irradiation, a colloidal absorption band appeared around λ = 425 nm. 10-min irradiation brought about a metallic luster on the film surface and at the same time, the increase of the absorbance at $\lambda >$ 600 nm is noticed. Prolonged irradiation yielded a clear silver mirror at the irradiated surface whose absorption spectrum was almost similar to that of thin silver film. Scanning electron micrographs of the ALAg film before and after UV irradiation are shown in Figure 4-8. Before irradiation, the surface appeared smooth. After prolonged irradiation, the film surface was densely covered with aggregated silver particles, which are the main product of photolysis in wet air at room temperature.

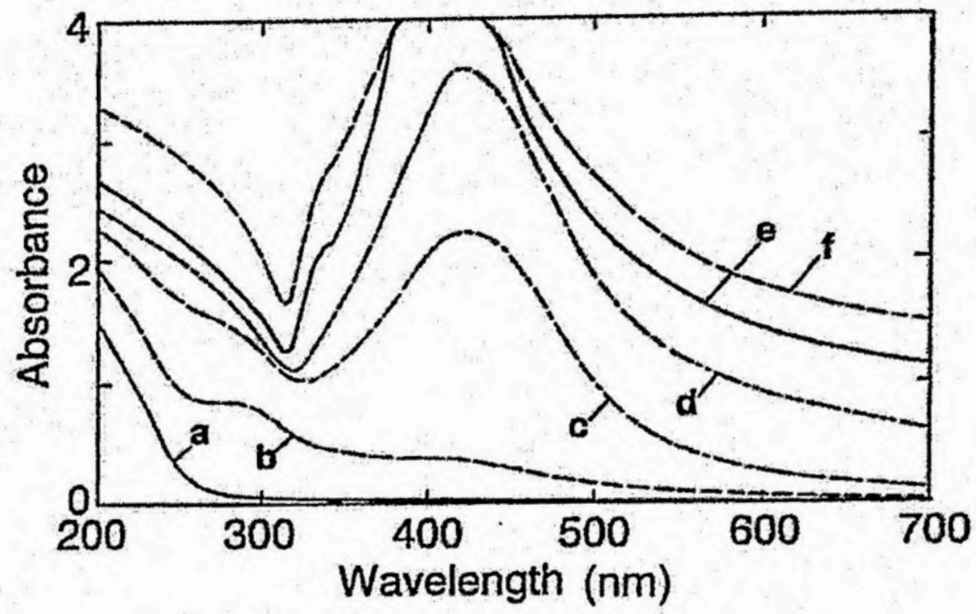

Figure 4-7. Absorption spectra of the ALAg film before and after UV irradiation. Irradiation time: (a) 0 min, (b) 5 min, (c) 10 min, (d) 20 min, (e) 60 min, (f) 120 min.

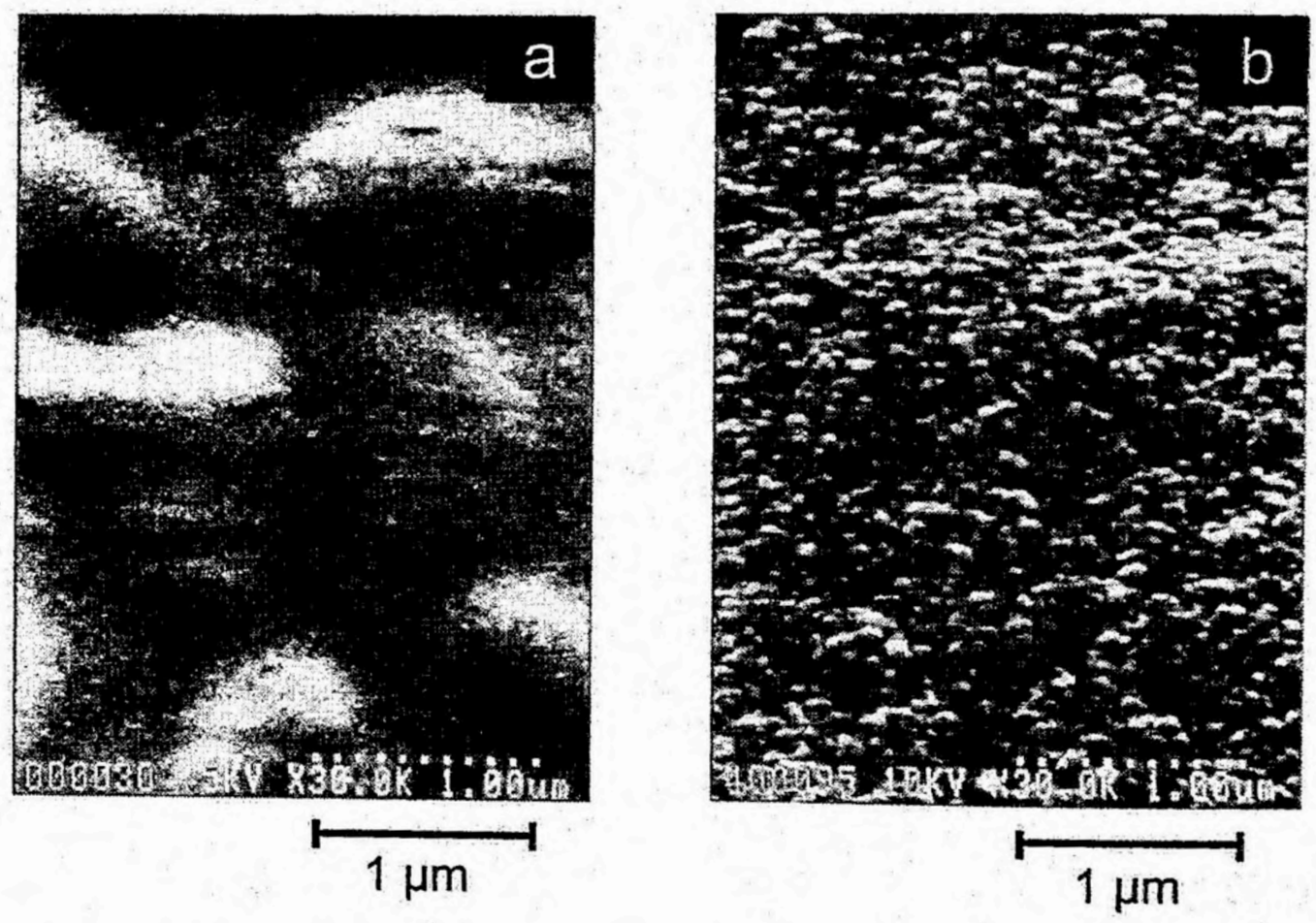

Figure 4-8. Scanning electron micrographs of the ALAg film. (a) Before irradiation. A thin layer of Pt/Pd was deposited on the film surface by sputtering. (b) After 120 min of irradiation with UV light. The Pt/Pd sputtering was not performed. The marker corresponds to 1 μm.

The author fabricated the reference film of ALNa on the circular Si wafer by dropping an aqueous solution of ALNa and drying. The ALNa film was subjected to irradiation with Ar-ion laser ($\lambda = 514.5$ nm) to diminish unspecified fluorescence of the film itself. After this treatment, the Raman spectrum was recorded (Figure 4-9). After an enlargement of the spectrum, the presence of many weak peaks are observed, aside from evident peaks of a fundamental band (522 cm^{-1}) and an overtone (950–982 cm^{-1}) of Si.[13,14] Among them, the band at 1415 cm^{-1} is

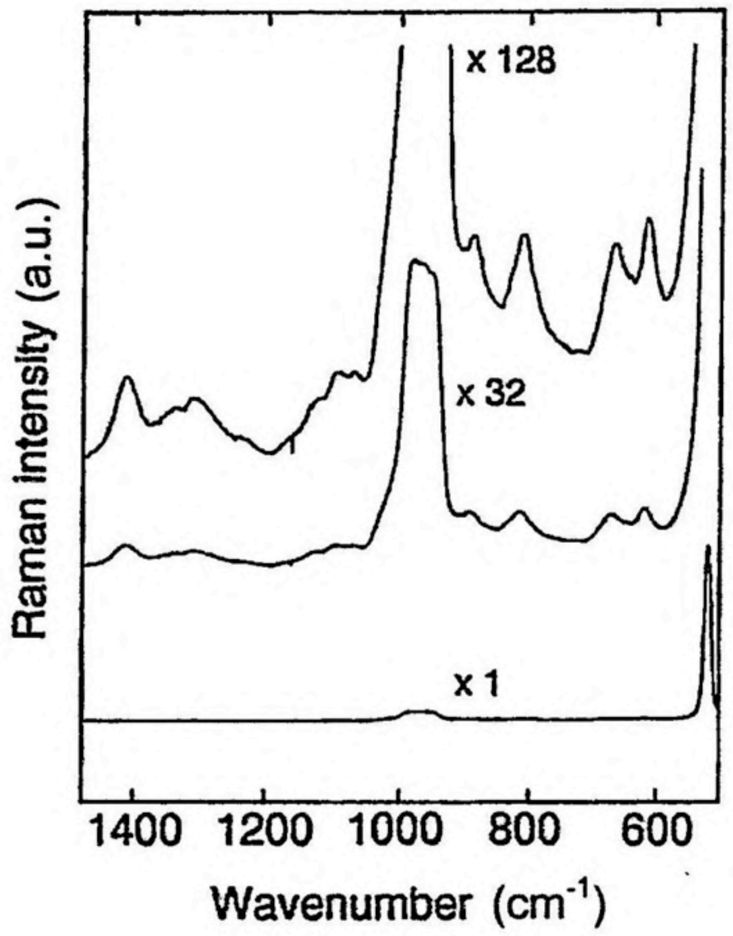

Figure 4-9. Raman spectrum of the ALNa film on the Si wafe. ×1, ×32, and ×128 in the figure indicate the magnitude of the enlargement.

assigned to symmetric COO^- stretching vibration and two bands at 675 and 624 cm^{-1} to deformation vibrations of the COO^- group, respectively.[12,25] The measurement of the Raman spectrum of the ALAg film was difficult before UV photolysis due to unspecified fluorescence. However, the Raman spectrum could be safely recorded after UV photolysis more than 5 min. Variation of the Raman spectra of the ALAg film with UV irradiation is shown in Figure 4-10. After 5-min irradiation, evident Raman bands were detected. 10-min irradiation resulted in an increase of Raman scattering. After irradiation for more than 20 min, the Raman intensity was gradually decreased. Raman bands around 1398–1405 cm^{-1}, 928–948 cm^{-1}, and 645–647 cm^{-1} correspond to $RCOO^-$ ions of silver alginate, i.e., symmetric COO^- stretching vibration, skeletal C-C stretching vibration adjacent to COO^- group, and deformation vibration of COO^- group, respectively.

The relative Raman intensity is defined as in the case of the CMCAg film. Due to the difficulty in measuring the Raman spectrum of the ALAg film before irradiation, the author has employed the ALNa film as a substitute, i.e., ALAg film for irradiation time, t = 0 min. Considering the intensity ratio of the Si overtone to the fundamental band (0.054) and the surface area of the Si wafer, the relative Raman intensity of symmetric COO^- stretching vibration at t = 0 (1415-cm^{-1} band) is 0.0067. The relative Raman intensities of three bands, symmetric COO^- stretching vibration (1398–1405 cm^{-1}), C-C (COO^-) stretching vibration

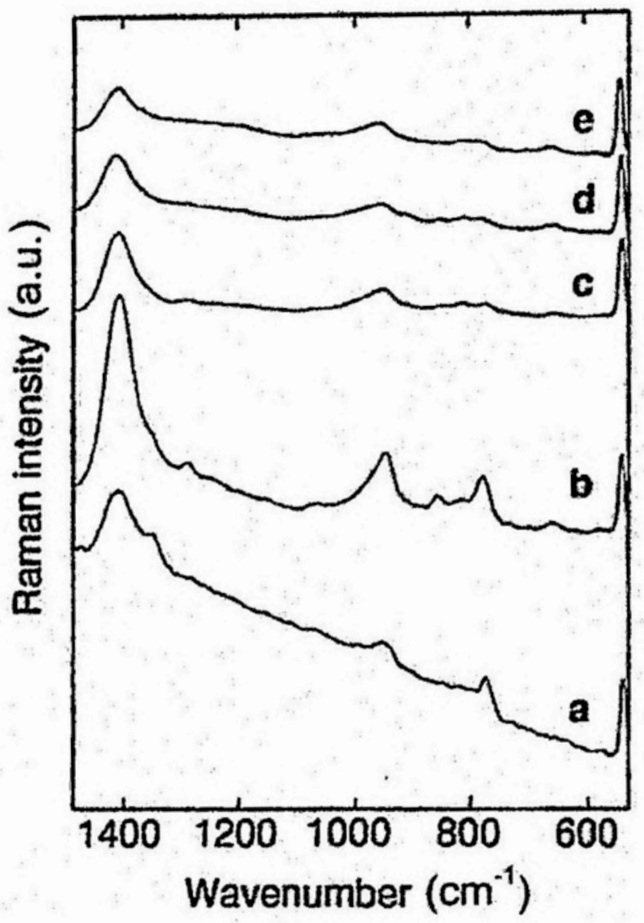

Figure 4-10. Variation of the Raman spectra of the ALAg film. Irradiation time: (a) 5 min, (b) 10 min, (c) 20 min, (d) 60 min, (e) 120 min. The spectra are given by using the fundamental band of Si as the intensity standard.

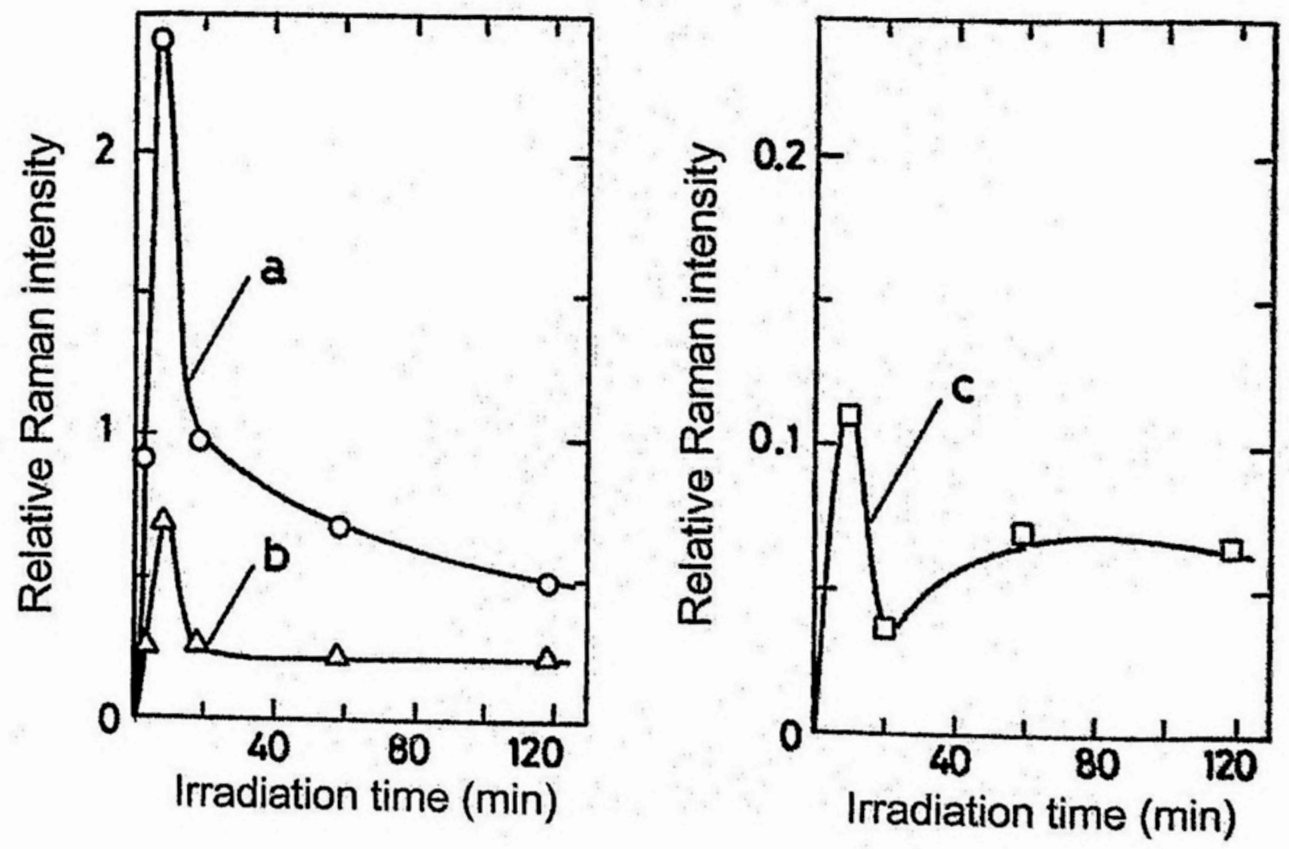

Figure 4-11. Variations of the relative Raman intensities of characteristic bands of the ALAg film with UV irradiation time. (a) symmetric COO^- stretching vibration (1398–1405 cm^{-1}), (b) C-C stretching vibration adjacent to COO^- group (928–948 cm^{-1}), (c) COO^- deformation vibration (645–647 cm^{-1}).

(928–948 cm^{-1}), COO^- deformation vibration (645–647 cm^{-1}), are plotted versus irradiation time in Figure 4-11. UV irradiation causes photolysis of silver alginate and the production of photolytic silver. As a result, the intensity of Raman scattering should decrease monotonically with irradiation time. On the other hand, similar to the CMCAg film, Figure 4-11 shows that the Raman intensity is increased by UV irradiation for 0–10 min. These observations demonstrate the realization of SERS in the ALAg film, too.

In this study, the author has focused on symmetric COO^- stretching vibration of silver alginate because SERS is most evident in this band. The relative Raman intensity I of symmetric COO^- stretching vibration has been evaluated. The author has tried to estimate the SERS enhancement factor just the same way as the previous section. A simple ratio of the relative Raman intensity of the ALAg film to the ALNa film is 136. To estimate γ to correct the number of COO^- ions contributing to Raman scattering, the author has assumed that a silver particle in the ALAg film is a sphere with a diameter of 10 nm or 40 nm, and that the particle is covered with a monolayer of carboxylate ions each of which occupies an area of 0.4 nm^2.[18,23] The corrected value of the SERS enhancement factor f are summarized in Table 4-2. f for $2a$ = 40 nm amounts to 1.1×10^5–1.9×10^5, which is in the same order to the CMCAg film photolyzed for 90–180 min. These results indicate the SERS effect is a common phenomenon for photolytic silver particles in high molecular weight carboxylic acids. Further, these values are not far from the usual value of 10^4–10^6 at the rough silver surface.[3]

f is increased by UV irradiation, attained to a maximum (t = 10 min), and then gradually

Table 4-2. Apparent SERS enhancement factor f of symmetric COO^- stretching vibration band of the ALAg film. The diameter of Ag particles $2a$ is either 10 nm or 40 nm

t	I	γ		f	
min		$2a$ = 10 nm	40 nm	$2a$ = 10 nm	40 nm
0	0.0067	1.0	1.0	1.0	1.0
5	0.91	0.0051	0.0013	2.7×10^4	1.1×10^5
10	2.4	0.0077	0.0019	4.7×10^4	1.9×10^5
20	0.97	0.0085	0.0021	1.7×10^4	6.8×10^4
60	0.68	0.0095	0.0024	1.1×10^4	4.4×10^4
120	0.50	0.011	0.0028	7.1×10^3	2.8×10^4

decreased after prolonged irradiation. As in the case of the CMCAg film, the increase of I and in $t = 0$–10 min is estimated to be in a close connection with the aggregation of silver particles. The author plots the electrical resistance R of the film surface versus irradiation time, together with the change of relative Raman intensity $\tilde{I}$ expressed relative to the maximum value of 2.4 (10-min irradiation) (Figure 4-12). R was decreased from 10^{10} Ω (before irradiation) to 10^5–10^7 Ω (after about 10-min irradiation), indicating the beginning of the contact of silver particles. It is likely that the increase of $\tilde{I}$ with irradiation from 5 to 10 min in Figure 4-12 is an example of further promotion of SERS by the aggregation of silver particles. The decrease of $\tilde{I}$ after irradiation of more than 20 min arises from the filter effect of photolytic silver as the same as CMCAg film. It has been proved that the silver salts of natural high molecular weight carboxylic acids are promising as a reagent to prepare small silver particles whose aggregation states could be monitored by Raman spectroscopy.

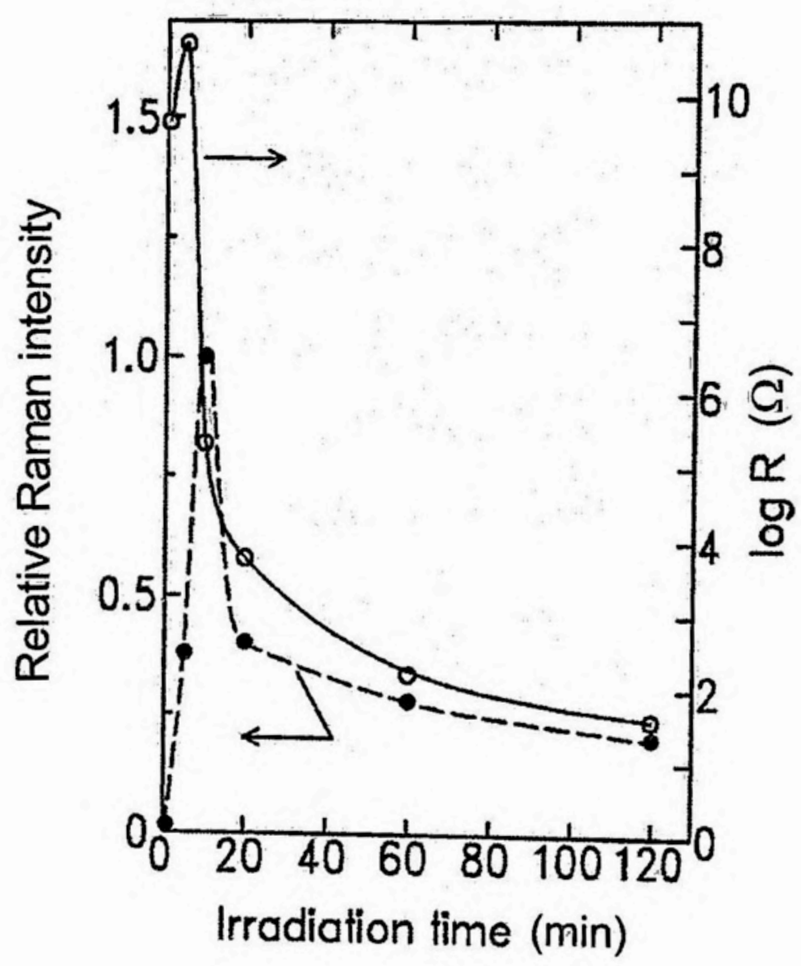

Figure 4-12. Changes of the relative enhancement factor $\tilde{I}$ and electrical sheet resistance R of the ALAg film with irradiation time. $\tilde{I}$ is given in arbitrary units.

4. 4 Summary

Raman scattering of the thin films of silver salt of high molecular weight carboxylic acids; carboxymethylcellulose (CMC) and alginic acid (AL) photolyzed with UV light has been studied. After UV irradiation, evident Raman bands related to $RCOO^-$ ions; symmetric COO^- stretching vibration (1390–1410 cm^{-1}), C-C (COO^-) stretching vibration (930–950 cm^{-1}), and

COO^- deformation vibration (640–650 cm^{-1}), were observed., manifesting the contribution of SERS. In the CMCAg film, the intensity of the symmetric COO^- stretching vibration band attained to the maximum after 180-min UV irradiation. At the same time, the electrical resistance of the film was decreased about 10^{-3}–10^{-2} times of unirradiated film. In the ALAg film, that band attained to the maximum after 10-min UV irradiation, in company with the reduction of electrical resistance by 10^{-5}–10^{-3}. These observations are closely related to the beginning of the contact of silver particles at the surface. When silver particles begin to aggregate, a contribution of multipole plasmon resonance to SERS becomes significant and causes the further promotion of SERS. In this sense, SERS is applicable as a probe to monitor the change of the aggregation state of silver particles. The maximum enhancement factor of 10^4–10^5 as estimated under several simplifying assumptions appeared to be in the same order reported by other research groups. After prolonged irradiation, the film surface changed into the clear silver mirror and the Raman intensity rather decreased due to the filter effect of deposited silver.

References

1. M. Fleischmann, P. J. Hendra, and A. J. McQuillan, *Chem. Phys. Lett.*, **26**, 163 (1971).
2. D. L. Jeanmaire and R. P. Van Duyne, *J. Electroanal. Chem.*, **84**, 1 (1977).
3. R. K. Chang and T. E. Furtak, *Surface Enhanced Raman Scattering*, Plenum Press, New York (1982).
4. J. A. Creighton, C. G. Blatchford, and M. G. Albrecht, *J. Chem. Soc. Faraday Trans. II*, **75**, 790 (1979).
5. D. Yogev and S. Efrima, *J. Phys. Chem.*, **92**, 5754, 5761 (1988).
6. J. E. Rowe, C. V. Shank, D. A. Zwemer, and C. A. Murray, *Phys. Rev. Lett.*, **44**, 1770 (1980).
7. A. M. Ahern and R. L. Garrell, *Anal. Chem.*, **59**, 2813 (1987).
8. F. -H. Haegel and A. Wokaun, *Chem. Phys. Lett.*, **157**, 328 (1989).
9. Y. Yonezawa, A. Takami, T. Sato, K. Yamamoto, T. Sasanuma, H. Ishida, and A. Ishitani, *J. Appl. Phys.*, **68**, 1297 (1990).
10. T. Miyama, Y. Yonezawa, T. Sato, J. Umemura, and T. Takenaka, *Chem. Lett.*, **1993**, 1537 (1993).
11. Y. Yonezawa, M. Kijima, and T. Sato, *Ber. Bunsenges. Phys. Chem.*, **96**, 1828 (1992).
12. E. Okamura, J. Umemura, and T. Takenaka, *J. Raman Spectroscopy*, **22**, 759 (1991).

13. J. P. Russell, *Appl. Phys. Lett.*, **6**, 223 (1965).

14. J. H. Parker Jr., D. W. Feldman, and M. Ashkin, *Phys. Rev.*, **155**, 712 (1967).

15. A. J. McQuillan and C. G. Pope, *Chem. Phys. Lett.*, **71**, 349 (1980).

16. T. W. Barret, *Spectrochim. Acta A*, **37**, 233 (1981).

17. J. H. Willey and R. H. Atalla, *Carbohydr. Res.*, **160**, 113 (1987).

18. M. Mabuchi, T. Takenaka, Y. Fujiyoshi, and N. Uyeda, *Surface Sci.*, **119**, 150 (1982).

19. O. Siiman, L. A. Bumm, R. Callagham, C. G. Blatchford, and M. Kerker, *J. Phys. Chem.*, **87**, 1014 (1983).

20. a) C. G. Blatchford, J. R. Campbell, and J. A. Creighton, *Surface Sci.*, **120**, 435 (1982).
    b) J. A. Creighton, *Surface Sci.*, **124**, 209 (1983).

21. M. Moskovits, *Rev. Mod. Phys.*, **57**, 783 (1985).

22. A. Wokaun, *Solid State Phys.*, **38**, 223 (1984).

23. M. Kerker, O. Siiman, L. A. Bumm, and D. -S. Wang, *Appl. Opt.*, **19**, 3253 (1980).

24. H. Ishida, H. Fukuda, G. Katagiri, and A. Ishitani, *Appl. Spectroscopy*, **40**, 322 (1986).

Chapter 5

Enhancement of Local Electric Field by a Metal Microsphere and Surface-Enhanced Raman Scattering of Silver Salts of High Molecular Weight Carboxylic Acids

5. 1 Introduction

Surface-enhanced Raman scattering (SERS); the molecules adsorbed at the surface of precious metals, such as Ag, Au, and Cu, display unusually strong Raman scattering, was discovered in the 1970s.[1] Although a number of theoretical models have been advocated as the mechanism of SERS, the electromagnetic mechanism and the chemical mechanism seem to be generally accepted. According to the electromagnetic mechanism, when UV-visible light is irradiated onto a coarse metal surface, surface plasmons (SP) are excited and very strong local electric field compared with the incident field is generated near the metal surface. The molecules adjacent to the metal surface are influenced by the local electric field in Raman scattering process, and consequently the Raman scattering cross-section of the molecule is enhanced significantly compared with that of the isolated molecule. Such effects of SP are not limited to Raman scattering. It is predicted theoretically that the existence of a coarse metal surface could bring about the enhancement of many other optical processes, such as absorption, fluorescence, energy transfer, and photochemical reactions of molecules. Actually, several research groups have reported on surface-enhanced electromagnetic process, surface-enhanced spectroscopy, and surface-enhanced photochemistry.[2,3] Especially, the applications of precious metal particles to the nonlinear optical materials and high-performance analytical devices have attracted much attention.[4,5]

Scattering of incidence plane electromagnetic wave by a single sphere can be analyzed by solving the basic equations of the Maxwell's electromagnetic field with suitable boundary conditions. Mie has obtained the analytical solutions of these problems and actually analyzed the spectroscopic properties of colloidal Au suspensions.[6] Sato et al. have examined scattering of the incident electromagnetic wave by metal, alloy and dielectric microspheres.[7] An approximate expression for the Mie's formula which expresses the extinction coefficient, the scattering coefficient and the absorption coefficient with the rational function of parameter α (which is defined by Eq. (4), later) has been proposed. The tractable formula has been applied to interpret the extinction spectra of the colloidal metals (Ag, Au, Pt) and their alloys in solutions. These calculations need only the information on asymptotic forms of scattering

electric and magnetic fields far from the sphere (wave zone, distance $r >>$ wavelength λ). O the other hand, in order to deal with the problems of the enhancement of the incid electromagnetic field by a metal microsphere, the information about the scattering electric an magnetic fields near the sphere surface are indispensable (near field zone, $r << \lambda$).

In this chapter, an effective enhancement factor Q_{NF} according to Mie and Messinger et al. has been introduced, and the enhancement of the incidence electric field by a Ag microsphere has been estimated.[8] Q_{NF} is a dimensionless quantity similar to the efficiency factors for extinction Q_{ext}, scattering Q_{sca}, and absorption Q_{abs} (Mie coefficients). In Chapter 4, Raman spectra of silver salts of high molecular weight carboxylic acids have been reported. Now, the author has attempted to interpret the enhancement of the Raman scattering of silver salts of high molecular weight carboxylic acids in terms of Q_{NF}.

5. 2 Method of Calculation

There have been many textbooks on the scattering problems of electromagnetic wave by spheres and spheroids.[9–11] In this work, the symbols have been taken from the Kerker's book.[11] The author shall analyze the scattering of linearly polarized monochromic plane by a sphere of radius a in an uniform medium (Figure 5-1). A center of the sphere (O) is located at the origin of the rectangular coordinates (x, y, z). The z and x axes are in parallel with the propagation direction of the wave and the electric field, respectively. The author has used the spherical coordinates (r, θ, ϕ) to represent an arbitrary position P. Time dependences of the electric and magnetic fields in the Maxwell equation are set equal to exp ($-i\omega t$), where an angular frequency of light is ω and i is an imaginary unit. The MKSA units have been used. The specific permeability of the medium and the sphere are equal to 1. Now, the sphere and the medium are discriminated by the subscript (1), (2), respectively and κ_1, κ_2, and k are defined by the dielectric constant $\varepsilon^{(1)}$, electric conductivity $\sigma^{(1)}$ of the sphere, and the dielectric constant of the medium $\varepsilon^{(2)}$.

Sphere

$$\kappa_1^{(1)} = i\omega\varepsilon^{(1)} + \sigma^{(1)}$$
$$\kappa_2^{(1)} = i\omega$$
$$k_1^{\,2} = -\kappa_1^{(1)}\kappa_2^{(1)}\mu_0$$

Medium (non-conductive)

$$\kappa_1^{(2)} = i\omega\varepsilon^{(2)}$$
$$\kappa_2^{(2)} = i\omega$$
$$k_2^{\,2} = -\kappa_1^{(2)}\kappa_2^{(2)}\mu_0$$

(1)

(μ_0 is permeability of free space.)

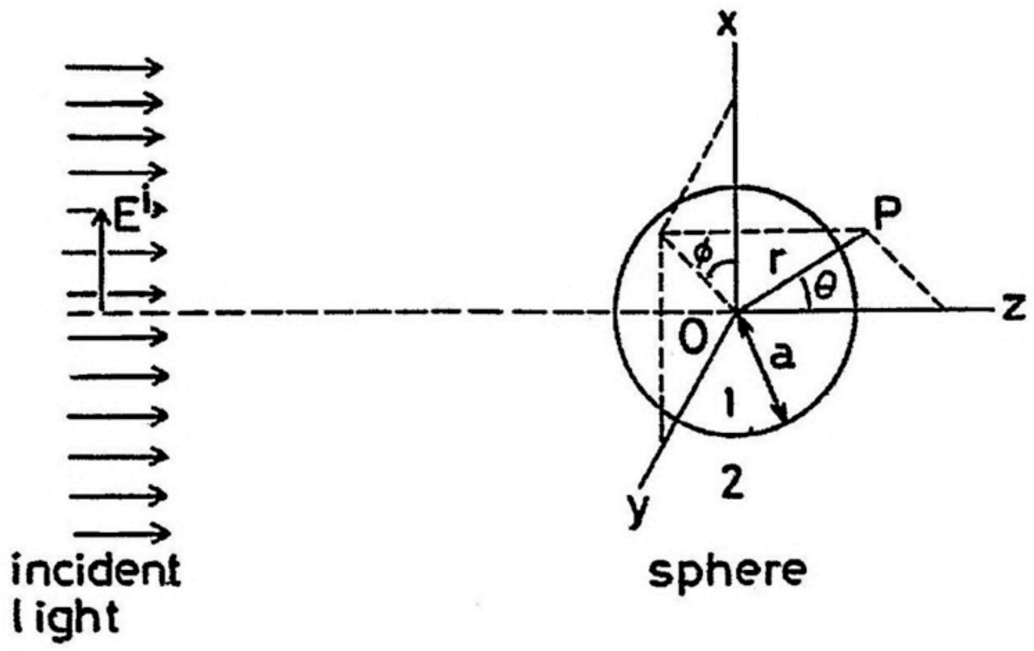

Figure 5-1. Geometry for scattering of a plane electromagnetic wave by a sphere. Incident wave travels along positive z-axis with electric vector polarized along x-axis. Particle with radius a has its center at origin (O). The position of the observer P is defined by the spherical coordinates (r, θ, ϕ). 1, 2 denote the sphere and the external medium, respectively.

The expansion coefficients a_n and b_n of the Debye potential of the scattering wave are determined by the boundary conditions. They are given by

$$a_n = \frac{\phi_n(\alpha)\phi_n'(\beta) - m_{12}\phi_n(\beta)\phi_n'(\alpha)}{\zeta_n(\alpha)\phi_n'(\beta) - m_{12}\phi_n(\beta)\zeta_n'(\alpha)}, \tag{2}$$

$$b_n = \frac{m_{12}\phi_n(\alpha)\phi_n'(\beta) - \phi_n(\beta)\phi_n'(\alpha)}{m_{12}\zeta_n(\alpha)\phi_n'(\beta) - \phi_n(\beta)\zeta_n'(\alpha)}. \tag{3}$$

Here, $(\ -\ )'$ express the differentiation with respect to each parameter. α and β are given by

$$\alpha = k_2 a, \quad \beta = k_1 a\ . \tag{4}$$

m_{12} is a complex refractive index of the sphere relative to the surrounding medium.

$$m_{12}^{\ 2} = \left(m_1^{\ 2} / m_2^{\ 2}\right) = \left(k_1^{\ 2} / k_2^{\ 2}\right) \tag{5}$$

Functions $\phi_n(z)$ and $\zeta_n(z)$ are Ricatti-Bessel functions, which are related to conventional spherical Bessel function of the first kind $j_n(z)$, and the spherical Bessel function of the 2nd kind $n_n(z)$ (n: positive integer).

$$\left.\begin{aligned}\phi_n(kr) &= krj_n(kr)\\ \chi_n(kr) &= -krn_n(kr)\\ \zeta_n(kr) &= \phi_n(kr) - i\chi_n(kr)\end{aligned}\right\} \tag{6}$$

As the spherical Hankel functions of the 1st and the 2nd kind, $h_n^{(1)}(z)$ and $h_n^{(2)}(z)$, are defined

$$\left.\begin{aligned}h_n^{(1)}(z) &= j_n(z) + in_n(z)\\ h_n^{(2)}(z) &= j_n(z) - in_n(z).\end{aligned}\right\} \tag{7}$$

$\zeta_n(kr)$ is related to $h_n^{(1)}(kr)$.

$$\zeta_n(kr) = krh_n^{(1)}(kr) \tag{8}$$

Mie's formula of the scattering cross section C_{sca}, the extinction cross section C_{ext}, and absorption cross section C_{abs} are given by the following formulas using a_n and b_n.[11]

$$C_{sca} = \frac{2\pi}{k_2^{\,2}}\sum_{n=1}^{\infty}(2n+1)\left(|a_n|^2 + |b_n|^2\right) \tag{9}$$

$$C_{ext} = \frac{2\pi}{k_2^{\,2}}\sum_{n=1}^{\infty}(2n+1)\mathrm{Re}(a_n + b_n) \tag{10}$$

The absorption cross section C_{abs} is given by subtraction of the scattering cross section C_{sca} from the total extinction cross section C_{ext}.

$$C_{abs} = C_{ext} - C_{sca} \tag{11}$$

Q_{sca}, Q_{ext}, and Q_{abs} follow from C_{sca}, C_{ext}, and C_{abs} divided by the geometrical cross section of the sphere (πa^2), respectively.

$$Q_{sca} = \frac{2}{a^2k_2^{\,2}}\sum_{n=1}^{\infty}(2n+1)\left(|a_n|^2 + |b_n|^2\right) \tag{12}$$

$$Q_{ext} = \frac{2}{a^2k_2^{\,2}}\sum_{n=1}^{\infty}(2n+1)\mathrm{Re}(a_n + b_n) \tag{13}$$

$$Q_{abs} = Q_{ext} - Q_{sca} \tag{14}$$

The author has introduced the effective enhancement factor Q_{NF} of the local electric field at the distance r from the center of the sphere. Q_{NF} is expressed as the sum of the vertical component Q_{NF}^{V} and the horizontal component Q_{NF}^{H} with respect to the sphere surface (Appendix).

$$Q_{NF} = Q_{NF}{}^{V} + Q_{NF}{}^{H} \tag{15}$$

$$Q_{NF}{}^{V} = \frac{2}{k_2{}^2 a^2}\sum_{n=1}^{\infty}(2n+1)n(n+1)\left|a_n\right|^2 \frac{1}{k_2{}^2 r^2}\zeta_n(k_2 r)\,\zeta_n^{\bullet}(k_2 r) \tag{16}$$

$$Q_{NF}{}^{H} = \frac{2}{k_2{}^2 a^2}\sum_{n=1}^{\infty}(2n+1)\left\{\frac{1}{k_2{}^2}\left|a_n\right|^2 \frac{d\zeta_n(k_2 r)}{dr}\frac{d\zeta_n^{\bullet}(k_2 r)}{dr} + \left|b_n\right|^2 \zeta_n(k_2 r)\,\zeta_n^{\bullet}(k_2 r)\right\} \tag{17}$$

Messinger et al. have obtained the formula similar to the Q_{NF} at the sphere surface ($r = a$).[8] The formulas (15)–(17) are more general because they are verified for arbitrary r. They have applied their formula to SERS of Ag, Au and Cu particles in aqueous solutions.[8] Wang has interpreted the structure resonance of the emission spectrum of the μm-sized semiconductor sphere according to Messinger's formula.[12] However, there have been few reports to evaluate Q_{NF} of metal particles with a view of the direct comparison with the experimental results of SERS.

The calculations of coefficients a_n and b_n in Eqs. (2) and (3) were performed in the same way of Sato et al.[7] The author took two or three term of n in the series expansion of the denominator and the numerator of a_n and b_n.[7] The spherical Bessel functions, the spherical Neumann functions, as well as the spherical Hankel functions were expressed by elementary functions. When $|z|$ was very small, the series expansion of spherical Bessel functions, spherical Neumann functions, and spherical Hankel functions were employed. The formulas of $\zeta_n(kr)$, $d\zeta_n(kr)/dr$ used for the calculation of Q_{NF} are summarized in Table 5-1. The complex refractive index of Ag for varying wavelengths was taken from the previous paper.[7] The refractive index of the polymer was assumed to be 1.5.[13] The wavelength region of calculations was λ = 300–700 nm.

5. 3 Results

In the first place, conventional efficiency factors Q_{ext}, Q_{sca}, and Q_{abs} of the Ag microsphere in the polymer film were calculated. Dependences of Q_{ext}, Q_{sca}, and Q_{abs} on the wavelength for the Ag sphere with a diameter of $2a$ = 10–200 nm are shown in Figure 5-2. In the cases of $2a$ = 10 nm and 40 nm, Q_{ext} has a single sharp peak. The peak position for the $2a$ = 10-nm particle is near λ = 420 nm, where $Q_{ext} \sim Q_{abs} = 10 >> Q_{sca}$. For the particle with $2a$ = 40 nm, Q_{ext} is more than 19 and Q_{sca} is larger than Q_{abs} at the peak position ($\lambda \sim$ 440 nm). Two broad peaks appear for $2a$ = 200 nm. They are at λ = 460 nm and 550 nm. Q_{ext} and Q_{sca} are about 5.8, while Q_{abs} is very small at λ = 460 nm.

Table 5-1. Supplementary table of $\zeta_n(kr)$ (Eq. (8)) and $d\zeta_n(kr)/dr$ for $n = 0, 1, 2, 3$.

n	$\zeta_n(kr)$
0	$\sin\theta - i\cos\theta$
1	$\left(-\frac{1}{\theta}\right)\times\{(\theta\cos\theta-\sin\theta)+i(\theta\sin\theta+\cos\theta)\}$
2	$\left(-\frac{1}{\theta^2}\right)\times\{(\theta^2\sin\theta+3\theta\cos\theta-3\sin\theta)+i(3\theta\sin\theta-\theta^2\cos\theta+3\cos\theta)\}$
3	$\left(-\frac{1}{\theta^3}\right)\times[\{(15\theta-\theta^3)\cos\theta-(15-6\theta^2)\sin\theta\}+i\{(15\theta-\theta^3)\sin\theta+(15-6\theta^2)\cos\theta\}]$

n	$\frac{d\zeta_n(kr)}{dr}$
0	$k(\cos\theta+i\sin\theta)$
1	$\left(\frac{1}{\theta^2}\right)\times\{k(\theta^2\sin\theta+\theta\cos\theta-\sin\theta)+ik(\theta^2\cos\theta-\cos\theta-\sin\theta)\}$
2	$\left(\frac{1}{\theta^3}\right)\times\left\{\begin{array}{l}k(3\theta^2\sin\theta-\theta^3\cos\theta+6\theta\cos\theta-6\sin\theta)\\ -ik(3\theta^2\cos\theta+\theta^3\sin\theta-6\cos\theta-6\theta\sin\theta)\end{array}\right\}$
3	$\left(\frac{1}{\theta^4}\right)\times\left\{\begin{array}{l}k(45\theta\cos\theta-6\theta^3\cos\theta-45\sin\theta+21\theta^2\sin\theta-\theta^4\sin\theta)\\ -ik(6\theta^3\sin\theta-45\cos\theta+21\theta^2\cos\theta-45\theta\sin\theta-\theta^4\cos\theta)\end{array}\right\}$

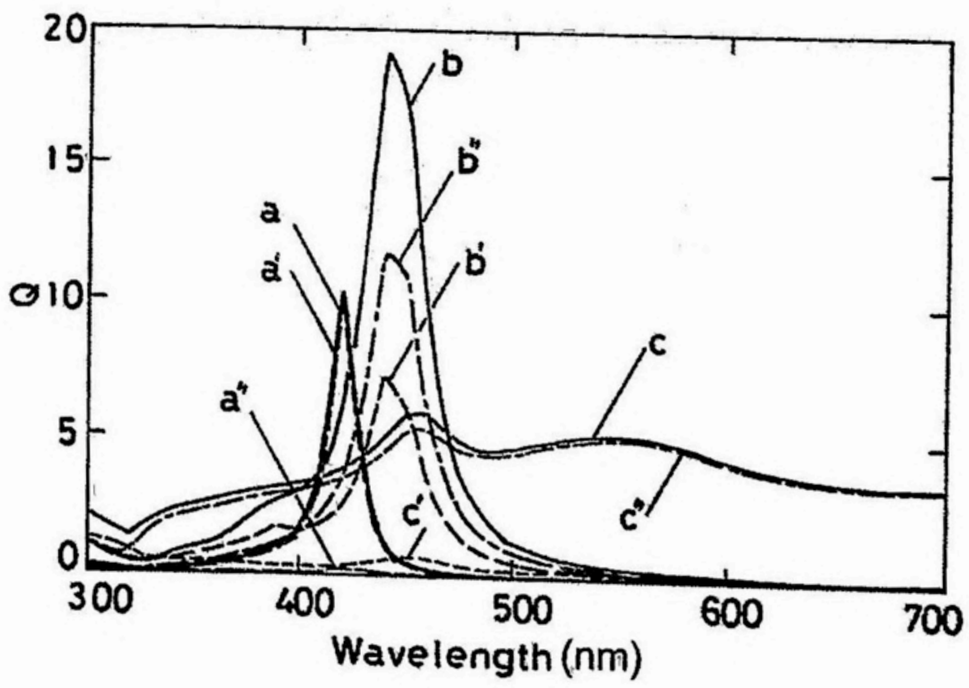

Figure 5-2. Extinction Q_{ext} (a, b, c, ———), absorption Q_{abs} (a', b', c', – – – –), and scattering Q_{sca} (a", b", c", ·····) efficiency factors of Ag spheres in polymer matrix. Diameter $2a$: (a), (a'), (a") 10 nm, (b), (b'), (b") 40 nm, (c), (c'), (c") 200 nm.

Dependences of Q_{NF} at the surface of Ag microsphere ($r = a$) on the wavelength are given in Figure 5-3. It has been shown that the wavelength dependence of Q_{NF} is similar to that of Q_{ext}. The peak position of Q_{NF} is shifted from $\lambda = 420$ nm to longer wavelengths with increasing particle diameter. When particle diameter is more than 100 nm, two peaks at $\lambda \sim 430$ nm and 580 nm are noticed. Q_{NF} at the peak position is about 3000 for $2a = 20$ nm. When particle diameter becomes larger, Q_{NF} is decreased to about 65 ($\lambda = 460$ nm) for $2a = 200$ nm.

Q_{NF} at the sphere surface was divided into the components $Q_{NF}{}^{V}$ and $Q_{NF}{}^{H}$, and the wavelength dependence of each component is given in Figure 5-4. The wavelength dependences of $Q_{NF}{}^{V}$ and $Q_{NF}{}^{H}$ are almost the same as Q_{NF}, and the ratio $\eta = (Q_{NF}{}^{V}/Q_{NF}{}^{H})$ is larger than 1. The values of η at the peak position of Q_{NF} are 2.0 for particle $2a = 10$ nm, 2.8 for $2a = 40$ nm, and 3.0 for $2a = 200$ nm, respectively. Dependences of Q_{NF}, $Q_{NF}{}^{V}$, and $Q_{NF}{}^{H}$ on the distance d from the sphere surface are summarized in Figure 5-5. Here, the wavelength of incident light was chosen $\lambda = 420$, 440, and 460 nm, which is near the peak position of Q_{NF} for the Ag sphere with $2a =$ 10, 40, and 200 nm, respectively. In the case of $2a = 10$ nm, Q_{NF} and η at the sphere surface ($d = 0$ nm) are 4400 and 2.1, respectively. Q_{NF} and η are 57 and 2.5 ($d = 10$ nm), and 0.25 and 0.10 ($d = 200$ nm), respectively. When $2a = 40$ nm, Q_{NF} and η are 1100 and 2.8 at the sphere surface. They are $Q_{NF} = 250$ and $\eta = 3.7$ ($d = 10$nm), and $Q_{NF} = 13$ and $\eta = 0.10$ ($d = 200$ nm). In the case of $2a = 200$ nm, Q_{NF} and η are 67 and 2.9 at the sphere surface. They are 39 and 3.2 ($d = 10$ nm), and 6.0 and 0.22 ($d = 200$ nm), respectively. Q_{NF} of Ag microspheres with $2a = 10$–40 nm is decreased to several % of that at the surface ($d = 0$ nm), when d is as large as the particle diameter.

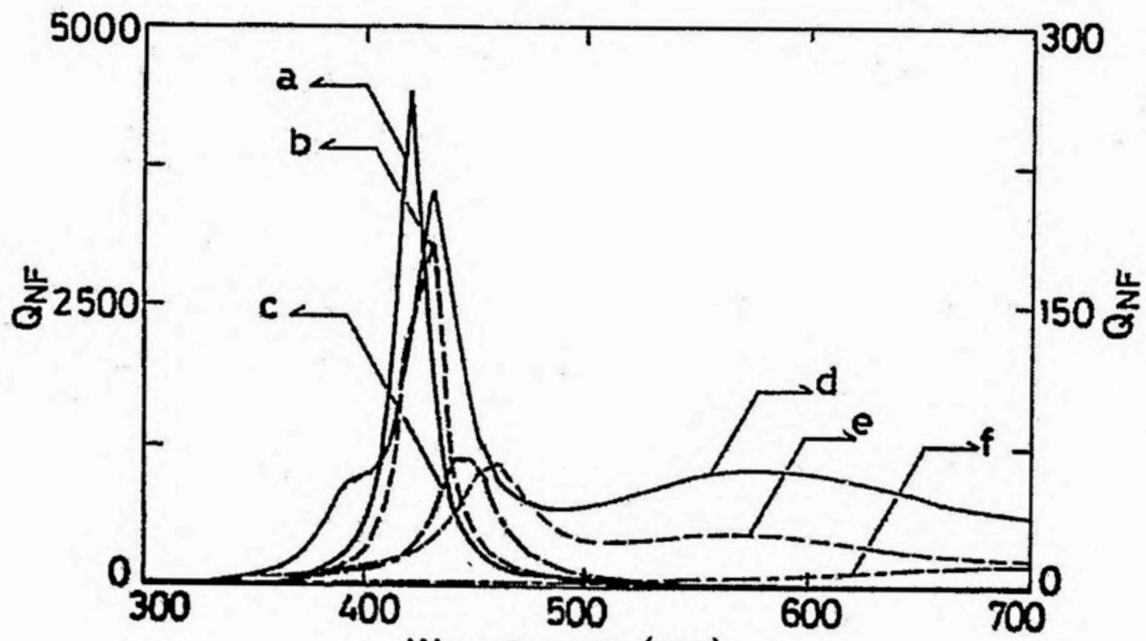

Figure 5-3. Effective enhancement factor Q_{NF} of Ag spheres in polymer matrix evaluated at sphere surface ($d = 0$ nm). Diameter $2a$: (a) 10 nm, (b) 20 nm, (c) 40 nm, (d) 100 nm, (e) 200 nm, (f) 400 nm.

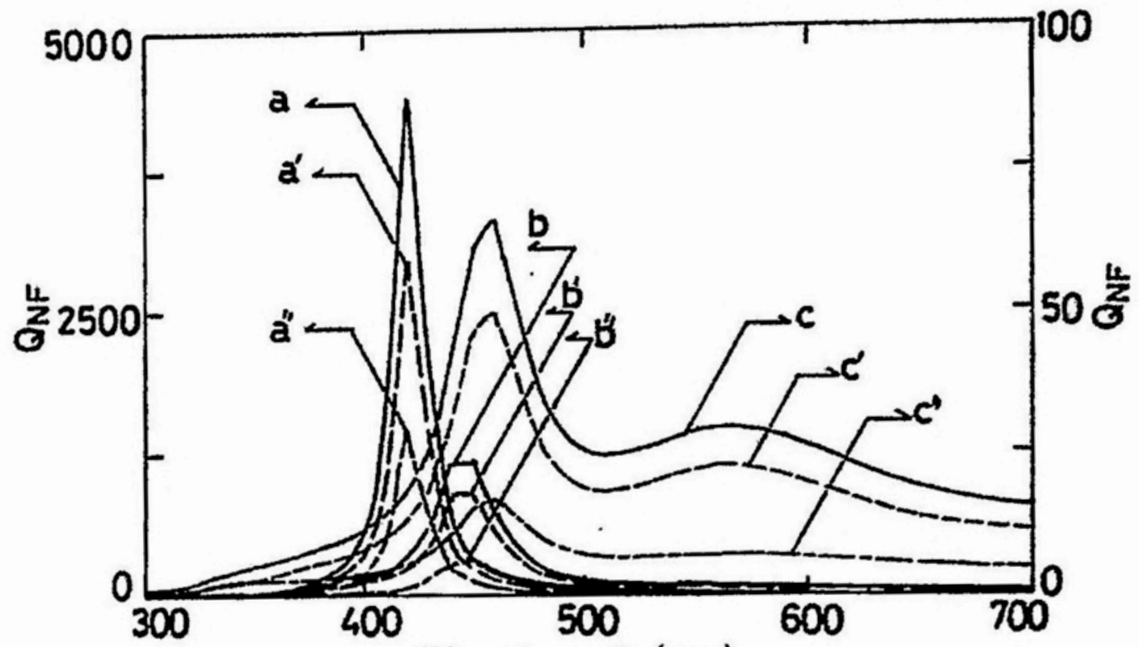

Figure 5-4. Decomposition of enhancement factor Q_{NF} (a, b, c, ———) of Ag spheres in polymer matrix into vertical $Q_{NF}{}^{V}$ (a', b', c', – – – –) and horizontal $Q_{NF}{}^{H}$ (a", b", c", ·····) components evaluated at the sphere surface ($d = 0$ nm).

Diameter $2a$: (a), (a') (a") 10 nm, (b), (b'), (b") 40 nm, (c), (c'), (c") 200 nm.

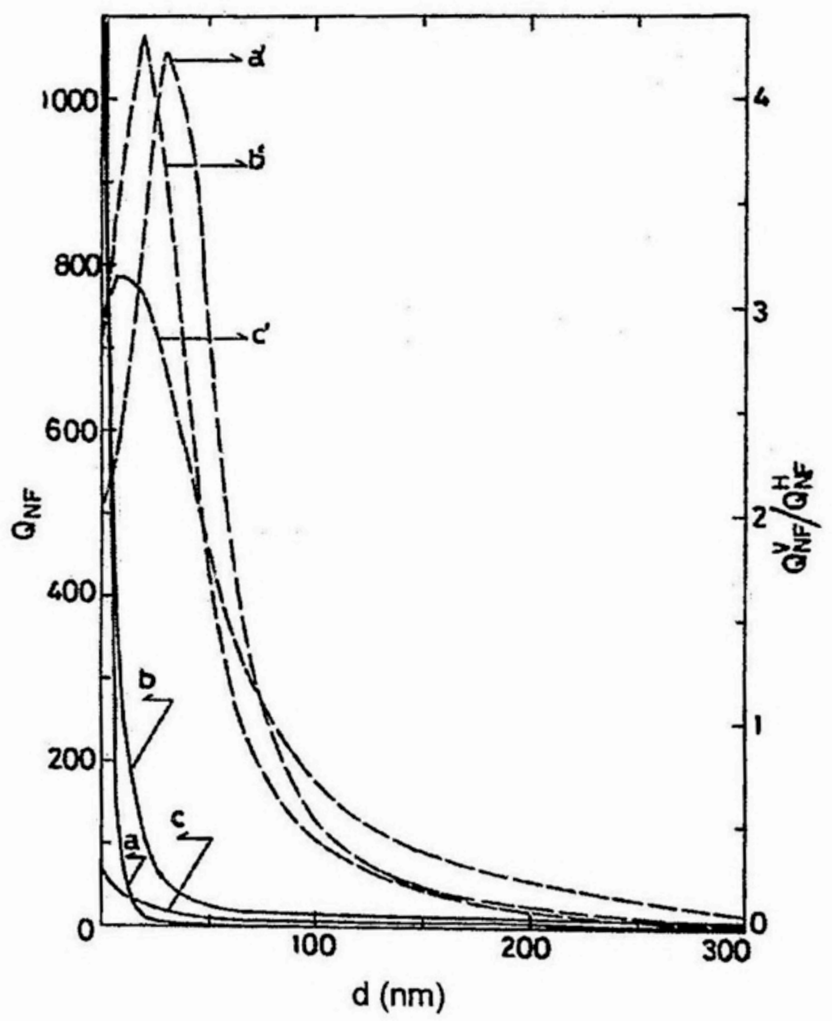

Figure 5-5. Dependences of enhancement factor Q_{NF} and its vertical $Q_{NF}{}^{V}$ and horizontal $Q_{NF}{}^{H}$ components on the distance d from the surface of Ag sphere in polymer matrix.

(a), (a') Diameter $2a = 10$ nm, incident wavelength $\lambda = 420$ nm,

(b), (b') Diameter $2a = 40$ nm, incident wavelength $\lambda = 440$ nm,

(c), (c') Diameter $2a = 200$ nm, incident wavelength $\lambda = 460$ nm,

a, b, c (———): Q_{NF}, a', b', c' (– – – –): Ratio $\eta = (Q_{NF}{}^{V}/Q_{NF}{}^{H})$.

5. 4 Discussion

The author has tried to discuss the Raman spectra of the CMCAg and ALAg films in Chapter 4 from the standpoint of the electromagnetic mechanism of SERS. According to Figure 5-3, the peak wavelength of Q_{NF} of the Ag particles with $2a$ = 10–200 nm ranges from λ = 420 to 460 nm. This wavelength is in considerably shorter than that of the excitation wavelength (λ = 514.5nm) used for measurements of Raman spectra. So that, the distance dependences of Q_{NF}, $Q_{NF}{}^{V}$, and $Q_{NF}{}^{H}$ at the incident wavelength λ = 510 nm were examined. The wavelength λ = 510 nm was selected because it is near the excitation wavelength of λ = 514.5nm. The results are given in Figure 5-6. In the case of the Ag microspheres of $2a$ = 10-nm size, Q_{NF} = 55, η = 2.0 at the sphere surface (d = 0) and Q_{NF} = 0.69 and η = 2.3 at d = 10 nm. In the case of $2a$ = 40 nm, Q_{NF} = 95, η = 2.6 at d = 0 and Q_{NF} = 2.1 and η = 3.5 at d = 40 nm. In the case of $2a$ = 200 nm, Q_{NF} = 5.1, η = 0.17 at d = 0 and Q_{NF} = 24, η = 2.9 at d = 200 nm.

for λ = 510 nm are considerable smaller than those for the incident wavelength near the eak position of Q_{NF} (Figure 5-5). It has been observed in Figure 5-6 that Q_{NF} is also reduced to several % of that at d = 0 when d is in the order of $2a$.

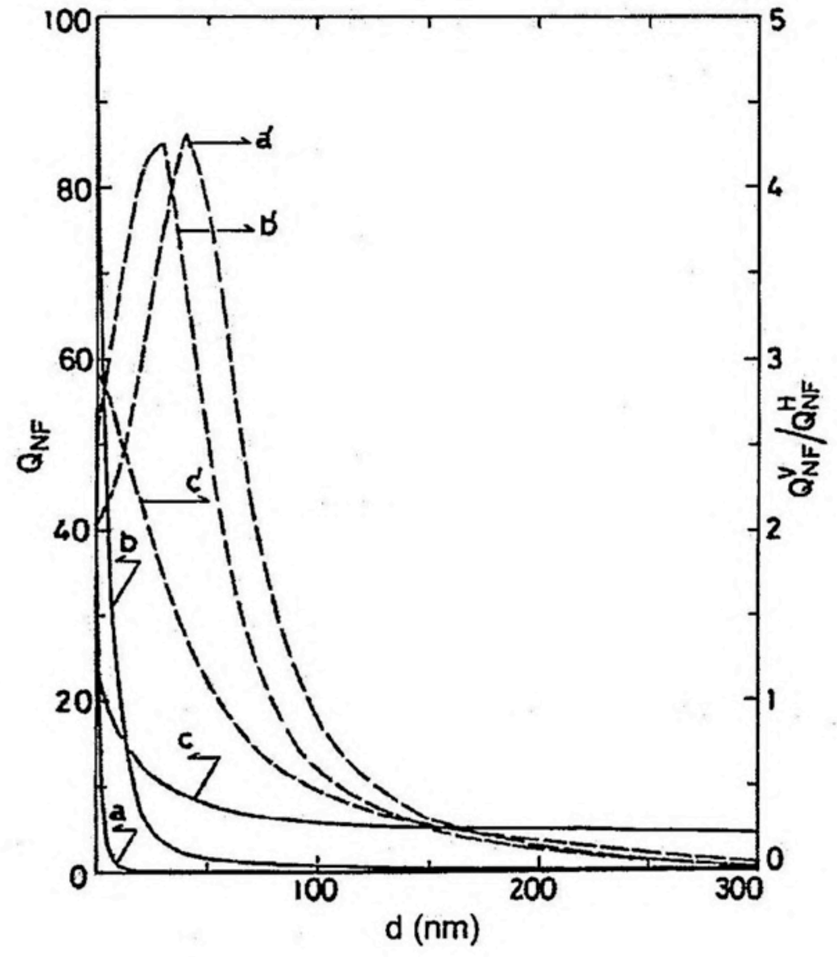

Figure 5-6. Dependences of enhancement factor Q_{NF} and its vertical $Q_{NF}{}^{V}$ and horizontal $Q_{NF}{}^{H}$ components on the distance d from the surface of Ag sphere in polymer matrix.

Diameter $2a$: (a), (a') 10 nm, (b), (b') 40 nm, (c), (c') 200 nm,

a, b, c (———): Q_{NF}, a', b', c' (– – – –): Ratio $\eta = (Q_{NF}{}^{V}/Q_{NF}{}^{H})$.

Incident wavelength λ = 510 nm.

Kerker et al. have dealt with SERS of the molecules adsorbed at the single sphere by exact classical electrodynamical model.[14] In their model, not only scattering of the incidenc plane wave by a sphere, the electromagnetic radiation from an oscillating dipole (molecule) and the scattering by the sphere are treated. Furthermore, the difference of the frequencies of the incidence light and Raman scattering light is also taken into account. However, it would be not suitable for the qualitative consideration of the enhancement of the local electric field on SERS because of the complicated calculations. Therefore, the author has examined the usefulness of the tractable factor Q_{NF}. According to a former papers on SERS of citric acid ions adsorbed at the Ag and Au colloids,[15,16] it is believed that carboxyl groups of the citric acid may adsorb at the Ag particles as COO^- form. Considering the distance dependence of Q_{NF} (Figure 5-6), this model agrees with the experimental observations that the strong SERS is obtained especially in the bands related to COO^-; symmetric stretching vibration and deformation vibration of COO^-, and C-C (COO^-) stretching vibration. In the Raman spectra of the CMCNa and ALNa films, a symmetric COO^- stretching vibration and two bands of deformation vibrations of COO^- are observed with similar intensity. On the other hand, in the silver salt films photolyzed with UV light, the symmetric COO^- stretching vibration is particularly remarkable. Considering the molecular structure of COO^- ion, it is plausible that the COO^- ions have a strong tendency to adsorb at the silver surface with a line segment which ties two O atoms parallel to the surface, and a line segment which connects the middle point between two O atoms and C atom vertical to the surface. Here, paying attention to $\eta > 1$, such an orientation of COO^- ions would be advantageous to the enhancement of the symmetric COO^- stretching vibration by the electromagnetic mechanism. Considering the distance dependence of Q_{NF}, the enhancement of the Raman scattering assigned to the pyranose ring, which is not in direct contact with the silver surface, would be weaker than that of COO^-.

The influence of the increased local electric field on the Raman scattering has to be considered twice; excitation and Raman scattering. They can be estimated by the square of Q_{NF} at the excitation wavelength.[12] Therefore, the author has compared $|Q_{NF}|^2$ in $\lambda = 510$ nm and the SERS enhancement factor f experimentally obtained in Chapter 4. $|Q_{NF}|^2$(s) on the sphere surface are 3.0×10^3 ($2a = 10$ nm), 9.0×10^3 (40 nm), and 5.9×10^2 (200 nm). The author has estimated f for the CMCAg film photolyzed for 30 min and for the ALAg film photolyzed for 5 min under the assumption that the diameter of Ag particles is 10–40 nm (Tables 4-1 and 4-2 in Chapter 4). It has been shown that f is 5 to 10 times larger than $|Q_{NF}|^2$. Kerker et al. have reported from the actual measurements by using excitation wavelength $\lambda = 514.5$ nm that the

SERS enhancement factor of citric acid adsorbed at the surface of colloidal Ag is 10–100 times of the theoretical value.[15] Therefore, it could be stated that $|Q_{NF}|^2$ is useful at least as a qualitative measure of the SERS enhancement factor.

The intensities I of the Raman bands are strongest at the irradiation time of 180 min (CMCAg film), and 10 min (ALAg film), respectively. At that time, f is 20–30 times larger than $|Q_{NF}|^2$. If Ag microspheres of the same size are formed as a result of UV photolysis and the increase of the amount of photolytic silver ΔN_{Ag} is equivalent to the increase in the number of the spatially isolated silver spheres, the ratio $I/\Delta N_{Ag}$ should be constant irrespective of irradiation time and then begins to decrease due to the filter effect of photolytic silver after a prolonged irradiation. Actually, the ratio $I/\Delta N_{Ag}$ is rather increased from 1.5 (30 min) to 6.7 (180 min), and then decreased to 1.5 (300 min) and 0.73 (600 min) in the case of the CMCAg film. For the ALAg film, it is increased from 3.6 (5 min) to 6.3 (10 min), and after that, decreased to 2.3 (20 min) and 0.96 (120 min). The decrease in $I/\Delta N_{Ag}$ after the long time irradiation would be caused by the filter effect. On the other hand, the existence of a maximum value of $I/\Delta N_{Ag}$, together with the decrease of the electric resistance of the film surface at the same time region (Figures 4-6 and 4-12 in Chapter 4) would indicate that the aggregation of Ag particles has an important effect on SERS.

There have been no reports that the aggregation of metal particles in a polymer film has profound effects on the Raman scattering. On the other hand, there have been several reports in the solution systems. Creighton et al. have observed the aggregation of Au colloids and the increase in SERS in the colloidal Au solutions added with pyridine.[17] Mabuchi et al. have examined the influence of aggregation of colloidal Au by aging on SERS of citric acid.[16] They have proposed, when the gold microspheres are aggregated, the electric field is enhanced more than being isolated, resulting in the increase in SERS. According to these studies, it is reasonable that further enhancement of local electric field is induced by the aggregation of Ag particles in the CMCAg and ALAg films. However, it is not easy to estimate quantitatively the variations of the local electric field by the aggregation of Ag particles. Then, the author will try qualitative estimation of correction coefficient Θ which expresses the aggregation qualitatively according to Wolkow & Moskovits.[18]

$$\Theta = 1/(1 - qG) \tag{18}$$

$$G = (\varepsilon_M - \varepsilon)/(\varepsilon_M + 2\varepsilon) \tag{19}$$

Here, q is a volume fraction of silver. ε_M and ε are complex dielectric constants of Ag and the medium (2.25), respectively. The effective enhancement factor $\tilde{Q}_{\mathrm{NF}}$ including the aggregati effect is given by the following formula.

$$\tilde{Q}_{\mathrm{NF}} = \Theta^2 Q_{\mathrm{NF}} \tag{20}$$

The author has calculated Θ^2 for $\lambda = 510$ nm and $q = 0$–0.3. Θ^2 were 1.0 (for $q = 0$), 1.8 ($q =$ 0.1), 4.2 ($q = 0.2$), and 19 ($q = 0.3$). These results may indicate that when q increases from 0 to 0.3, $|Q_{\mathrm{NF}}|^2$ is increased by 10^1 to 10^2 times. Thus, although such estimation is very rough, it can reproduce the increase in f to some extent. That is, the aggregation of Ag particles could bring about the increase in f. These estimations would be not valid for larger q because Q_{NF} is originally calculated under the assumption that the Ag particle is isolated in a medium. More exactly, the author has to treat the interaction between the randomly dispersed aggregated metal particles and electromagnetic waves from the first-principle. Such problems have been intensively studied in the field of nonlinear optics,[19] which is beyond the scope of the present study.

After a prolonged irradiation, the SERS enhancement factor is reduced by the "filter effect" of aggregated silver particles at the surface of polymer films. Our research group has carried out preliminary measurements of SERS and the nonlinear optical effect of Ag colloids formed by UV photolysis of an aqueous solution containing both $AgClO_4$ and the ALNa as a protective agent. In the Raman spectrum of the solution photolyzed with UV light, the strong SERS effect has been observed. The enhancement factor of the symmetric COO^- stretching vibration (1405 cm^{-1}) is estimated by about 1×10^5, when a particle diameter $2a = 40$ nm. This value is very close to f of the ALAg film (5-min photolysis). The enhancement factor amounts to about 2×10^6, when photolysis of the solution is continued until the aggregation of Ag particles occurs. As the absorbance of excitation light and the Raman scattering light is low in the solution system, the influence of a filter effect is negligible and the author can successfully observe the enhancement induced by the aggregation of Ag particles. These results may be a supporting evidence of "further enhancement of SERS by aggregation of silver particles" in the CMCAg and ALAg films.

The author has shown that Q_{NF} is useful to predict SERS by electromagnetic mechanism. Because Q_{NF} can be easily obtained from the usual Mie coefficients, it is applicable for the diverse surface-enhanced electromagnetic process as well. Surface-enhanced electromagnetic processes, surface-enhanced spectroscopy, and surface-enhanced photochemistry caused by the

interaction of metal particles with light would provide many interesting subjects for the development of optoelectronic devices, imaging materials, and the applications to material analysis.[20–23]

5. 5 Summary

The author has defined the effective enhancement factor Q_{NF} of the local electromagnetic field, and calculated the Q_{ext}, Q_{sca}, Q_{abs}, and Q_{NF} of Ag microspheres in a polymer film. The author have proposed an explicit formula of Q_{NF} useful for arbitrary distance r ($\geq a$) from the center of the microsphere. The surface plasmon (SP) peak appeared at the wavelemgth $\lambda = 420$ nm for particle diameter $2a = 10$ nm, $\lambda = 440$ nm for $2a = 40$ nm, $\lambda = 460$ nm and 550 nm for $2a = 200$ nm in the absorption spectra of the Ag microsphere. Q_{NF} at the sphere surface ($r = a$) at these wavelengths are ≥ 4000 (10 nm), ≥ 1000 (40 nm), and < 100 (100 nm), respectively. Especially, Q_{NF} is quite larger than Q_{sca} for the particle with $2a$ less than 40 nm. When the distance d from the sphere surface is in the order of particle diameter, Q_{NF} is decreased to several % of the maximum value. In the distance far from the surface ($d >> a$), $Q_{NF}{}^{V}$ becomes to be zero and $Q_{NF}{}^{H}$ is reduced to Q_{sca}. Based on the calculation, it is proposed that the Ag particles in a polymer film can display a number of surface enhanced electromagnetic processes. The author has estimated the SERS enhancement factor f of the silver salt films of high molecular weight carboxylic acids in Chapter 4. Q_{NF} has been compared with f. Q_{NF} of $2a$ = 10–40 nm particles is 55–95, and $|Q_{NF}|^2$ is (3–9) $\times 10^3$ for $\lambda = 510$ nm. Although $|Q_{NF}|^2$ is 1/10–1/5 of f, Q_{NF} is useful for a qualitative measure of the enhancement factor of SERS. The Raman scattering becomes maximum at the irradiation time of 180 min for the CMCAg film and 10 min for the ALAg film, respectively. It is due to the aggregation of silver particles in the film. The local electric field enhancement by the aggregation of silver particles was evaluated using the correction coefficient Θ. When the volume fraction of silver increased from 0 to 0.3, Θ^2 increased 1–20, resulting the increase in $|\tilde{Q}_{NF}|^2$ by $10^1 - 10^2$ times.

5. 6 Appendix

The quantity Σ_{NF} obtained by the fallowing angle integration of the scalar product of the electric field E^S of the scattering wave at the position r ($\geq a$) from the center of the sphere is introduced to examine the enhancement of the incident electromagnetic field near the sphere.

$$\Sigma_{NF} = \int_0^{\pi} \int_0^{2\pi} \boldsymbol{E}^S \cdot \boldsymbol{E}^{S*} r^2 \sin\theta d\theta d\phi \qquad \text{(A1)}$$

The electric field is expressed using Debye potentials. The integral is given by the sum of tw terms.

$$\Sigma_{\mathrm{NF}} = \Sigma_{\mathrm{NF}}^{1} + \Sigma_{\mathrm{NF}}^{2}$$

Here,

$$\Sigma_{\mathrm{NF}}^{1} = \frac{2\pi}{{k_2}^2}\sum_{n=1}^{\infty}(2n+1)\left(\frac{1}{{k_2}^2}\left|a_n\right|^2\frac{d\zeta_n}{dr}\frac{d\zeta_n^*}{dr} + \left|b_n\right|^2\zeta_n\zeta_n^*\right) \tag{A2}$$

$$\Sigma_{\mathrm{NF}}^{2} = \left(-\frac{1}{{k_2}^2}\right)\left(-\frac{1}{{k_2}^2}\right)^*\sum_{n=1}^{\infty}2\pi r^2\left|a_n\right|^2\frac{(2n+1)}{n(n+1)} \times\left(\frac{d^2\zeta_n}{dr^2}\frac{d^2\zeta_n^*}{dr^2} + k_2^2(k_2^2)^*\zeta_n\zeta_n^* + k_2^2\zeta_n\frac{d^2\zeta_n^*}{dr^2} + (k_2^2)^*\zeta_n^*\frac{d^2\zeta_n}{dr^2}\right). \tag{A3}$$

Now, $j_n(r)$, $n_n(r)$, $h_n^{(1)}(r)$, and $h_n^{(2)}(r)$ are expressed with $\xi_n(r)$ on behalf of them, and the author notes that $\xi_n(r)$ is a solution of the following differential equation.

$$\frac{d^2\xi_n(r)}{dr^2} + \frac{2}{r}\frac{d\xi_n(r)}{dr} + \left(1 - \frac{n(n+1)}{r^2}\right)\xi_n(r) = 0 \tag{A4}$$

A formula (8) is used, then,

$$\frac{d^2\zeta_n(k_2r)}{dr^2} = \left(\frac{n(n+1)}{r^2} - k_2^2\right)\zeta_n(k_2r). \tag{A5}$$

Therefore,

$$\Sigma_{\mathrm{NF}}^{2} = \left(-\frac{1}{{k_2}^2}\right)\left(-\frac{1}{{k_2}^2}\right)^*\sum_{n=1}^{\infty}\pi r^2\left|a_n\right|^2\frac{2(2n+1)}{n(n+1)}\cdot\frac{n^2(n+1)^2}{r^4}\zeta_n(k_2r)\zeta_n^*(k_2r) = \frac{2\pi}{k_2^2}\sum_{n=1}^{\infty}(2n+1)\,n(n+1)\left|a_n\right|^2\frac{1}{{k_2}^2r^2}\zeta_n(k_2r)\zeta_n^*(k_2r). \tag{A6}$$

Here, the effective enhancement factor Q_{NF}, is defined according as the effective scattering factor Q_{sca} of the Mie theory. It is divided into the vertical component ${Q_{\mathrm{NF}}}^{\mathrm{V}}$ and horizontal component ${Q_{\mathrm{NF}}}^{\mathrm{H}}$ and then formula (15)–(17) are obtained.

$$Q_{\mathrm{NF}} = {Q_{\mathrm{NF}}}^{\mathrm{V}} + {Q_{\mathrm{NF}}}^{\mathrm{H}} \tag{15}$$

$${Q_{\mathrm{NF}}}^{\mathrm{V}} = \frac{2}{{k_2}^2a^2}\sum_{n=1}^{\infty}(2n+1)n(n+1)\left|a_n\right|^2\frac{1}{{k_2}^2r^2}\zeta_n(k_2r)\,\zeta_n^*(k_2r) \tag{16}$$

$$Q_{NF}{}^{H} = \frac{2}{k_2{}^2 a^2} \sum_{n=1}^{\infty} (2n+1) \left\{ \frac{1}{k_2{}^2} |a_n|^2 \frac{d\zeta_n(k_2 r)}{dr} \frac{d\zeta_n{}^*(k_2 r)}{dr} + |b_n|^2 \zeta_n(k_2 r)\, \zeta_n{}^*(k_2 r) \right\} \qquad (17)$$

From the following asymptotic form,

$$\zeta_n(k_2 r)\zeta_n^*(k_2 r) \approx 1, \quad \frac{1}{k_2{}^2} \frac{d\zeta_n}{dr} \frac{d\zeta_n^*}{dr} \approx 1 \qquad (A7)$$

$Q_{NF}{}^{V}$ approaches zero and $Q_{NF}{}^{H}$ is reduced to Q_{sca} at the wave region ($r >> a$). When $r = a$, the formulas (15) and (16) agree with the formulas of Messinger et al.

References

1. R. K. Chang and T. E. Furtak eds, *Surface Enhanced Raman Scattering*, Plenum Press, New York (1982).
2. A. Wokaun, *Solid State Phys.*, **38**, 223 (1984).
3. M. Moskovits, *Rev. Mod. Phys.*, **57**, 783 (1985).
4. a) F. Hache, D. Ricard, and C. Flytzanis, *J. Opt. Soc. Am. B*, **3**, 1647 (1987).
   b) F. Hache, D. Ricard, C. Flytzanis, and U. Kreibig, *Appl. Phys. A*, **47**, 347 (1988).
5. K. Fukumi, A. Chayahara, K. Kadono, T. Sakaguchi, Y. Horino, M. Miya, J. Hayakawa, and M. Sato, *Japanese J. Appl. Phys.*, **30**, L742 (1991).
6. G. Mie, *Ann. Phys.*, **25**, 377 (1908).
7. T. Sato, Y. Yonezawa, and H. Hada, *J. Soc. Photogr. Sci. Technol. Jpn.*, **51**, 122 (1988).
8. B. J. Messinger, K. Ulrich von Raben, R. K. Chang, and P. W. Barbar, *Phys. Rev. B*, **24**, 649 (1981).
9. H. C. van de Hulst, *Light Scattering by Small Particles*, John Wiley, New York (1957).
10. M. Born and E. Wolf, *Principles of Optics (5-th ed.)*, Pergamon Press, Oxford (1974).
11. M. Kerker, *The Scattering of Light and Other Electromagnetic Radiation*, Academic Press, New York (1969).
12. Y. Wang, *J. Phys. Chem.*, **95**, 1119 (1991).
13. T. Miyama, Y. Yonezawa, and T. Sato, *J. Soc. Photogr. Sci. Technol. Jpn.*, **57**, 1 (1994).
14. M. Kerker, D.-S. Wang, and H. Chew, *Appl. Opt.*, **19**, 4159 (1980).
15. a) M. Kerker, O. Siiman, L. A. Bumm, and D.-S. Wang, *Appl. Opt.*, **19**, 3253 (1980).
    b) O. Siiman, L. A. Bumm, R. Callaghan, C. G. Blatchford, and M. Kerker, *J. Phys. Chem.*, **87**,1014 (1983).

16. M. Mabuchi, T. Takenaka, Y. Fujiyoshi, and N. Uyeda, *Surface Sci.*, **119**, 150 (1982).

17. a) J. A. Creighton, C. G. Blatchford, and M. G. Albrecht, *J. Chem. Soc. Faraday II*, **75**, 790 (1979).

b) C. G. Blatchford, J. R. Campbell, and J. A. Creighton, *Surface Sci.*, **120**, 435 (1982).

18. R. A. Wolkow and M. Moskovitz, *J. Chem. Phys.*, **87**, 5858 (1987).

19. a) V. M. Shalaev and M. I. Stockman, *Z. Phys.D*, **10**, 71 (1988).

b) M. I. Stockman, V. M. Shalaev, M. Moskovits, R. Botet, and T. F. George, *Phys. Rev. B*, **46**, 2821 (1992).

20. B. Rothenhausler and W. Knoll, *Nature*, **332**, 615 (1988).

21. J. Wessel, *J. Opt. Soc. Am. B*, **2**, 1538 (1985).

22. a) K. Kneipp, W. Jahr, and G. Roewer, *Chem. Phys. Lett.*, **163**, 105 (1989).

b) K. Kneipp and H. Kneipp, *Spectrochim. Acta A*, **49**, 167 (1993).

23. Y. Nishikawa, K. Fujiwara, and T. Shima, *Appl. Spectrosc.*, **44**, 691 (1990).

Chapter 6

Quenching of Dye Fluorescence by Thin Silver Films Formed by Photolysis of Silver Salt of Carboxymethylcellulose

6. 1 Introduction

When thin films of silver salt of high molecular weight carboxylic acids such as alginic acid and carboxymethylcellulose (CMC) are photolyzed with UV light, photolytic silver particles are formed.[1,2] The aggregation state of photolytic silver changes from atom to cluster, colloid and bulk metal according as the reaction conditions; temperature, relative humidity, ratio of Ag^+ substitution and evacuation.[3]

An application of the Langmuir-Blodgett (LB) technique to the study of energy transfer between excited molecules and solids has been initiated by Kuhn et al. in connection with spectral sensitization of silver halide photography.[4,5] Metal films of a few nanometer thickness have been mainly used for those studies. It has been assumed that certain photophysical effects; surface-enhanced Raman scattering (SERS), enhanced absorption, enhanced luminescence, enhanced photochemistry, energy transfer, non-linear optics, are influenced by the morphology and the aggregation states of silver particles. However, experimental verification has not developed so much except for SERS.[6,7] Silver salt of CMC (CMCAg) is interesting as a model system for such studies. The silver metal film formed by photolysis of the CMCAg films is attractive as the substrate to deposit dye monolayers from the air/water interface by the LB technique.

In this chapter, the author has deposited dye monolayers onto the silver particulate film ($CMCAg^C$) and the silver mirror ($CMCAg^M$) formed by photolysis of the CMCAg films and examined the luminescence properties of dye molecules. Here, films of silver salt of CMC before irradiation are denoted as $CMCAg^+$. In the $CMCAg^M$ formed by 600-min photolysis, the film surface has been densely covered with colloidal silver particles of 10–30 nm in size. At the same time, the film surface tends to assume bulk metal-like properties. In the $CMCAg^C$ formed by 5-min photolysis, small silver particles formed by photolysis are dispersed uniformly in the film. In this study, N-ethyl-octadecylrhodamine B (dye I) and 10-(1-pyrene)-decanoic acid (dye II) has been used because there have been a number of reports on spectroscopic properties of those dyes.[8,9] In the fluorescence spectra, dye I shows a broad luminescence band around wavelength λ_{em} = 600 nm and dye II shows characteristic sharp peaks around λ_{em} = 400 nm. Since a colloidal absorption band of silver develops around 410

nm after photolysis of the CMCAg film, which is near the fluorescence peaks of dye II, might give additional influences on fluorescence quenching. In this study, the author has detailed examinations on the distance-dependent fluorescence quenching of dye molecules by energy transfer from excited dye molecules to photolytic silver and attempted to interpret the experimental results based on Kuhn's classical electromagnetic theory.[10]

6. 2 Experimental

6. 2. 1 Preparation and photolysis of $CMCAg^+$ films

Sodium salt of CMC (CMCNa: Figure 6-1) was purchased from Nacalai Tesque Co. and purified by reprecipitation with methanol. A 0.5 wt% aqueous solution of CMCNa was dropped on a quartz plate ($10 \times 40 \times 1$ mm^3) by the amount of 0.05 $mL \cdot cm^{-2}$. The CMCNa film was dried and then immersed in 0.1 M (1 M = 1 $mol \cdot dm^{-3}$) $AgNO_3$ aqueous solution for 60 min to substitute Na^+ with Ag^+. The film was washed with distilled water and dried again in the dark. The $CMCAg^+$ (1–5 μm in thickness) on the quartz plate was colorless and transparent. The ratio of Ag^+ substitution was determined more than 85% by means of atomic absorption spectrometry.[2] A 15-W sterilization lamp, Type GT-1511N (Toshiba Co.), used for the light source emitted UV light at 253.7 nm strongly. The CMCAg was exposed to UV light at room temperature (293–303 K) in air at the relative humidity more than 70%. The irradiation time was 0–600 min.

6. 2. 2 Preparation and transfer of dye monolayers

N-ethyl-octadecylrhodamine B (dye I) was synthesized by Nippon Kanko Shikiso Co.[11] 10-(1-pyrene)-decanoic acid (dye II) was purchased from Molecular Probe Co. Structure formulas of dye I and dye II are given in Figure 6-1. Arachidic acid (C_{20}) as the matrix molecule was purchased from Nacalai Tesque Co. Dye assemblies dye/C_{20} were prepared by the spreading method in a trough filled with a 0.3 mM aqueous solution of $Ca(NO_3)_2$. The spreading solution was a mixture of dye and C_{20} in $CHCl_3$. The molar ratio of spreading solutions was 1 : 9 for dye I and 1 : 1 for dye II. These solutions contained 0.3 mM of dye I and 0.54 mM of dye II. The preparation of dye monolayers was performed using a surface pressure gauge FSD-22 (San-es Keisoku Co.) and the monolayers were transferred onto the substrate by means of a motor-driven elevator Type HBM (Kyowa Interface Science Co., Ltd.). The mixed $CHCl_3$ solution of dye and C_{20} was spread over the aqueous subphase at the temperature of T = 289–292 K. After 10 min, the monolayer was carefully compressed until surface pressure

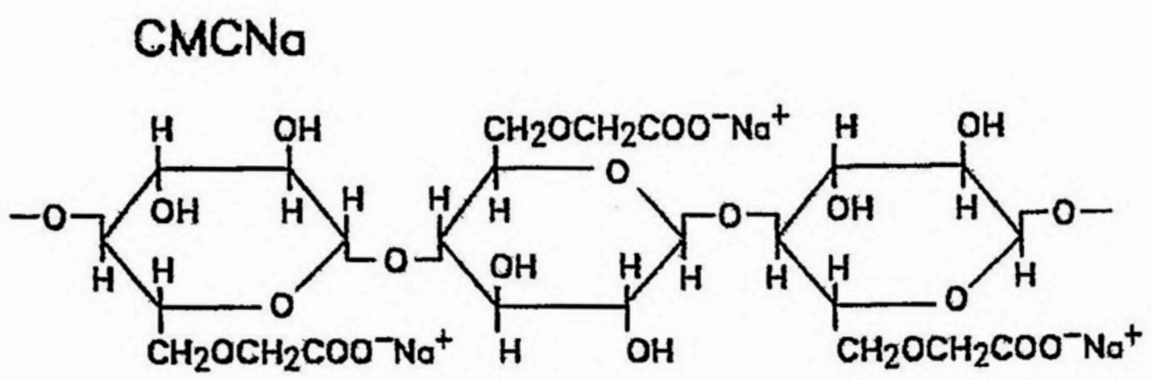

Figure 6-1. Structure formulas of sodium salt of carboxymethylcellulose (CMCNa) and dyes. dye I: N-ethyl-octadecylrhodamine B, dye II: 10-(1-pyrene) decanoic acid.

reached $\pi = 30\ mN \cdot m^{-1}$. The monolayer was transferred onto the quartz plate and the CMC substrates ($CMCAg^+$, $CMCAg^C$, $CMCAg^M$) under constant surface pressure by vertical deposition technique. The quartz plate was made hydrophobic by the deposition of cadmium arachidate (CdC_{20}) monolayers. The surfaces of the $CMCAg^+$, $CMCAg^C$, and $CMCAg^M$ substrates were proved to be almost hydrophilic. Dye layers on the side of the quartz surface were wiped off. The number of monolayers on one side of the plate was two for dye I (2×1) and one for dye II (1×1), respectively. Here, ($m \times 1$) means the m-dye monolayers deposited on one side of the plate. The 0–11 monolayeres of calcium arachidate (CaC_{20}) were deposited on the CMCAg substrates at the surface pressure $\pi = 30\ mN \cdot m^{-1}$ to change the distance *d* between the CMC film and the dye layer. After that, the (2×1) dye I layer or the (1×1) dye II layer was deposited on it. The schematic structures of monolayer assemblies are shown in Figure 2. Here, it is assumed that the surface of the CMCAg films is partly covered with ultra-thin film of CMC according to the studies of XPS and Raman scattering as given in Chapter 2 and Chapter 4.

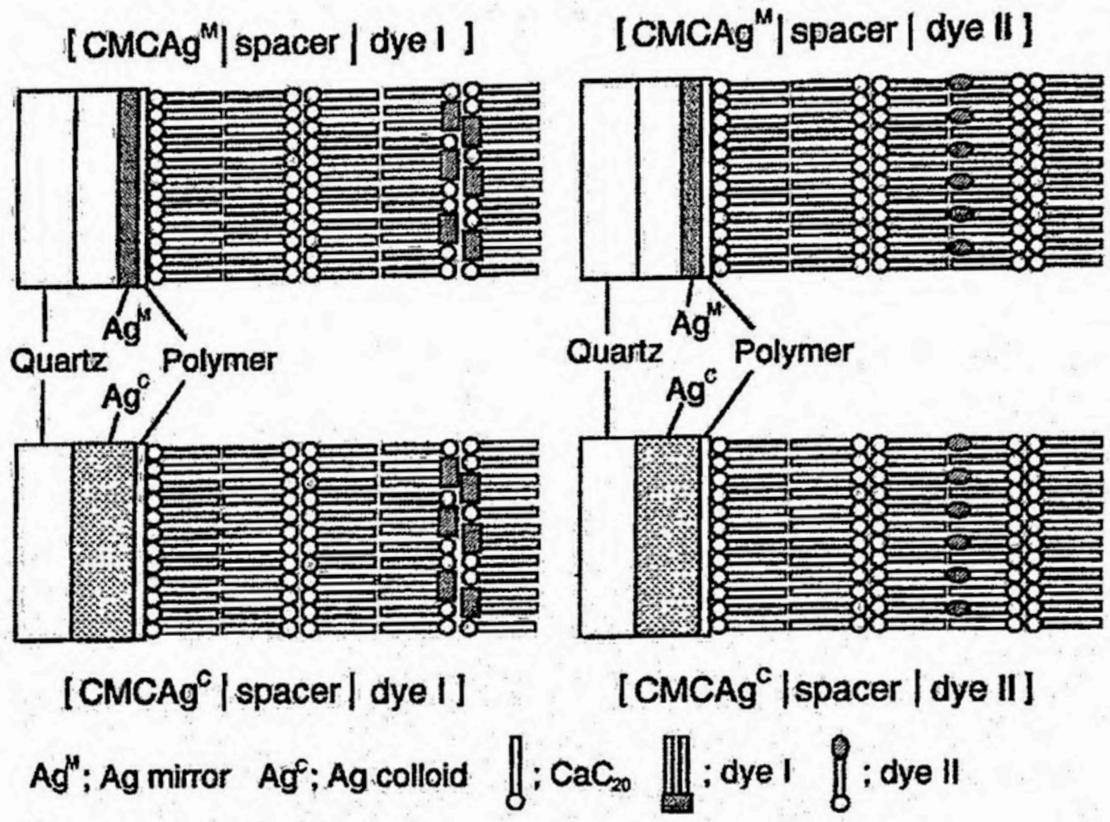

Figure 6-2. Monolayer assemblies of dye I and dye II arranged on the $CMCAg^M$ substrate ([$CMCAg^M$ | spacer | dye]) and the $CMCAg^C$ substrate ([$CMCAg^C$ | spacer | dye]). Dye monolayers were deposited on one side of the substrate whose surface was previously covered with suitable number of calcium arachidate (CaC_{20}) spacer layers.

6. 2. 3 Spectroscopic measurements

Transmittance spectra of the CMCAg film before and after photolysis were recorded on a UV-260 spectrophotometer (Shimadzu Co.). Absorption spectra and fluorescence spectra of dye layers were recorded on a UV-260 spectrophotometer (Shimadzu Co.) and an 850 spectrofluorometer (Hitachi, Ltd), respectively. The excitation wavelength for fluorescence measurements was λ_{ex} = 365 nm for dye I and λ_{ex} = 337 nm for dye II. The fluorescence intensity was corrected for the number of dye molecules in the monolayer assembly because of the variation of transfer ratio of dye. After fluorescence spectra were measured, dye molecules in the monolayers on the substrates were dissolved with 3 ml of methanol (dye I) or 3 ml of chloroform (dye II). From the absorption spectra of dye solutions, the optical density (OD) at λ = 545–548 nm (dye I) and at λ = 326–328 nm (dye II) was determined. Then the calibrated fluorescence intensity I was estimated by the intensity of fluorescence peak divided by the OD.

6. 3 Results

6. 3. 1 Photolysis of CMCAg films

Variation of transmittance spectra of the CMCAg film with irradiation time is shown in Figure 6-3. The absorption band around λ = 250 nm is assigned to electron transfer band, i.e., light-induced electron transfer from carboxylate ion (COO^-) to Ag^+ ions. The film became

yellow-brown colored and colloidal absorption band of silver at $\lambda \sim 410$ nm appeared and developed with irradiation time. When photolysis was continued, the film surface gradually wore a metallic luster and finally it changed into a clear silver mirror. In the CMCAg irradiated more than several hours, a so-called absorption window due to the bulk plasmon of silver was seen at around 310 nm. Such an observation would indicate that the properties of aggregated lloidal silver are not so different from those of bulk silver. The direct current (DC) electrical resistance of the $CMCAg^+$ was over 10^{10} Ω before irradiation. The electrical resistance was sharply decreased with irradiation and attained to less than 1000 Ω after 600 min of irradiation. It may indicate the precipitation of colloidal silver particles at the irradiated side of the film, forming the densely-packed silver particulate film. These speculations have been confirmed with aids of high-resolution scanning electron microscopy in Chapter 2. In this study, CMCAg films before irradiation ($CMCAg^+$), and irradiated for 600 min ($CMCAg^M$) and 5 min ($CMCAg^C$) were used for the substrates to deposit dye monolayers. The optical properties of the $CMCAg^M$, in which colloidal silver particles aggregated at the surface, would resemble those of the bulk silver film. The $CMCAg^C$ was dark brown in color and small silver particles are likely to disperse in the polymer film.

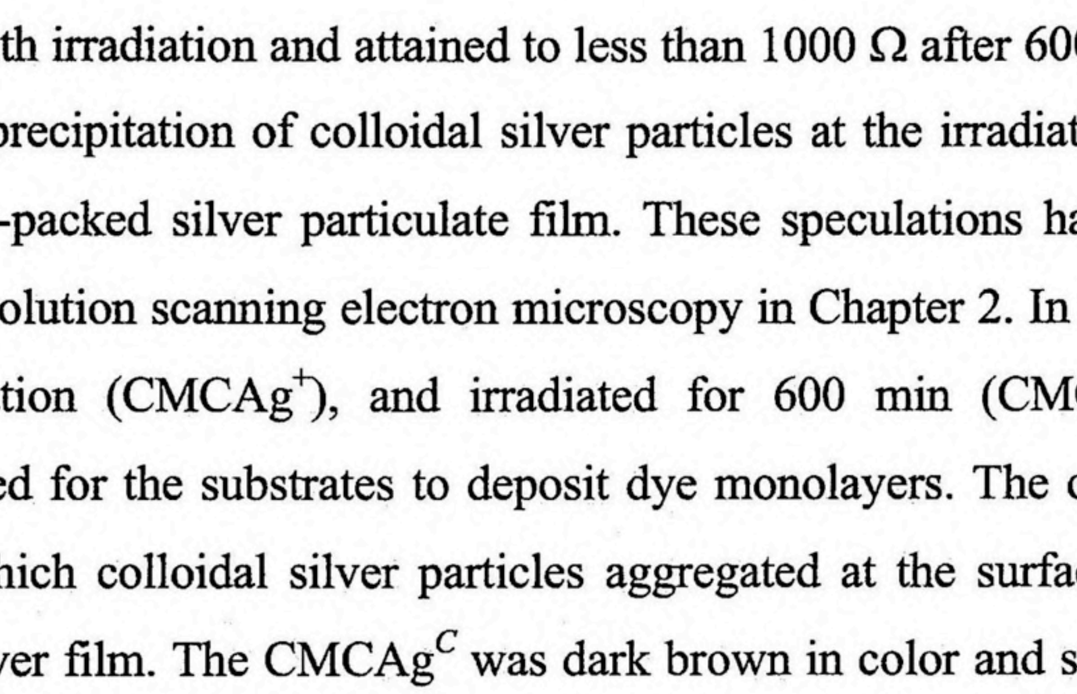

Figure 6-3. Variation of the transmittance spectra of the CMCAg film on the quartz plate with irradiation time. (a) 0 min, (b) 1 min, (c) 5 min, (d) 60 min, (e) 120 min, (f) 300 min, (g) 600 min.

6. 3. 2 Fluorescence spectra and fluorescence quenching of dye I LB films

Typical absorption and fluorescence spectra of the (2 × 1) layers of C_{20} : dye I = 9 : 1 on the quartz plate and on the $CMCAg^+$ substrate are given in Figure 6-4(A)(B). In the absorption spectra of dye layers on both substrates, a monomer band and a shoulder of the dimer band

were observed at $\lambda = 568$ nm and $\lambda \sim 525$ nm, respectively. The fluorescence peak was loca at $\lambda_{em} = 600$ nm.[11] In the case of the $CMCAg^+$, the shape of fluorescence spectra was changed probably due to the emission of impurities in the substrate itself. However, if its contribution is properly corrected, the fluorescence spectrum of dye I on the $CMCAg^+$ appears to be similar to that on the quartz plate.

The strong light absorption of the CMCAg film after photolysis hindered the measurements of the absorption spectra of dye I layer on the $CMCAg^M$. The fluorescence spectra of dye I deposited on the $CMCAg^M$ with 11 spacer monolayers ($d = 32.7$ nm) (a) and without spacer monolayers (b) are shown in Figure 6-5. A monomer fluorescence band was located at $\lambda_{em} =$ 600 nm which is the same as on the quartz plate. The fluorescence intensity of dye layers directly deposited on the $CMCAg^M$ (b) was less than 10% of that for $d = 32.7$ nm (a). It is

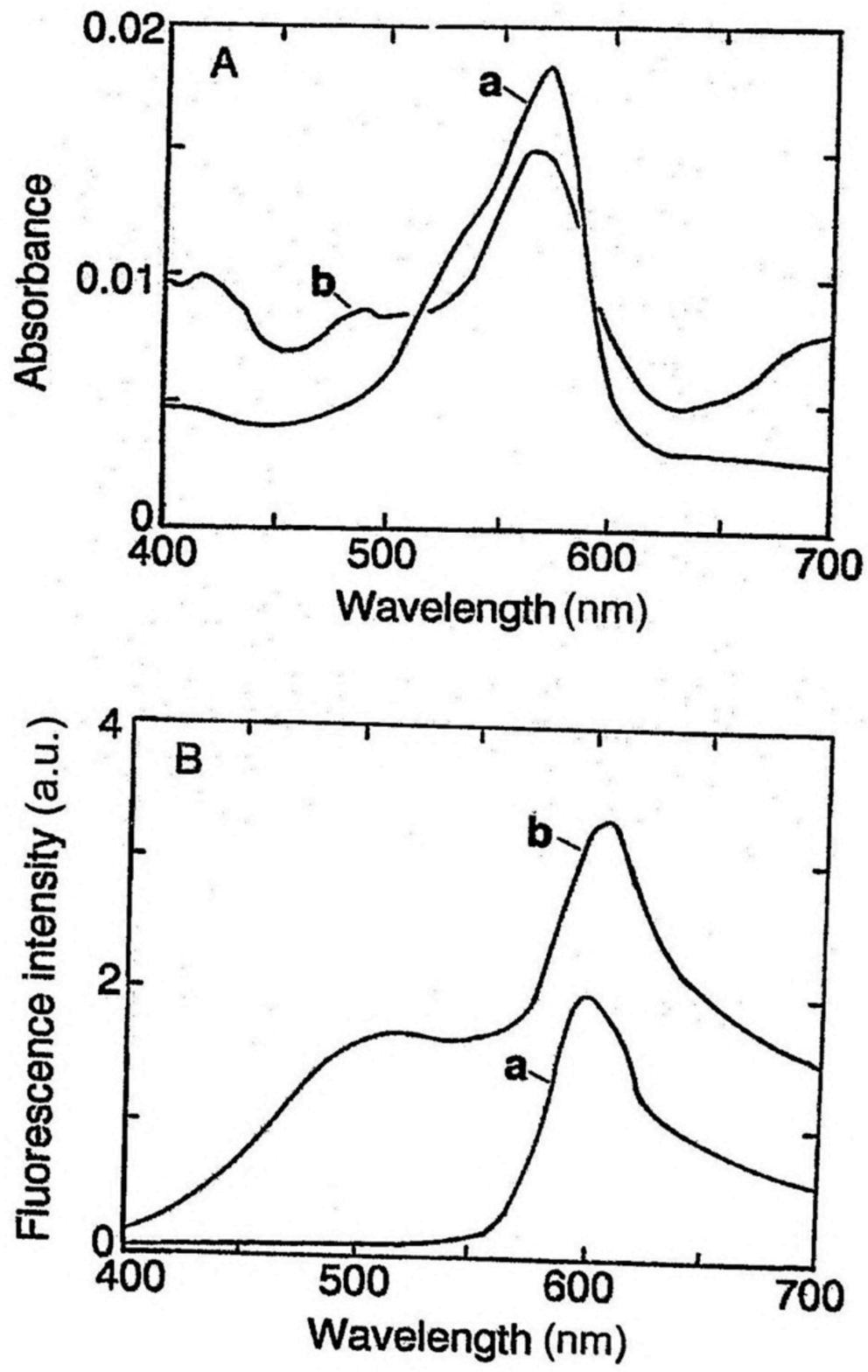

Figure 6-4. Absorption spectra (A) and fluorescence spectra (B) of dye I layers on the quartz (a) and the $CMCAg^+$ (b) substrates.

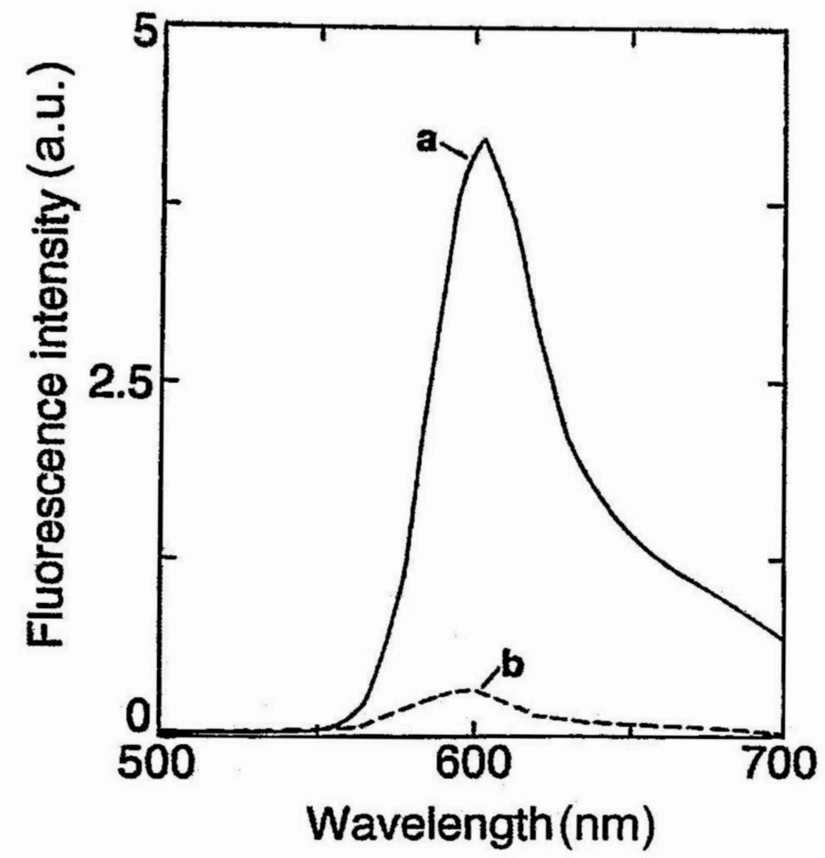

Figure 6-5. Fluorescence spectra of dye I layers on the CMCAg^M substrate. The number of spacer layers is 11 (a) and 0 (b).

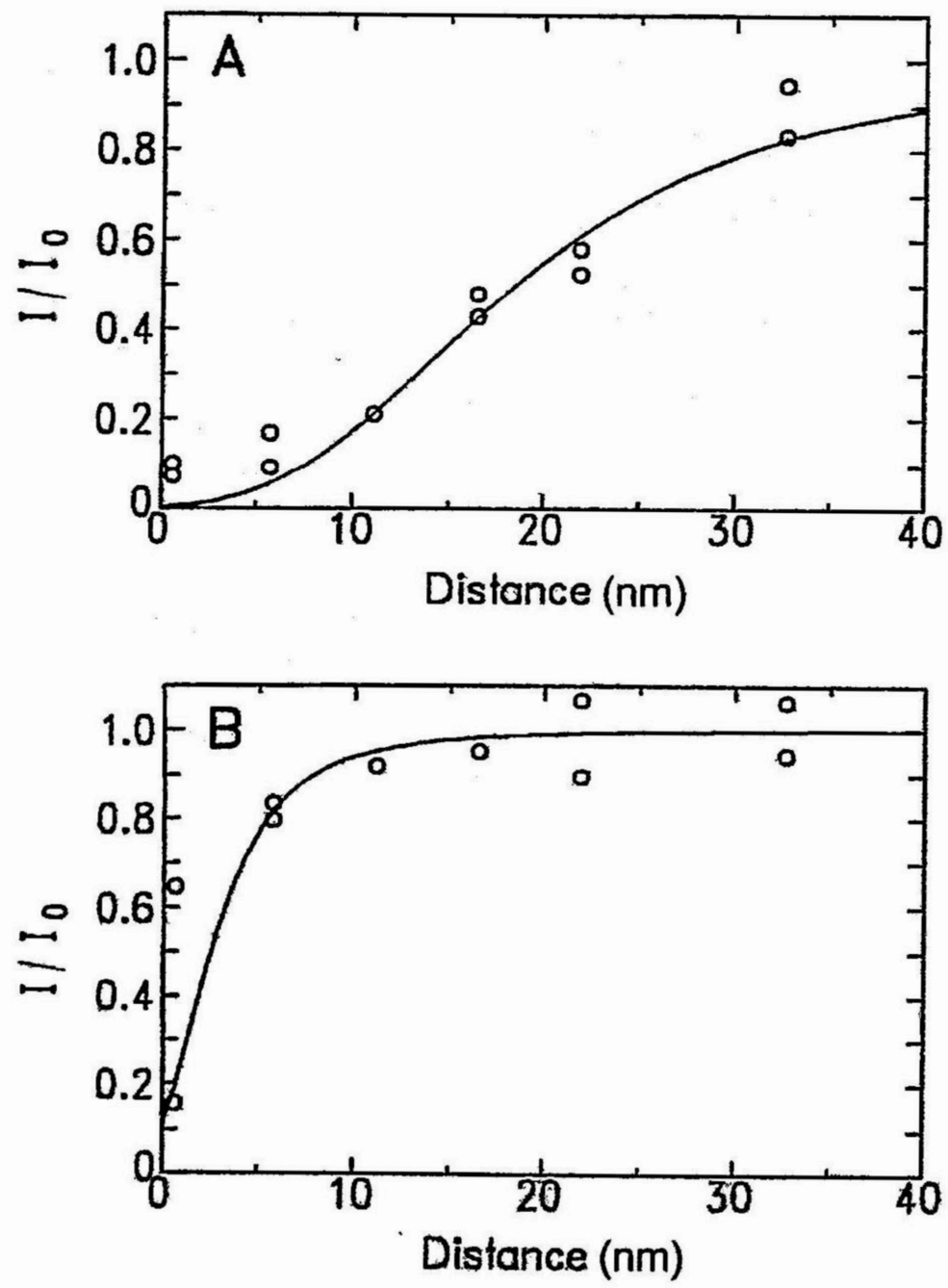

Figure 6-6. Dependences of the relative fluorescence intensity I/I_0 of the [CMCAg^M | spacer | dye I] assembly (A) and the [CMCAg^C | spacer | dye I] assembly (B) on the distance. ——— : Theoretical curves given by Eq. (30) with parameters $\tilde{d}_0 = 21$ nm (A) and $\tilde{d}_0 = 5$ nm (B), respectively.

reasonable to assume that the decrease in the fluorescence intensity is caused by excitation energy transfer from the excited dye molecules to silver films. The relative fluorescence intensity I/I_0 of the [$CMCAg^M$ | spacer | dye I] assembly is plotted versus the distance d in Figure 6-6(A). I_0 denotes the fluorescence intensity for infinite distance from the silver film. In experimental data, the author has assumed that I_0 is equal to the value of $I = 270$ when $d = 32.7$ nm. The author has also examined the distance dependence of the fluorescence intensity of the [$CMCAg^C$ | spacer | dye I] assembly and the results are plotted in Figure 6-6(B). In this case, $I_0 = 74$ was taken with reference to the value of I when $d > 21.9$ nm. The reason why I_0 of [$CMCAg^M$ | spacer | dye I] and [$CMCAg^C$ | spacer | dye I] are different one another is not clear at present. The author has supposed that it may be related to the reflection of excitation light and fluorescence light at the $CMCAg^M$/air interface.

6. 3. 3 Fluorescence spectra and fluorescence quenching of dye II LB film

Absorption and fluorescence spectra of the (1 × 1) layer of C_{20} : dye II = 1 : 1 on the quartz plate and on the $CMCAg^+$ substrate are given in Figure 6-7(A)(B). A series of sharp peaks, $\lambda =$ 270, 280, 320, 340, and 360 nm were seen in the absorption spectrum of dye II on the quartz plate.[12] In the fluorescence spectra, the monomer bands at $\lambda_{em} = 380$, 400, and 420 nm and a broad excimer band at $\lambda_{em} = 450$–480 nm were observed. Because of the strong absorption of the $CMCAg^+$ substrate itself, two peaks at $\lambda = 340$ and 360 nm remained in the absorption spectra of dye II. Due to the substrate emission of $CMCAg^+$, an exact fluorescence spectrum of dye II was difficult to obtain. Fluorescence spectra of dye II on the $CMCAg^M$ with 1 or 11 spacer monolayers are shown in Figure 6-8. It is noticed that the intensity of excimer fluorescence on the $CMCAg^M$ was smaller than that on the quartz plate. It is supposed that the excimer formation of pyrene molecules may be affected by the difference between the quartz surface and the $CMCAg^M$ surface. On the other hand, the ratio of the intensities of the monomer fluorescence and the excimer fluorescence in the [$CMCAg^M$ | spacer | dye II] assembly appeared to be almost constant irrespective of the number of spacer layers. Therefore, the author has focused on the fluorescence peak at $\lambda_{em} = 400$ nm to examine the fluorescence quenching in detail. The dependences of the relative fluorescence intensity of the [$CMCAg^M$ | spacer | dye II] assembly and the [$CMCAg^C$ | spacer | dye II] assembly on the distance d are given in Figure 6-9(A)(B). Here, I_0 is 1100 for the $CMCAg^M$ and I_0 is 280 for the $CMCAg^C$, respectively. The fluorescence quenching was observed as in the case of dye I, but it was effective only at the short distance. I was almost equal to I_0 when d is larger than 20 nm.

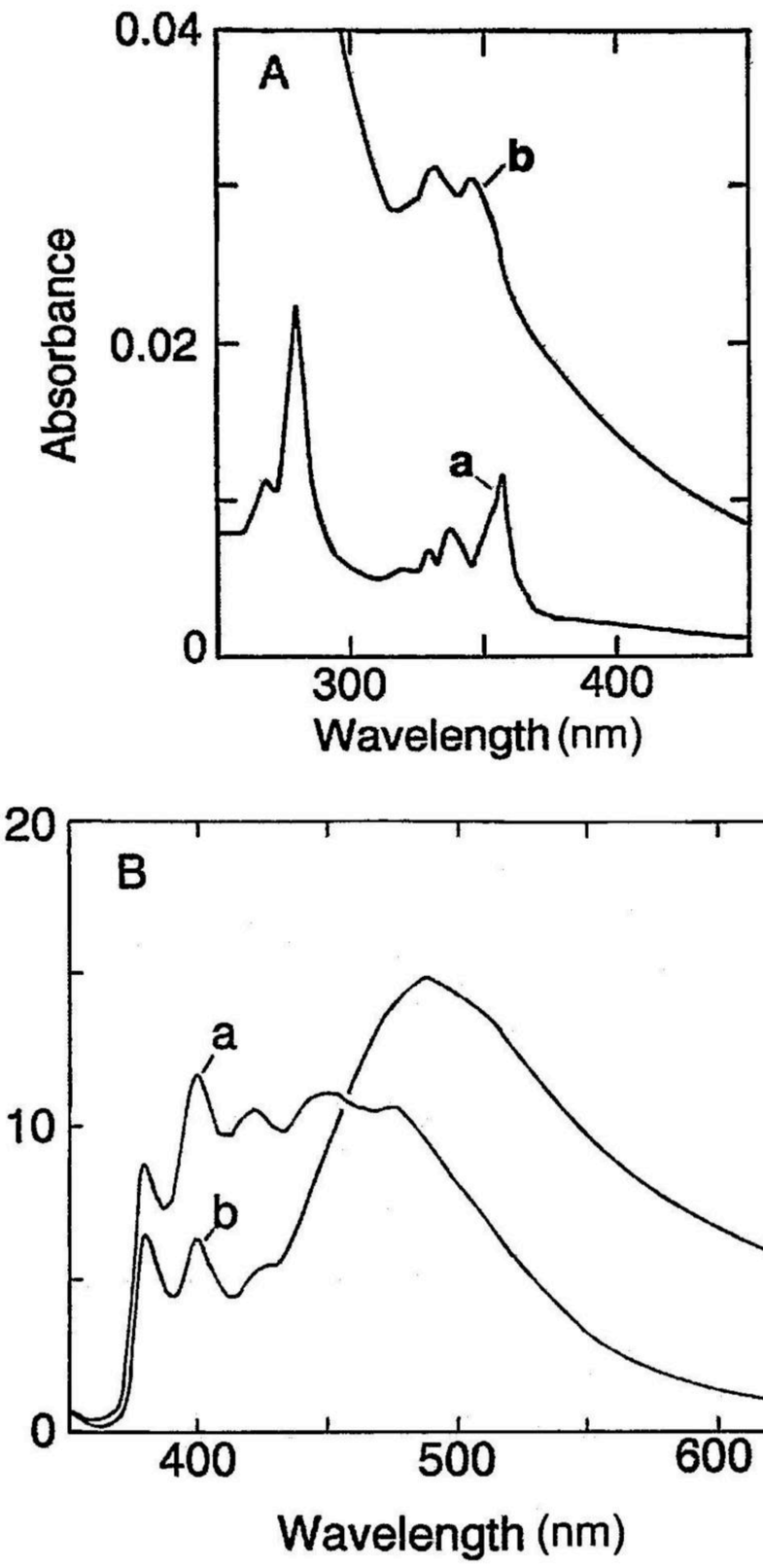

Figure 6-7. Absorption spectra (A) and fluorescence spectra (B) of dye II monolayer on the quartz (a) and the $CMCAg^{+}$ (b) substrates.

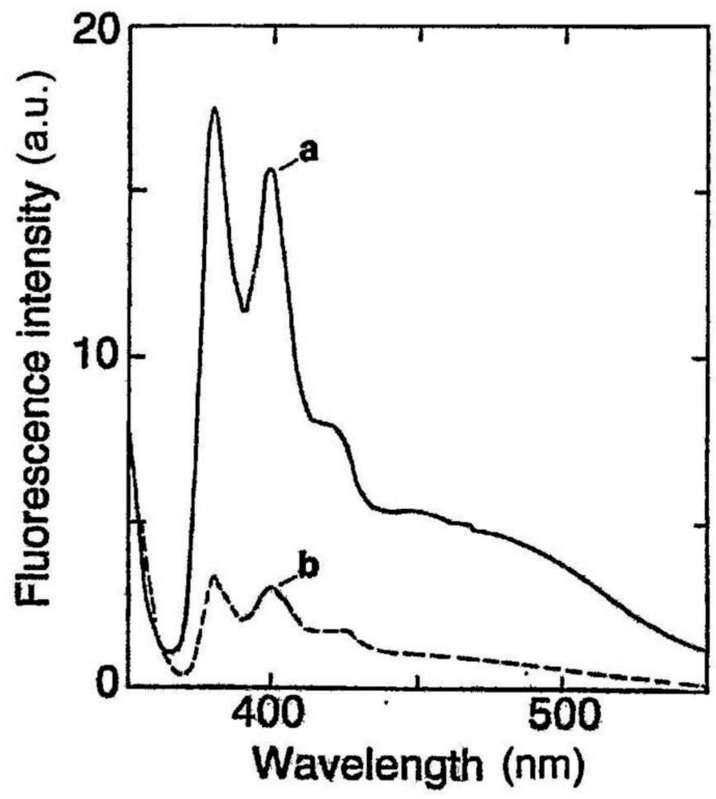

Figure 6-8. Fluorescence spectra of dye II monolayer on the $CMCAg^{M}$ substrate. The number of spacer layers is 11 (a) and 1 (b).

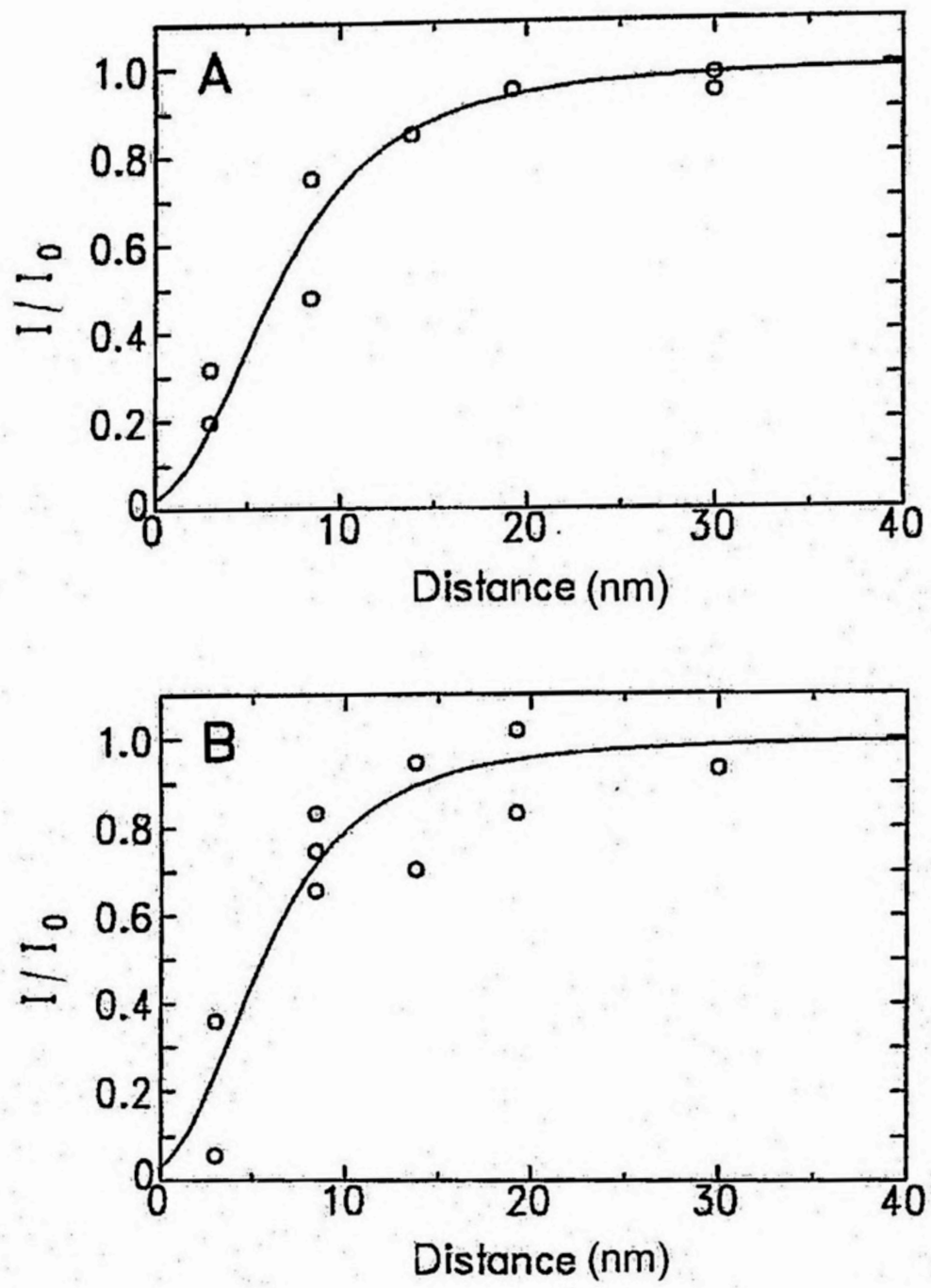

Figure 6-9. Dependences of the relative fluorescence intensity I/I_0 of the [CMCAg^M | spacer | dye II] assembly (A) and the [CMCAg^C | spacer | dye II] assembly (B) on the distance. ———: Theoretical curves given by Eq. (30) with parameters $\tilde{d}_0 = 9$ nm (A) and $\tilde{d}_0 = 8$ nm (B), respectively.

6. 4 Discussion

6. 4. 1 Kuhn's energy transfer theory

Kuhn's group has carried out a skilful experimental research on excitation energy transfer between dye molecules and thin metal films using LB technique.[4] A theoretical research based on the classical electrodynamics has been started by Kuhn and coworkers.[10,13] and completed by Chance et al. (CPS theory).[14] In this study, the author has attempted to interpret the experimental results on the basis of Kuhn's energy transfer theory. First, the author has rearranged the Kuhn's theory into the form suitable for the present study. To formulate energy transfer from emitting molecule S to accepter plane *A*, a molecule in the monolayer is considered as an isolated point dipole (S). S is defined as oscillating along the z-direction and located at the distance *d* from the smooth metal surface of thickness Δ (Figure 6-10). n_f is an

average radiation energy of S per unit time in the absence of A. Also, non-radiative energy loss n_t is introduced. The fluorescence quantum yield q of S is given by

$$q = \frac{n_f}{n_f + n_t}. \tag{1}$$

Then, the fluorescence quantum yield q_d of S when accepter plane A is located at the distance of d, and the time average of radiation energy n_a absorbed by A per unit time are introduced.

$$\frac{q}{q_d} = \frac{n_f + n_t + n_a}{n_f + n_t} = 1 + \frac{n_a}{n_f / q} \tag{2}$$

When S is a oscillating dipole with amplitude μ_0 and oscillating angular frequency ω, n_f is expressed in next equation (MKSA unit).[15] Here, n is the refractive index of medium surrounding the oscillating dipole and c is light velocity. ε_0 is permittivity of free space.

$$n_f = \frac{{\mu_0}^2 \omega^4 n}{12\pi\varepsilon_0 c^3} \tag{3}$$

A power loss of S in the absence of A is named L and a power absorbed by A when A exists is L_a.

$$L = n_f + n_t = n_f / q \tag{4}$$

$$q/q_d = 1 + L_a/L \tag{5}$$

The accepter layer is very thin and absorbs light with an angular frequency ω by the absorbance Θ. In general, the energy absorption dL_a in small area of a surface $dxdy$ is given in next formula when light with electric field amplitude F_0 is incident perpendicularly into the surface.

$$dL_a = \Theta \frac{c\varepsilon_0}{2} {F_0}^2 dxdy \tag{6}$$

It has been assumed that the same expression is applicable to electromagnetic field irradiated by the oscillating dipole. Further, the author assumes that existence of plane A does not affect

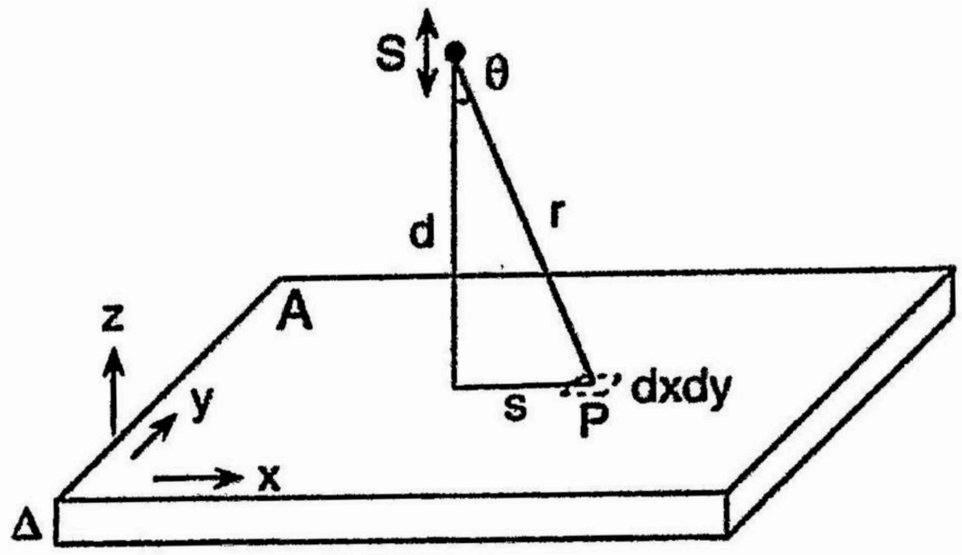

Figure 6-10. Geometry of oscillating dipole-mirror problem. A dipole S at the distance *d* of an absorbing layer *A* is oscillating in the z-direction (perpendicular to the acceptor layer). The thickness of the layer is *Δ*. *r*, *s*, *θ* define a small area *dxdy* at the position P on the layer surface.

the electromagnetic radiation by the oscillating dipole. Then, the electric field radiated from S oscillating along the z direction at the point *P* in the *xy*-plane consists of three components as follows.[15]

$$
\begin{aligned}
\boldsymbol{E}^{(0)} &= \left\{ -\frac{\boldsymbol{p}}{n^2 r^3} + \frac{3\boldsymbol{x}(\boldsymbol{x}\cdot\boldsymbol{p})}{n^2 r^5} \right\} \times \frac{1}{4\pi\varepsilon_0} \\
\boldsymbol{E}^{(1)} &= \left\{ -\frac{\omega \boldsymbol{p}}{ncr^2} + \frac{3\boldsymbol{x}(\omega\boldsymbol{x}\cdot\boldsymbol{p})}{ncr^4} \right\} \times \frac{1}{4\pi\varepsilon_0} \\
\boldsymbol{E}^{(2)} &= \left\{ -\frac{\omega^2 \boldsymbol{p}}{c^2 r} + \frac{\boldsymbol{x}(\omega^2\boldsymbol{x}\cdot\boldsymbol{p})}{c^2 r^3} \right\} \times \frac{1}{4\pi\varepsilon_0}
\end{aligned}
\qquad (7)
$$

The accepter is assumed to interact only with planar component of the radiative electric field. The first term in each component of Eq. (7) does not contribute because $\boldsymbol{p}$ // z. So, the *x* components of $\boldsymbol{E}^{(0)}$, $\boldsymbol{E}^{(1)}$, $\boldsymbol{E}^{(2)}$ are given by

$$
\begin{aligned}
\boldsymbol{E}_x^{(0)} &= \left(\frac{3r^2 \mu_0 \cos\theta \sin\theta}{n^2 r^5} \right) \times \frac{1}{4\pi\varepsilon_0} \\
\boldsymbol{E}_x^{(1)} &= \left(\frac{3\omega r^2 \mu_0 \cos\theta \sin\theta}{ncr^4} \right) \times \frac{1}{4\pi\varepsilon_0} \\
\boldsymbol{E}_x^{(2)} &= \left(\frac{\omega^2 r^2 \mu_0 \cos\theta \sin\theta}{c^2 r^3} \right) \times \frac{1}{4\pi\varepsilon_0}.
\end{aligned}
\qquad (8)
$$

Therefore, the square of the electric field amplitude F_0^2 at the arbitrary point of distance r and angle θ from S on the plane is expressed by

$$F_0^2 = \mu_0^2 \sin^2\theta\cos^2\theta \times \left(\frac{9}{n^4 r^6} + \frac{9\omega^2}{n^2 c^2 r^4} + \frac{\omega^4}{c^4 r^2} \right) \times \frac{1}{4\pi\varepsilon_0} . \tag{9}$$

F_0^2 of Eq. (9) is substituted in Eq. (6) and integrated over x, y to calculate L_a. A term coming from the first term of Eq. (9) is

$$L_a = \iint \Theta \frac{c\varepsilon_0 n}{2} F_0^2 dxdy = \left(\iint \Theta \frac{c\varepsilon_0 n}{2} \mu_0^2 \sin^2\theta\cos^2\theta \frac{9}{n^4 r^6} dxdy \right) \times \frac{1}{4\pi\varepsilon_0} . \tag{10}$$

Here, planar polar coordinate is introduced.

$$dxdy = sds \cdot d\beta,\ r^2 = d^2 + s^2 \tag{11}$$

where,

$$\cos\theta = d/r,\ \sin\theta = s/r, \tag{12}$$

$$\begin{aligned} L_a &= \Theta \frac{c\varepsilon_0 n}{2} \mu_0^2 \left(\int_0^{2\pi} d\beta \int_0^{\infty} \frac{s^2 d^2}{\left(d^2 + s^2\right)^2} \frac{9}{n^4 \left(d^2 + s^2\right)^3} sds \right) \times \frac{1}{4\pi\varepsilon_0} \\ &= \Theta \frac{c\varepsilon_0 n}{2} \mu_0^2 2\pi \frac{9}{n^4} d^2 \left(\int_0^{\infty} \frac{y}{2\left(y + d^2\right)^5} dy \right) \times \frac{1}{4\pi\varepsilon_0} . \end{aligned} \tag{13}$$

By using a formula,

$$\int_0^{\infty} \frac{y}{\left(y + d^2\right)^5} dy = \frac{1}{12d^6}, \tag{14}$$

$$L_a = \Theta \frac{c\varepsilon_0 n}{2} \mu_0^2 \frac{3\pi}{4d^4 n^4} \times \frac{1}{4\pi\varepsilon_0} . \tag{15}$$

Now, wavelength in vacuum λ_0 is introduced.

$$\lambda_0 = 2\pi c/\omega . \tag{16}$$

Then,

$$L_a = \Theta \times \frac{c\varepsilon_0 n}{2}\mu_0{}^2 \times \frac{1}{4\pi\varepsilon_0} \times \frac{3\pi}{4n^4 d^4} \times \frac{1}{(2\pi)^4} \times \left(\frac{\omega\lambda_0}{c}\right)^4 \tag{17}$$

$$= \Theta \frac{1}{16} cn\mu_0{}^2 \frac{\omega^4}{c^4} \frac{3}{2}\left(\frac{\lambda_0}{2\pi nd}\right)^4 .$$

The contributions of the second and the third terms of Eq. (9) are similarly calculated. Final equation is given by

$$L_a = \Theta \frac{1}{16} cn\mu_0{}^2 \frac{\omega^4}{c^4}\left\{\frac{3}{2}\left(\frac{\lambda_0}{2\pi nd}\right)^4 + \left(\frac{\lambda_0}{2\pi nd}\right)^2 + 1\right\}. \tag{18}$$

At the near field region of the oscillating dipole ($d << \lambda$), the third term is negligible. Then, by introducing the following quantities

$$d_0 = (\Theta q)^{1/4}\alpha(\lambda_0 / n), \alpha = (1/4\pi)(9/2)^{1/4}$$
$$\eta = (\Theta q)^{1/2}\left(\sqrt{2}/4\right), \tag{19}$$

Eq. (5) is summarized by

$$\frac{q}{q_d} = 1 + \left(\frac{d_0}{d}\right)^4 + \eta\left(\frac{d_0}{d}\right)^2 . \tag{20}$$

Considering that certain dye molecules in LB films are represented by the point dipoles oscillating parallel to the plane A, the author regards α as an adjustable parameter varying from 0.05 to 0.15 according as the orientation of dye molecules. In many cases, d^{-2} term of Eq. (18) can be ignored in comparison with d^{-4} term. Therefore, d^{-4} rule is realized between I; emission intensity when the accepter layer is in the distance d and I_0; emission intensity when $d = +\infty$.[4]

$$\frac{q}{q_d} = \frac{I_0}{I} = 1 + \left(\frac{d_0}{d}\right)^4 \tag{21}$$

In the CMCAg^M, the thickness of the silver mirror is estimated to 100–200 nm (Chapter 3),

so the condition of very thin layer ($\Delta << d$) is not satisfied. Hence, the author has to extend the Kuhn's theory to the case of which the accepter layer is thick ($d << \Delta$).[16] A thin layer of which thickness is dz at the depth of z from the accepter surface is considered. According to Eq. (21),

$$\frac{1}{I} = \frac{1}{I_0} + \frac{1}{I_0}\left(\frac{d_0}{d+z}\right)^4 = \frac{1}{I_0} + \frac{1}{I_0}\Theta\frac{1}{(d+z)^4}\alpha^4 q\frac{{\lambda_0}^4}{n^4}. \tag{22}$$

When an extinction constant of the metal is denoted as κ_c, Θ is expressed by

$$\Theta = \frac{4\pi\kappa_c dz}{\lambda_0}. \tag{23}$$

By integrating Eq. (22) in the depth direction,

$$\int_0^{\Delta}\frac{1}{(z+d)^4}dz = \frac{1}{3}\left\{\frac{1}{d^3} - \frac{1}{(\Delta+d)^3}\right\}. \tag{24}$$

Therefore,

$$\frac{I_0}{I} = 1 + \frac{4\pi\kappa_c}{\lambda_0}q\alpha^4\frac{{\lambda_0}^4}{n^4}\frac{1}{3}\left\{\frac{1}{d^3} - \frac{1}{(\Delta+d)^3}\right\}. \tag{25}$$

Now, because of $\Delta >> d$,

$$\frac{I_0}{I} = 1 + \frac{4\pi\kappa_c}{\lambda_0}q\alpha^4\frac{{\lambda_0}^4}{n^4}\frac{1}{3}\frac{\Delta}{d^3\Delta} = 1 + \frac{4\pi\kappa_c\Delta}{\lambda_0}q\alpha^4\left(\frac{\lambda_0}{n}\right)^4\frac{1}{3d^3\Delta}. \tag{26}$$

Here, equivalent quantities to d_0 and Θ, $\tilde{d}_0$ and $\tilde{\Theta}$ were introduced.

$$\tilde{d}_0 = \left(\tilde{\Theta}q\right)^{1/3}\alpha^{4/3}\left(\lambda_0/n\right)^{4/3}\left(1/3\Delta\right)^{1/3} \tag{27}$$

$$\tilde{\Theta} = 4\pi\kappa_c\Delta/\lambda_0 \tag{28}$$

Finally,

$$\frac{I_0}{I} = 1 + \left(\frac{\tilde{d}_0}{d}\right)^3 . \tag{29}$$

Here, $\tilde{d}_0$ is the value of d when I is one-half of I_0. In this way, the distance dependence of the fluorescence quenching is expected to follow a d^{-3} rule.[17]

6. 4. 2 Distance dependence of fluorescence quenching

The author has assumed that the surface of the CMCAg substrates is covered with thin CMC film with a thickness of $W = 2.5$ nm and transformed the Eq. (29) as follows.

$$\frac{I_0}{I} = 1 + \left(\frac{\tilde{d}_0}{d + W}\right)^3 \tag{30}$$

Theoretical curves (Eq. (30)) of the distance dependence of fluorescence quenching for [$CMCAg^M$ | spacer | dye] assemblies are shown in Figures 6-6 (A) and 6-9 (A). In the case of [$CMCAg^M$ | spacer | dye I], a theoretical curve of eq. (30) with a fitting parameter $\tilde{d}_0 = 21$ nm has well reproduced the observed data. Therefore, it is confirmed that energy transfer from dye I to the silver layer follows the d^{-3} rule. Next, the author has tried to estimate $\tilde{d}_0$ by Eq. (27). Parameters and calculated $\tilde{d}_0$ value are given in Table 6-1. The absorbance of thin silver films at the fluorescence wavelength was difficult to estimate because of high reflectance of the $CMCAg^M$. Therefore, the author has employed $\tilde{\Theta} = 1.6$ calculated by the method given in Appendix. The film thickness $\Delta = 200$ nm of the $CMCAg^M$ has been estimated by TEM observation (Chapter 2). The value $\tilde{d}_0 = 23$ nm using $\alpha^{4/3} = 0.0565$ of Eq. (19) for the

Table 6-1. Comparison of the observed $\tilde{d}_0$ with those estimated from Eq.(27).

	$\tilde{d}_0$ (nm)					$\tilde{d}_0$ (nm)
	observed	λ_0 (nm)	Q	Δ (nm)	$\tilde{\Theta}$	theoretical
[$CMCAg^M$ | spacer | dye I]	21	600	1.0	200	1.6	23
[$CMCAg^C$ | spacer | dye I]	5	600	1.0	1000	0.25	7
[$CMCAg^M$ | spacer | dye II]	9	400	0.1	200	11	12
[$CMCAg^C$ | spacer | dye II]	8	400	0.1	1000	2.5	4

CMCAg^M agrees well with the measured value $\tilde{d}_0$ = 21 nm. Although, $\tilde{d}_0$ is considerably larger than that estimated from usual Förster-type energy transfer theory between organic dye molecules; 5–10 nm,[18] such long distance energy transfer has been reported in other dye monolayer-metal film combinations.[19] Kuhn has assumed that the surface of thin metal film is completely flat. In reality, because the CMCAg^M is composed of the aggregate of small silver particles, the surface may have many concavo-convexes. However, judging from the coincidence of $\tilde{d}_0$ in Table 6-1, the surface of the CMCAg^M seems to be flat enough for dye molecules in the LB film.

In the [CMCAg^M | spacer | dye II] assembly, $\tilde{d}_0$ = 9 nm has been observed. The fluorescence lifetime of dye II in monolayer assemblies on the quartz plate was about τ = 5–10 nsec. This value is quite shorter than the literature value for fluorescence lifetime of pyrene; τ = 100 nsec.[8] About one-order shorter fluorescence lifetime of dye II in LB films would be caused by fluorescence quenching by oxygen in air.[20] The fluorescence quantum yield q in Eq. (27) is taken to be 0.1. The author has confirmed that $\tilde{d}_0$ changes only within 10–20% if q is in the range of 0.05–0.2. When $\tilde{\Theta}$ = 11 is used, $\tilde{d}_0$ amounts to 12 nm. Indeed the calculated $\tilde{d}_0$ is close to the observed one, but $\tilde{\Theta}$ = 11 is unreasonably large. The estimation of $\tilde{\Theta}$ in the wavelength range close to surface plasmon band (λ_{sp} ~ 410 nm) is not easy.

In Figures 6-6(B) and 6-9(B), theoretical curves of distance dependence of fluorescence quenching (Eq. (30)) in the [CMCAg^C | spacer | dye] assemblies are given. Originally, excitation energy transfer in such a system is beyond the subject of the Kuhn's theory. The author has assumed that the CMC film incorporating colloidal silver particles is regarded as a sort of a "metal film" with Δ = 1000 nm and having a certain effective dielectric constant. Then, the author can apply Eq. (30) to the [CMCAg^C | spacer | dye] assemblies. As the number density of colloidal silver particles acting as the energy accepter is rather low, the observed value $\tilde{d}_0$ of [CMCAg^C | spacer | dye I] is only 5 nm. The author has estimated $\tilde{\Theta}$ = 0.25 from the transmittance spectrum of the CMCAg^C. The calculated $\tilde{d}_0$ = 7 nm is nearly equal to the observed one.

In the case of [CMCAg^C | spacer | dye II] assembly, $\tilde{d}_0$ = 8 nm has been observed. By using $\tilde{\Theta}$ = 2.5 and Δ = 1000 nm, $\tilde{d}_0$ = 4 nm has been estimated, which is about a half of the observed one. It may indicate that the CMCAg^C has stronger fluorescence quenching ability towards dye II than those given by Eq. (27)–(30).

The author has next compared the observed $\tilde{d}_0$ with calculated ones in four systems. The observed order $\tilde{d}_0$ (CMCAg^M-dye I) >> $\tilde{d}_0$ (CMCAg^C-dye I) would reflect the difference in

the number density of colloidal silver particles. The order $\tilde{d}_0$ (CMCAg^M-dye I) > $\tilde{d}_0$ (CMCAg^M-dye II) would be caused by the different wavelength in Eq. (27); λ_0 = 600 nm for dye I, λ_0 = 400 nm for dye II, together with the fluorescence quantum yield q; q = 1.0 for dye I, q = 0.1 for dye II.[7,8] On the other hand, the agreement is not satisfactory in the dye II assembly. For the calculated value $\tilde{d}_0$ (CMCAg^M-dye II) > $\tilde{d}_0$ (CMCAg^C-dye II), but the observed one $\tilde{d}_0$ (CMCAg^M-dye II) ~ $\tilde{d}_0$ (CMCAg^C-dye II). These observations may reflect unconventional conditions that fluorescence wavelength of dye II, λ_{em} = 400 nm is close to the surface plasmon absorption band λ_{sp} = 410 nm. It may be related to the possibility that strong electric field induced at the colloidal silver particles can influence the energy transfer from the excited dye molecules to silver.[21–23] However, as the fluorescence quantum yield q is small in the dye II assembly, the estimation of $\tilde{\Theta}$ near $\lambda = \lambda_{sp}$ may be accompanied with relatively large errors. If dye molecule whose fluorescence wavelength is located at shorter side of λ_{em} is used, special features of excitation energy transfer of dye II may become more evident. Until now, studies on fluorescence properties and excitation energy transfer in small metal particles-dye systems have not advanced much because of the difficulty in sample preparation. The polymer films incorporating silver clusters and colloids formed by photolysis of the CMCAg films seem to be promising matrix to promote such a direction of research.

6. 5 Summary

When the thin films of CMCAg was photolyzed with UV light, either the deep brown colored film, CMCAg^C containing colloidal silver or CMCAg^M, whose surface was covered with a silver mirror, was formed according to the irradiation time. The C_{20} : dye I or C_{20} : dye II monolayer was formed on the subpahse consisting of an aqueous $Ca(NO_3)_2$ solution. Dye monolayers were deposited on the CMCAg substrates (CMCAg$^+$, CMCAg^M, and CMCAg^C) by the LB technique. Fluorescence spectra of the [CMCAg^M | spacer | dye] assemblies and the [CMCAg^C | spacer | dye] assemblies were measured. Fluorescence quenching of dye I and dye II was observed when the spacer thickness between the silver layer and dye layers was decreased. Fluorescence quenching is caused by excitation energy transfer from excited dye molecules to silver films. The dependence of fluorescence quenching of the [CMCAg^M | spacer | dye] assemblies on the distance has been analyzed on the basis of the classical electromagnetic theory of Kuhn. The author has shown that fluorescence quenching follows a d^{-3} distance law. The characteristic distance $\tilde{d}_0$ in which fluorescence intensity is one-half of that in the infinite separation of the silver layer is as follows; $\tilde{d}_0$ = 21 nm for dye I, $\tilde{d}_0$ = 9 nm

for dye II. The Kuhn's theory has been applied to the [CMCAg^C | spacer | dye] assemblies. In this system, the author has also observed that fluorescence quenching obeys the d^{-3} distance law. $\tilde{d}_0$ are 5 nm for dye I, and 8 nm for dye II, respectively. In the [CMCAg^M | spacer | dye] assemblies, the absorbance $\tilde{\Theta}$ of the silver layer has been estimated by the Wolter's formula combined with the Maxwell-Garnett theory. The calculated value $\tilde{d}_0$ = 23 nm for the [CMCAg^M | spacer | dye I] assembly well agrees with the observed one. Also, the calculated value $\tilde{d}_0$ = 7 nm for the [CMCAg^C | spacer | dye I] assembly well agrees with the observed one. Although the calculated value $\tilde{d}_0$ =12 nm in the [CMCAg^M | spacer | dye II] assembly is relatively close to the observed one, $\tilde{\Theta}$ is unreasonably large. The calculated $\tilde{d}_0$ is 4 nm in the [CMCAg^C | spacer | dye II] assembly, which is about a half of the observed one. Those results indicate that the fluorescence properties of dye II system are not fully analyzed by the Kuhn's theory because the fluorescence peak of dye II is near the surface plasmon band of colloidal silver.

6. 6 Appendix: Optical properties of the CMCAg^M

The formation of colloidal silver and a silver mirror by UV photolysis of silver alginate films has been studied.[1,2] It has been found that the colloidal silver formed by short time irradiation are uniformly dispersed inside of the film of the thickness 1–5 μm. On the other hand, after long-time photolysis, silver atoms and clusters are precipitated at the irradiated side of the film, forming a "metal layer" of the thickness 100–200 nm. This layer consists of colloidal silver particles surrounded by silver salt of alginic acid. Judging from the dependence of electric sheet resistance on the amount of photolytic silver, a volume fraction Q of silver has been estimated to be 0.2–0.6. The author has assumed that these considerations are applicable to the CMCAg films as well. Then, three layered film; [air | polymer film containing metal particles | quartz plate] has been introduced and the transmittance spectrum and the reflectance spectrum are calculated by Wolter's formula. Here, a refractive index of the CMCAg is taken to be n_s = 1.5,[24] which is common to general polymer materials. According to Wolter,[25] transmittance (T) and reflectance (R) are given by the following equations.

$$T = \frac{16 n_s \left(n^2 + \kappa^2\right)}{\rho\tau e^{k\tau} + \chi\rho e^{-k\tau} + 2s\cos(n\tau) + 2t\sin(n\tau)}, \quad \text{(A1)}$$

$$R = \frac{\chi\tau e^{k\tau} + \rho\sigma e^{-k\tau} + 2q\cos(n\tau) + 2v\sin(n\tau)}{\rho\tau e^{k\tau} + \chi\rho e^{-k\tau} + 2s\cos(n\tau) + 2t\sin(n\tau)}, \quad \text{(A2)}$$

where,

$$\chi = (n-1)^2 + \kappa^2$$
$$q = \left(n^2 + \kappa^2\right)\left(1 + {n_s}^2\right) - \left(n^2 + \kappa^2\right)^2 - {n_s}^2 - 4n_s\kappa^2$$
$$\rho = (n+1)^2 + \kappa^2$$
$$s = \left(n^2 + \kappa^2\right)\left(1 + {n_s}^2\right) - \left(n^2 + k^2\right)^2 + {n_s}^2 + 4n_s\kappa^2$$
$$\sigma = (n - n_s)^2 + \kappa^2,\ \nu = 2\kappa(n_s - 1)\left(\kappa^2 + n^2 + n_s\right)$$
$$\tau = (n + n_s)^2 + \kappa^2,\ t = 2\kappa(n_s + 1)\left(\kappa^2 + n^2 - n_s\right) \qquad \text{(A3)}$$

$$r = 4\pi\delta / \lambda_0 \qquad \text{(A4)}$$

Here, δ is the film thickness and λ_0 is wavelength.

A complex dielectric constant of the silver particles / polymer composite ε_c is estimated by the Maxwell-Garnett theory.[26]

$$\frac{\varepsilon_c - \varepsilon_0}{\varepsilon_c + 2\varepsilon_0} = Q\frac{\varepsilon - \varepsilon_0}{\varepsilon + 2\varepsilon_0} \qquad \text{(A5)}$$

Here, ε is a complex dielectric constant of silver metal. A real and imaginary part of ε, ε_1 and ε_2, are related with the refractive index n and extinction constant κ.[27]

$$\varepsilon = \left\{\left(n^2 - \kappa^2\right) - 2n\kappa i\right\} \times \frac{\mu_0\varepsilon_0}{\mu} = \varepsilon_1 - i\varepsilon_2 \qquad \text{(A6)}$$

μ is permeability and μ_0 is permeability of free space, respectively. The real and imaginary part of the complex dielectric constant of the composite system, ε_{1c} and ε_{2c}, are expressed in a similar form.

$$\varepsilon_c = \left\{\left({n_c}^2 - {\kappa_c}^2\right) - 2n_c\kappa_c i\right\} \times \frac{\mu_0\varepsilon_0}{\mu} = \varepsilon_{1c} - i\varepsilon_{2c} \qquad \text{(A7)}$$

Then, the refractive index n_c and extinction constant κ_c of the composite system are given by

$$n_c = \sqrt{1/2}\sqrt{\left\{\varepsilon_{1c} + \sqrt{{\varepsilon_{1c}}^2 + {\varepsilon_{2c}}^2}\right\} \times \frac{\mu}{\mu_0\varepsilon_0}}$$
$$\kappa_c = \left(\varepsilon_{2c} / 2n_c\right) \times \frac{\mu}{\mu_0\varepsilon_0}. \qquad \text{(A8)}$$

Calculated transmittance spectra are shown in Figure 6-A1 (A). The observed transmittance spectrum of the CMCAg^M is well reproduced by using $\delta = 200$ nm and $Q = 0.5$. $\tilde{\Theta}$ of the CMCAg^M are given by

$$\tilde{\Theta} = 4\pi\kappa_c\delta / \lambda_0 . \qquad \text{(A9)}$$

Calculated reflectance spectrum is shown in Figure 6-A1 (B). The transmittance spectrum and the reflectance spectrum of bulk silver ($\delta = 200$ nm) are added to Figures 6-A1(A) and (B) to compare with composite systems. Parameters and the calculated $\tilde{\Theta}$ are summarized in Table 6-A1.

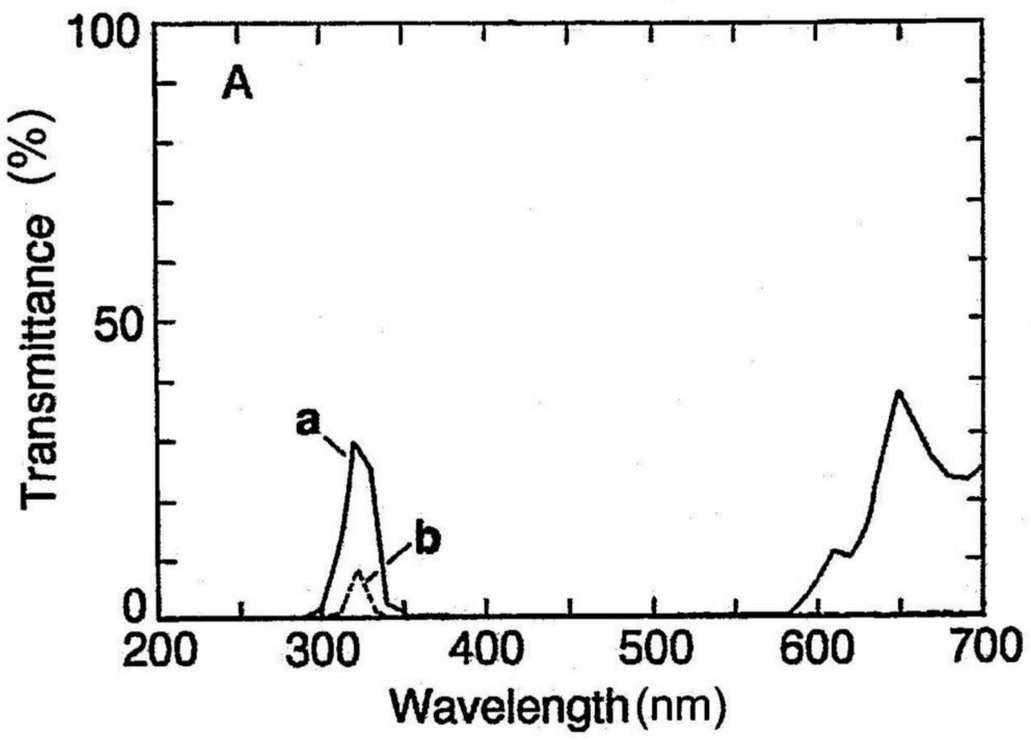

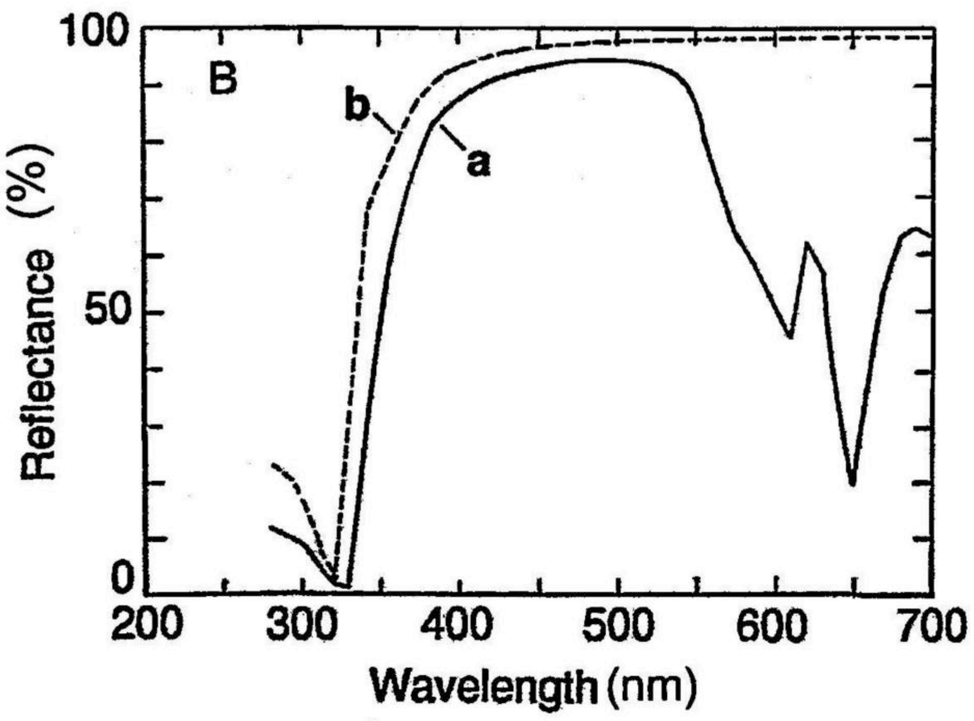

Figure 6-A1. Calculated transmittance spectra (A) and reflectance spectra (B) of the CMCAg^M (a) and bulk silver film (b) whose thickness is assumed to be $\delta = 200$ nm. (A) Transmittance spectra estimated by Eq.(A1). (B) Reflectance spectra estimated by Eq. (A2). The volume fraction of silver Q in the CMCAg^M (a) is assumed to be 0.5.

Table 6-A1. Absorbance $\tilde{\Theta}$ of the silver mirror formed at the surface of the CMCAg film

	δ (nm)	Q	λ_0 (nm)	κ_C	$\tilde{\Theta}$
[CMCAg^M | spacer | dye I]	200	0.5	600	0.386	1.6
[CMCAg^M | spacer | dye II]	200	0.5	400	1.81	11

References

1. Y. Yonezawa, A. Takami, T. Sato, K. Yamamoto, T. Sasanuma, H. Ishida, and A. Ishitani, *J. Appl. Phys.*, **68**, 1297 (1990).
2. Y. Yonezawa, Y. Konishi, H. Hada, K. Yamamoto, and H. Ishida, *Thin Solid Films*, **218**, 109 (1992).
3. Y. Yonezawa and M. Kijima, *J. Soc. Photogr. Sci. Tech. Jpn.*, **56**, 3 (1993).
4. H. Kuhn, D. Möbius, and H. Bücher, *Physical Methods of Chemistry*, Vol I, Part 3B, A. Weissberger and B. Rossiter eds., John Willey&Sons Inc., New York (1972), p.577.
5. H. Kuhn, *Proc. 1980 Tokyo Symposium on Advances in Photography – Interactions between Light and Material for Photographic Applications*, The Society of Photographic Science and Technology of Japan, (1980), p.199.
6. M. Moskovits, *Rev. Mod. Phys.*, **57**, 783 (1985).
7. F. Hache, D. Ricard and C. Flytzanis, *J. Opt. Soc. Am.*, **B3**, 1647 (1986).
8. J. B. Birks ed., *Organic Molecular Photophysics*, Vol. 1, John Willey&Sons Inc., New York (1973).
9. J. B. Birks ed., *Organic Molecular Photophysics*, Vol. 2, John Willey&Sons Inc., New York (1975).
10. H. Kuhn, *J. Chem. Phys.*, **53**, 101 (1970).
11. Y. Yonezawa, M. Ohno, K. Wataya, S. Suga, and H. Hada, *J. Soc. Photogr. Sci. Tech. Jpn.*, **50**, 294 (1987).
12. I. Yamazaki, N. Tamai, and T. Yamazaki, *J. Phys. Chem.*, **91**, 3572 (1987).
13. H. Bücher, H. Kuhn, B. Mann, D. Möbius, L. von Szentpaly, and P. Tillmann, *Photogr. Sci. Eng.*, **11**, 233 (1967).
14. R. R. Chance, A. Prock, and R. Silbey, *Adv. Chem. Phys.*, **37**, 1 (1978).

15. M. Born and E. Wolf, *Principle of Optics*, Tokai Daigaku Syuppansya, Tokyo, (1974) p.118.
16. H. Kallmann, G. Vaubel, and H. Baessler, *Phys. Stat. Sol. (b)*, **44**, 813 (1971).
17. R. R. Chance, A. Prock, and R. Silbey, *J. Chem. Phys.*, **62**, 2245 (1975).
18. Th. Förster, *Discuss. Faraday Soc.*, **27**, 7 (1959).
19. H. Bücher, K. H. Drexhage, M. Fleck, H. Kuhn, D. Möbius, F. P. Schäfer, J. Sondermann, W. Sperling, P. Tillmann, and J. Wiegand, *Molecular Crystals*, **2**, 199 (1967).
20. F. Wilkinson, *Organic Molecular Photophysics*, Vol. 2, J. B. Birks ed., John Willey&Sons Inc., New York (1973), p.95.
21. J. Gersten and A. Nitzan, *J. Chem. Phys.*, **75**, 1139 (1981).
22. R. Ruppin, *J. Chem. Phys.*, **76**, 1681 (1982).
23. C. Pineda and D. Ronis, *J. Chem. Phys.*, **83**, 5330 (1985).
24. The Chemical Society of Japan ed., *Kagaku Binran, Kisohen II (second edition)*, Maruzen, Tokyo (1975) p.1259.
25. H. Wolter, *Z. Phys.*, **105**, 269 (1937).
26. J. C. Maxwell Garnett, *Phil. Trans. Roy. Soc.*, **203**, 385 (1904); **205**, 237 (1906).
27. T. Sato, Y. Yonezawa, and H. Hada, *J. Soc. Photogr. Sci. Tech. Jpn.*, **51**, 122 (1988).

Conclusion

In this thesis, fabrication, characterization and physicochemical properties of photolytic metal nanoparticles in the films of polysaccharide derivatives; carboxymethylcellulose (CMC) and chitosan (CTO), have been studied. A special feature of our method of fabrication is the photoreduction of metal ions in polymer films under fairly mild conditions. Silver and gold nanoparticles in the films of polysaccharide derivatives have been recognized to be important starting materials for matrix-supported metal particles and thin metal films, which have attracted considerable attention from a technological viewpoint because of unique physicochemical properties different from bulk metals.

In Chapter 1, thin films of silver salt of CMC (CMCAg) and chloroauric acid salt of CTO (CTOAu) were photolyzed with 253.7-nm light under several reaction conditions. When the CMCAg film was irradiated in wet air at room temperature, the formation of a clear silver mirror at the irradiated side of the film was observed. Similarly, a clear gold mirror was formed when the CTOAu film was photolyzed under similar conditions. It was found that the clear silver or gold mirror is made of aggregated metal particles stabilized by CMC or CTO. When the CMCAg film was photolyzed in vacuum at liquid nitrogen temperature and then gradually heated, 300 and 335 nm peaks overlapped with a structureless absorption band appeared, indicating the existence of silver clusters. Although no distinct peaks were noticed in the CTOAu film photolyzed in vacuum at liquid nitrogen temperature, heating the film until room temperature followed by the introduction of air brought about the development of colloidal absorption band of gold. It has been proved that silver and gold in various aggregation states (atom, cluster, colloid, bulk metal) can be produced and stabilized in the form of polymer-supported metal particles and thin films under controlled reaction conditions.

Chapter 2 dealt with the aggregation of silver nanoparticles at the surface of CMCAg film photolyzed with UV light in wet air at room temperature. Surface composition analysis by X-ray photoelectron spectroscopy (XPS) has been proved to be helpful to examine the mechanism of formation and growth of metal nanoparticles, as well as photochemical reactions of the CMCAg film. The total silver concentration (silver ions and reduced silver) at the surface as estimated by XPS was increased from 5.4 atomic % (31.6 wt%) before irradiation to 45.0 atomic % (87.0 wt%) after 600 min of irradiation. FE-SEM and TEM observations of the CMCAg film, as well as the surface composition analysis have indicated the precipitation of silver nanoparticles at the film surface. Average particle size changed from 11 nm to 33 nm

during 30–600 min of irradiation. Some details of the reaction mechanism have been discussed with aids of the XPS and IR analysis.

Aggregation of photolytic gold nanoparticles at the surface of CTOAu film in wet air at room temperature has been investigated in Chapter 3. Detailed XPS study and FE-SEM observation were carried out to characterize gold nanoparticles. Gold clusters formed at the early stage were characterized by the 0.5–0.8 eV peak shift and 0.1–0.25 eV line broadening of the XPS spectrum of Au(4f) region compared with bulk gold. FE-SEM observation demonstrated the change of the average particle size, from 13 nm (t = 10 min) to 50 nm (t = 120 min). After prolonged irradiation, the peak position and FWHM of the Au(4f) line approached those of bulk gold. The concentration of reduced gold at the surface layer was increased from 0.6 atomic % (5.4 wt%) before irradiation to 21.2 atomic % (77.4 wt%) after 120 min of irradiation, indicating that gold atoms and clusters can migrate inside the film and precipitate at the irradiated surface. Based on the XPS analysis of the CTOAu film, a reasonable reaction scheme has been proposed.

In Chapter 4, Raman spectra of the CMCAg film and a silver alginate film (ALAg film) photolyzed with UV light were measured. Raman bands related to $RCOO^-$ ion; symmetric COO^- stretching vibration, C-C (COO^-) stretching vibration, and COO^- deformation vibration, became evident after photolysis. The enhancement of Raman scattering due to photolytic silver has been interpreted in terms of surface-enhanced Raman scattering (SERS). The intensity of the symmetric COO^- stretching vibration band attained to the maximum by 180 min and 10 min of UV irradiation for the CMCAg film and the ALAg film, respectively. At the same time, the electrical resistance of the film surface was decreased about 10^{-5}–10^{-2} times of that of the unirradiated films, which is caused by the contact of silver particles. A close connection between the Raman intensity and the aggregation state of photolytic silver has been noted. When metal particles begin to aggregate, a contribution of multipole plasmon resonance to SERS may become significant. In this sense, SERS is applicable as a probe to monitor the change of the aggregation state of silver particles. The maximum enhancement factor of 10^4–10^5 as estimated under several simplifying assumptions appeared to be in the same order as reported by other research groups. After prolonged irradiation, the film surface changed into the clear silver mirror, resulting in the decrease of the Raman intensity due to the filter effect of deposited silver.

With a help of Mie theory, a tractable formula for the enhancement efficiency of the local electric field Q_{NF} was introduced in Chapter 5. For the Ag sphere embedded in the polymer

matrix, Q_{NF} was calculated as functions of incident wavelength (λ = 300–700 nm) and particle diameter ($2a$ = 10–400 nm). When the incident wavelength was in resonance with surface plasmon mode of the small Ag sphere, Q_{NF} had the distinct maximum value. Q_{NF} evaluated for the incident wavelength λ = 510 nm was compared with many features of SERS of the CMCAg and the ALAg films obtained in Chapter 4. It has been suggested that Q_{NF} is useful as a practical index for the small metal particles to promote surface-enhanced electromagnetic processes.

In Chapter 6, the CMCAg film containing colloidal silver particles ($CMCAg^C$) and the CMCAg film whose surface was covered with silver mirror ($CMCAg^M$) were used for the substrate to deposit dye monolayers by Langmuir-Blodgett (LB) technique. Two dyes having long alkyl chains; dye I (N-ethyl-octadecylrhodamine B), dye II (10-(1-pyrene)-decanoic acid), were taken up. The monolayer assemblies; [$CMCAg^M$ | spacer | dye I], [$CMCAg^C$ | spacer | dye I], exhibited a broad fluorescence peak around λ_{em} = 600 nm, while the [$CMCAg^M$ | spacer | dye II] assembly and [$CMCAg^C$ | spacer | dye II] assembly were characterized by sharp fluorescence peaks around 400 nm. The fluorescence intensity of those assemblies was considerably reduced when the thickness of the calcium arachidate spacer separating the dye layer from the substrate was decreased. It has been concluded that fluorescence quenching is caused by electronic energy transfer from an excited dye molecule (energy donor) to the silver particles (acceptor). The characteristic distance, d_0, in which fluorescence intensity is one-half of that in the case of infinite separation of the acceptor layer, was estimated. They were 21 nm ([$CMCAg^M$ | spacer | dye I]), 5 nm ([$CMCAg^C$ | spacer | dye I]), 9 nm ([$CMCAg^M$ | spacer | dye II], and 8 nm ([$CMCAg^C$ | spacer | dye II]), respectively. These observations have been interpreted with the help of the electromagnetic theory of energy transfer.

The metal salt films of polysaccharide derivatives, such as CMC and CTO, are unique materials, which have dual roles; the reaction agent of metal nanoparticle synthesis and the protective agent for metal nanoparticles. It is demonstrated that the aggregation states of deposited metals are controllable from atoms, clusters, colloids to bulk metals by changing reaction conditions. The photolytic metal nanoparticles have been proved to cause the enhancement of the Raman scattering of adjacent molecules and the fluorescence quenching of adsorbed dyes. Judging from the basic research carried out in this thesis, future applications of noble metal particulate films based on naturally occurring polymer for optical devices, optoelectronic devices, photocatalysts, high-sensitivity analytical devices, as well as imaging materials are highly promising.

List of Publications

Chapter 1

1. Formation of Metal Particles and Thin Films by Photolysis of Metal Salts of Polysaccharide Derivatives

   Yoshiro Yonezawa, Noritsugu Kometani, Masayuki Seki, Takeshi Sakagami, Hirotoshi Tanaka, Sei-ichi Koyanagi, and Toshihito Miyama

   Transactions of the Materials Research Society of Japan, **27**, 197–200 (2002).

Chapter 2

2. Photoinduced Formation and Aggregation of Silver Nanoparticles at the Surface of Carboxymethylcellulose Films

   Toshihito Miyama and Yoshiro Yonezawa

   Journal of Nanoparticle Research, **6**, 457–465 (2004).

Chapter 3

3. Aggregation of Photolytic Gold Nanoparticles at the Surface of Chitosan Films

   Toshihito Miyama and Yoshiro Yonezawa

   Langmuir, **20**, 5918–5923 (2004).

Chapter 4

4. Surface-Enhanced Raman Scattering from Silver Salt of Carboxymethylcellulose Photolyzed with UV-Light

   Toshihito Miyama, Yoshiro Yonezawa, Tomoo Sato, Junzo Umemura, and Tohru Takenaka

   Chemistry Letters, **1993**, 1537–1540 (1993).

5. Photoinduced Formation of Aggregated Silver Particles from Silver Salt of Polysaccharide

   Yoshiro Yonezawa, Tomoo Sato, Toshihito Miyama, Akinori Takami, Junzo Umemura, and Tohru Takenaka

   Surface Review and Letters, **3**, 1109–1112 (1996).

Chapter 5

6. Enhancement of Local Electric Field by a Metal Microsphere and Surface Enhanced Raman Scattering of Silver Salts of High Molecular Weight Carboxylic Acids
   Yoshiro Yonezawa, Toshihito Miyama, and Tomoo Sato
   Journal of the Society of Photographic Science and Technology of Japan, **58**, 109–121 (1995).

Chapter 6

7. Transfer of Dye Monolayers onto Silver Metal Films Formed by Photolysis of Silver Salt of Carboxymethylcellulose
   Yoshiro Yonezawa, Toshihito Miyama, and Tomoo Sato
   Chemistry Letters, **1992**, 2455–2458 (1992).

8. Quenching of Dye Fluorescence by Thin Silver Films Formed by Photolysis of Silver Salt of Carboxymethylcellulose
   Toshihito Miyama, Yoshiro Yonezawa, and Tomoo Sato
   Journal of the Society of Photographic Science and Technology of Japan, **57**, 1–11 (1994).

The following papers are not included in this thesis.

9. Monolayer Assemblies Incorporating Two Types of Cyanine Dyes: Possibility of Formation of an Amalgamation-type J-Aggregate
   Yoshiro Yonezawa, Toshihito Miyama, and Hideaki Ishizawa
   Journal of Imaging Science and Technology, **39**, 331–340 (1995).

10. Geographical Effect on the Weatherability of Plasticized Polyvinylchloride
    Toshihito Miyama and Hirotsugu Yoshida
    Materials Life, **9**, 135–139 (1997).

Acknowledgments

This thesis work was carried out in 2003–2005 at Osaka City University and in 1992–1994 at Kyoto University. The author wishes to express his deepest gratitude to Professor Yoshiro Yonezawa of Osaka City University for his kind direction and continuous encouragement throughout this work.

The author also expresses his deep gratitude to Professor Tsutomu Ohzuku and Professor Akikazu Matsumoto of Osaka City University for their helpful suggestions and discussions. Sincere gratitude is due to Dr. Kouichi Tsuji and Dr. Noritsugu Kometani of Osaka City University, and Dr. Tomoo Sato of University of Tsukuba (formally of Kyoto University) for their helpful advices and kind support.

The author is grateful to Mr. Masato Azuma, Dr. Kazuo Doyama, Mr. Taro Ichijo, Mr. Shigeki Nomura and Mr. Masashi Kanou of Sekisui Chemical Co., Ltd. for their kind support and encouragement. Grateful acknowledgment is made to all the colleagues of Development Center of Sekisui Chemical Co., Ltd.

Special thanks are due to the collaborating students, Dr. Akinori Takami and Mr. Itaru Kawabata of Kyoto University, Mr. Masayuki Seki, Mr. Takeshi Sakagami, Mr. Hirotoshi Tanaka and Mr. Sei-ichi Koyanagi of Osaka City University, for their experimental help in Chapter 1, Chapter 3 and Chapter 4. A heartfelt appreciation is extended to all the colleagues and friends in Yonezawa Laboratory for their warm help and daily discussions.

The author is deeply indebted to Emeritus Professor Tohru Takenaka and Professor Junzo Umemura of Kyoto University for Raman scattering measurements and fruitful discussions in Chapter 4.

The author is grateful to Professor Shinzaburo Ito and Dr. Masataka Ohoka of Kyoto University for their experimental help in fluorescence spectroscopy in Chapter 6.

The author is sincerely grateful to his parents for their warm support and encouragement.

Finally, the author would like to express his deepest feeling of gratitude to his wife, Yuko, and daughter, Maho, for their mental support and encouragement that have been of greatest importance throughout this work.

January, 2005

Toshihito Miyama